

FABRICATION, CHARACTERIZATION AND MODELING OF MAGNETORHEOLOGICAL ELASTOMERS

Ashkan Dargahi

A Thesis
in
The Department
of
Mechanical and Industrial Engineering

Presented in Partial Fulfillment of the Requirements
for The Degree of Masters of Applied Science at
Concordia University
Montreal, Quebec, Canada

August 2017

© Ashkan Dargahi, 2017

CONCORDIA UNIVERSITY
School of Graduate Studies

This is to certify that the thesis prepared

By: **Ashkan Dargahi**

Entitled: **“Fabrication, Characterization and Modeling of Magnetorheological Elastomers”**

and submitted in partial fulfillment of the requirements for the degree of

Master of Applied Science (Mechanical Engineering)

complies with the regulations of the University and meets the accepted standards with respect to originality and quality.

Signed by the final examining committee:

_____ Chair
Dr. Hoi Dick Ng

_____ MIE Examiner
Dr. Sivakumar Narayanswamy

_____ External Examiner
Dr. Hassan Rivaz

_____ Supervisor
Dr. Subhash Rakheja

_____ Supervisor
Dr. Ramin Sedaghati

Approved by _____
Dr. S. Narayanswamy, Graduate Program Director

Dr. Amir Asif, Dean
Faculty of Engineering & Computer Science

Date _____

ABSTRACT

FABRICATION, CHARACTERIZATION AND MODELING OF MAGNETORHEOLOGICAL ELASTOMERS

by Ashkan Dargahi

Magnetorheological elastomers (MREs) are a novel class of magneto-active materials comprised of an elastomeric matrix impregnated by micron-sized ferromagnetic particles, which exhibit adjustable mechanical properties such as stiffness and damping coefficient in a reversible manner under the application of an external magnetic field. MREs are solid state of magnetorheological (MR) materials. In contrast to MR fluids, which provide field-dependent apparent viscosity, MREs, being a smart viscoelastic material, are capable of providing controlled field dependent moduli. Yet having a solid grasp of highly complex behavior of this active composite is a fundamental necessity to design any adaptive structure based on the MRE. This study is concerned with investigation of the static and dynamic behavior of the magnetorheological elastomers. To this end, six different types of MREs with varying contents of the rubber matrix as well as ferromagnetic particles are fabricated and characterized statically in the shear mode as a function of the magnetic field intensity. The MRE containing the highest percentage of iron particles (40% volume fraction) exhibited a notable relative MR effect of 555% with 181.54 KPa increase in the MRE shear modulus. This particular MRE was then chosen for subsequent dynamic characterization. The dynamic responses of magnetorheological elastomers revealed strong dependence on the strain and strain rate as well as the applied magnetic field intensity. Dynamic characterization is performed in shear mode under harmonic excitations under the broad ranges of shear strain amplitude (2.5-20%), frequency (0.1-50 Hz) and magnetic field intensity (0-450 mT). The strain softening, strain stiffening, strain rate stiffening and the magnetic field stiffening phenomena are identified as the nonlinear properties of MRE stress-strain hysteresis loops. Subsequently, an operator-based Prandtl-Ishlinskii (PI) phenomenological model is developed to predict the nonlinear hysteresis behavior of the MREs as functions of strain, strain rate and field intensity. The stop-operator-based classical PI model using only 10 hysteresis operators provided very accurate predictions, and it involved identification of only four parameters, which were dependent on the loading conditions. The validity of the developed Classical Prandtl-Ishlinskii model is assessed using the laboratory-measured data for MRE over a wide range of inputs. The proposed model is further generalized to predict the dynamic behavior of MRE independent of the loading conditions, which could be beneficial for controlling the MRE-based adaptive devices in real time. The results demonstrated that the proposed generalized model could accurately characterize the nonlinear hysteresis properties of MRE under a wide range of loading conditions and applied magnetic fields.

To my Parents,

Akbar Darghai & Forouzan Vasighi

Without whom none of my success would be possible

Acknowledgment

I would like to express my most sincere gratitude to my supervisors, Profs. Subhash Rakheja and Ramin Sedaghati; I wish to express my honest appreciation for their patience and invaluable guidance and advice throughout my Master's program.

I would like to also extend a special vote of gratitude towards Prof. Javad Dargahi, and his senior PhD student, Mr. Amir Hooshir for their invaluable suggestions and comments.

I would like to wholeheartedly thank my brother, Mr. Shayan Dargahi who unconditionally supported me in all the steps throughout my master's studies.

Last, but not least, my warm and heartfelt thanks goes to my cousin and his wife, Pouya Lamerad and Golia Shafiee, and all my close friends and office-mates at Concordia University: Kaveh Rahbardar Mojaver, Mahsa Mousavi, Mana Mirmirani, Milad Javadi Aghdam, Niranjana Mehendaleh, Hossein Vatandoost, Hadi Shamieh, Shahram Shokouhfar, Masoud Hemmatian, Ali Fallah Jahromi, Mostafa Asadi, Morteza Sadeghifar and Behzad Jafari for their inspiration and support.

List of Figures

Figure 1.1: MRE fabrication process [20].	3
Figure 1.2: Operational modes of MREs: (a) shear mode; (b) squeeze mode; and (c) field-active mode [17].	4
Figure 1.3: Different configurations of the Adaptive tuned vibration absorbers based on MR, proposed by: (a) Ginder et al. [29]; (b) Deng et al. [27]; (c) Deng and Gong [26]; and (d) Dong et al. [28].	5
Figure 1.4: (a) Typical laminated rubber bearing/isolator and (b) Cross-section of the MRE base isolator by Li et al. [33].	5
Figure 1.5: Experimental setup designed by Lokander et al. [48] for measurement of MR effect in the shear mode.	12
Figure 1.6: (a) Schematic of the double lap-shear test setup; and (b) experimental setup for double lap-shear testing designed by Gordaninejad et al. [12] (LVDT: linear variable differential transformer).	13
Figure 1.7: Experimental setup employed for characterizations of the MRE specimens with permanent magnets by Norouzi et al. [4].	13
Figure 1.8: Schematic diagram and experiment setup designed by Yu et al. [34] for characterization of a multi-layered MRE vibration isolator.	14
Figure 1.9: Shear stress versus shear strain of a MRE sample under different magnetic fields [20].	15
Figure 1.10: Shear stress - shear strain characteristics of a large capacity MRE-based seismic isolator [32].	15
(a)	16
Figure 1.11: (a) shear stress-strain responses of the MRE under different magnetic field intensities ($\gamma = 4\%$); (b) variations in the shear storage modulus with frequency ($\gamma = 4\%$); and (c) variations in the shear storage modulus with frequency ($\gamma = 16\%$) [4].	16
Figure 1.12: Loss factor versus frequency for different magnetic flux densities: (a) $\gamma = 4\%$ and (b) $\gamma = 16\%$ [4].	17
Figure 1.13: (a) Absolute and (b) relative MR effect versus frequency at high frequencies ranging from 100 to 1250 Hz with different applied magnetic fields [48].	17
Figure 1.14: Loss factor versus frequency under higher frequency excitations, ranging from 100 to 1250 Hz under different magnetic fields intensities [48].	18
Figure 1.15: Variations in the loss angle ($\tan\delta$) in the lower frequency range (1 to 21 Hz) under different magnetic field intensities [48].	18
Figure 1.16: Shear strain- shear stress hysteresis loops obtained at different frequencies with 16% strain and magnetic flux density of 272 mT [4].	19

Figure 1.17: Variations in the storage modulus with shear strain applied at different frequencies under different magnetic flux intensities: (a) $f = 0.1$ Hz; and (b) $f = 3$ Hz [4].....	20
Figure 1.18: Variations in the loss factor with shear strain applied at different frequencies under different magnetic flux intensities: (a) $f = 0.1$ Hz; and (b) $f = 3$ Hz [4].....	20
Figure 1.19: Schematic diagram of the phenomenological models incorporating Bouc–Wen element (a) in parallel with a Voigt element proposed by Yang et al. [3] for a seismic isolator; (b) proposed by Behrooz et al. [2] for a variable stiffness and damping isolator.	22
Figure 1.20: (a) Modified viscoelastic Kelvin-Voigt model proposed by Norouzi et al. [4]; and (b) Schematic of the phenomenological model proposed by Yu et al. 2016 [34].	24
Figure 1.21: The (a) stop and (b) Play Hysteresis operators [70].	25
Figure 2.1: MRE Fabrication set-up.....	35
Figure 2.2: Fabricated MRE – type 3 (a) in and (b) out of the designed circular molds.....	35
Figure 3.1: Typical test piece arrangement – ISO 1827 (1: two external plates, 2: two internal plates, 3: pin and fixture for tensile loading) [73].	38
Figure 3.2: Typical stress-strain response of viscoelastic materials under sinusoidal deformation [74].....	41
Figure 3.3: Load deflection hysteresis loop (X: deflection, Y: load) [74].....	43
Figure 3.4: Double lap shear test arrangement [75].	44
Figure 3.5: Double lap shear test specimens design[75].	45
Figure 3.6: ElectroForce 3200 test instrument – Axial Configuration.	46
Figure 3.7: (a) 3D designed test arrangement, (b) manufactured test specimens and MRE samples and (c) actual test arrangement.	48
Figure 3.8: Experimental set-up designed for applying magnetic field on the test arrangement.....	49
Figure 3.9: Simple shear test set-up placed between the two sets of permanent magnets.	49
Figure 3.10: Magnetic field intensity at 5mm from center point versus distance between the permanent magnets.	51
Figure 3.11: Schematic diagram for calculating the magnetic field on the central axis (a) of a rectangular block at a distance x and (b) between the two rectangular magnet at a distance x from the center point.	52
Figure 3.12: Comparison between the measured and analytical magnetic field intensities at 5 mm from the center point for varying values of magnetic remanence.....	53
Figure 3.13: Distribution of magnetic field intensity between two permanent magnets along the central x axis in different distances between the magnets.	53
Figure 3.14: Stress-strain curve of fabricated MREs (a) type1, (b) type2, (c) type3, (d) type4, (e) type5, (f) type6, at 4 different magnetic field intensities.	56

Figure 3.15: Shear modulus versus magnetic field intensity for MRE (a) type1, (b) type2, (c) type3, (d) type4, (e) type5, (f) type6.	57
Figure 3.16: Effects of magnetic field intensity on the shear modulus of fabricated MREs obtained from static tests.	60
Figure 3.17: Bar graph representation of magneto-mechanical properties of MREs.	60
Figure 3.18: Proposed model of shear modulus at different magnetic field densities and the measured data.	61
Figure 3.19: Measured hysteresis nonlinearities of MRE in simple shear mode under different frequencies with 10% shear strain and (a) magnetic field intensity: 0mT, (b) magnetic field intensity: 150mT, (c) magnetic field intensity: 300mT, (d) magnetic field intensity: 450mT.	64
Figure 3.20: Measured hysteresis nonlinearities of MRE in simple shear mode under different strain amplitudes at 10 Hz and (a) magnetic field intensity: 0mT, (b) magnetic field intensity: 150mT, (c) magnetic field intensity: 300mT, (d) magnetic field intensity: 450mT.	65
Figure 3.21: Measured hysteresis nonlinearities of MRE in simple shear mode at different magnetic field intensities under excitation frequency of 10 Hz and (a) shear strain amplitude: 2.5%, (b) shear strain amplitude: 5%, (c) shear strain amplitude: 10%, (d) shear strain amplitude: 20%.	66
Figure 3.22: Effects of excitation frequency on the elastic shear modulus of MRE at different strain amplitudes and (a) magnetic field intensity: 0mT, (b) magnetic field intensity: 150mT, (c) magnetic field intensity: 300mT, (d) magnetic field intensity: 450mT.	67
Figure 3.23: Effects of excitation frequency on the loss shear modulus of MRE at different strain amplitudes and (a) magnetic field intensity: 0mT, (b) magnetic field intensity: 150mT, (c) magnetic field intensity: 300mT, (d) magnetic field intensity: 450mT.	68
Figure 3.24: Effects of strain amplitude on the elastic shear modulus of MRE at different excitation frequencies and (a) magnetic field intensity: 0mT, (b) magnetic field intensity: 150mT, (c) magnetic field intensity: 300mT, (d) magnetic field intensity: 450mT.	69
Figure 3.25: Effects of strain amplitude on the loss shear modulus of MRE at different excitation frequencies and (a) magnetic field intensity: 0mT, (b) magnetic field intensity: 150mT, (c) magnetic field intensity: 300mT, (d) magnetic field intensity: 450mT.	70
Figure 3.26: Effects of magnetic field intensity on the elastic shear modulus of MRE at different excitation frequencies and (a) shear strain amplitude: 2.5%, (b) shear strain amplitude: 5%, (c) shear strain amplitude: 10%, (d) shear strain amplitude: 20%.	71
Figure 3.27: Effects of magnetic field intensity on the loss shear modulus of MRE at different excitation frequencies and (a) shear strain amplitude: 2.5%, (b) shear strain amplitude: 5%, (c) shear strain amplitude: 10%, (d) shear strain amplitude: 20%.	72
Figure 3.28: A typical stress-strain curve of MRE in simple shear mode under applied magnetic field.	73
Figure 3.29: Measured stress-strain hysteresis loop of MRE type 6 at 20% shear strain, 0.1 Hz excitation frequency and 300 mT magnetic field intensity.	74

Figure 4.1: The input-output properties of the stop hysteresis operator.....	78
Figure 4.2: Input-output characteristics of: (a) stop hysteresis operators with different threshold values; and (b) the classical Prandtl-Ishlinskii model integrating five stop operators under $v(t) = 20\sin 2\pi t$	80
Figure 4.3: Comparisons between of the stress-strain properties obtained from the Classical PI model with the measured data under varying strain amplitudes and $0mT$ magnetic field intensity, and different excitation frequencies (a) $0.1 Hz$ (b) $1 Hz$ (c) $10 Hz$ (d) $50 Hz$ (- - Measured, - Model).....	84
Figure 4.4: Comparison between of the stress-strain properties obtained from the Classical PI model with the measured data under varying strain amplitudes and $150mT$ magnetic field intensity, and different excitation frequencies (a) $0.1 Hz$ (b) $1 Hz$ (c) $10 Hz$ (d) $50 Hz$, (- - Measured, - Model).	85
Figure 4.5: Comparison between of the stress-strain properties obtained from the Classical PI model with the measured data under varying strain amplitudes and $300mT$ magnetic field intensity, and different excitation frequencies (a) $0.1 Hz$ (b) $1 Hz$ (c) $10 Hz$ (d) $50 Hz$, (- - Measured, - Model).	86
Figure 4.6: Comparison between of the stress-strain properties obtained from the Classical PI model with the measured data under varying strain amplitudes and $450mT$ magnetic field intensity, and different excitation frequencies (a) $0.1 Hz$ (b) $1 Hz$ (c) $10 Hz$ (d) $50 Hz$, (- - Measured, - Model).	87
Figure 4.7: Variations in model constant $c1$ with the loading frequency.....	88
Figure 4.8: Variations in the classical PI model parameter $k1$ with: (a) loading frequency; and (b) the magnetic field intensity.	90
Figure 4.9: Variations in the classical PI model parameter $k2$ with: (a) loading frequency; and (b) the magnetic field intensity.	90
Figure 4.10: The relationships between the model parameters (a) $k1$, (b) $k2$ with the loading frequency and the magnetic field intensity.....	91
Figure 4.11: The stress-strain hysteresis loops obtained from the generalized Prandtl-Ishlinskii model over the range of the strain amplitudes (2.5, 5, 10 and 20%) under: (a) $10 Hz$ excitation frequency and $300 mT$ magnetic field intensity; and (b) $1 Hz$ excitation frequency and $150 mT$ magnetic field intensity.....	93
Figure 4.12: The stress-strain hysteresis loops obtained from the generalized Prandtl-Ishlinskii model over the range of the excitation frequencies (0.1, 1, 10 and 50 Hz) under $300 mT$ magnetic field intensity and the strain amplitude: (a) 10%; and (b) 20%.....	93
Figure 4.13: The stress-strain hysteresis loops obtained from the generalized Prandtl-Ishlinskii model over the range of the magnetic field intensities (0, 150, 300 and 450 mT) under 10 % strain amplitude and the excitation frequency: (a) $1 Hz$; and (b) $10 Hz$	94

List of Tables

Table 1.1: Composition of different samples fabricated by gong et al. [38].	7
Table 1.2: A summary of constitutes of the reported fabricated MRE samples.	8
Table 2.1: Technical properties of Ecoflex 00-20, extra soft silicone rubber.	30
Table 2.2: The effects slacker on the softness of the silicone rubber.	31
Table 2.3: The Effects of silicone thinner on the properties of mold max 30 silicone rubber.	31
Table 2.4: The volume fraction of each component in fabricated MREs.	32
Table 2.5: The density of MRE components.	33
Table 2.6: The Physical properties of fabricated MREs.	36
Table 3.1: Shear test conditions for small-sized apparatus[74].	42
Table 3.2: Recommended dimensions for double lap shear test specimens[75].	45
Table 3.3: Specifications of Bose - ElectroForce 3200.	47
Table 3.4: Comparison between the magneto-mechanical properties of fabricated MREs.	60
Table 4.1: Variations in parameters of the classical Prandtl-Ishlinskii model with the excitation frequency and magnetic field intensity.	82

Nomenclature

a_1, a_2	Constants of the equation proposed for magnetic field intensity at the center point between two permanent magnets
A	Bonded area of one face of one test sample
B	Magnetic field intensity
$B(x)$	Magnetic field intensity at $5mm$ from the center point between the magnets
B_r	Remanence magnetism
c	Thickness of one rubber element
c_1, c_2	Constants of threshold function
$CPVC$	Critical particles volume concentration
C_0	Viscous coefficient
$C_m[0, T]$	Space of piecewise monotone continuous functions defined on the time interval $[0, T]$
d	Deformation of the test piece in shear mode
$E_r[.](0)$	Initial condition of stop operator
$E_r[.]$	Stop operator
$E_r[.](t)$	Output of stop operator
f	Frequency
F	Force
F_0	Maximum load amplitude
$F_r[.](0)$	Initial condition of play operator

$F_r[.]$	Play operator
$F_r[.](t)$	Output of play operator
G	Shear modulus
G'	Elastic shear modulus
G''	Loss shear modulus
G_0	Shear modulus in absence of magnetic field intensity
G_{max}	Shear modulus in presence of maximum magnetic field intensity
$ G^* $	Absolute value of the complex shear modulus
h	Thickness of one test piece
k_1, k_2	Constants of density function
K_0	Stiffness
L	Length of rectangular magnet
m	Weight
m_1, m_2, m_3, m_4	Constants of equation proposed for shear modulus in terms of magnetic field intensity
M	Number of inputs
n	Non-dimensional parameters of Bouc-Wen model
p	Density function
q	Positive constant of the Prandtl-Ishlinskii model based on play operator
r	Threshold function of the Prandtl-Ishlinskii model
R^2	Coefficient of determination
T	Thickness of rectangular magnet
$u(t)$	System output

$v(t)$	System input
V	Volume
w_1, w_2	Constants of density function
$w(t)$	System output
w_i	Mass fraction of component i
W	Width of rectangular magnet
x	Displacement
\dot{x}	Velocity
x_0	Maximum deflection amplitude
z	Evolutionary variable in Bouc-Wen model
\dot{z}	Rate of the evolutionary variable in Bouc-Wen model
β	Non-dimensional parameters of Bouc-Wen model
γ_0	Shear strain amplitude
ρ_{apparent}	Apparent density
ρ_{true}	True density
φ_i	Volume fraction of component i
ΔG_r	Relative magnetorheological effect
ΔG	Absolute magnetorheological effect
Π	Play operator-based Prandtl-Ishlinskii model
$\Pi[.](t)$	The output of play operator-based Prandtl-Ishlinskii model
Ω	Stop operator-based Prandtl-Ishlinskii model
$\Omega[.](t)$	Output of stop operator-based Prandtl-Ishlinskii model

α	Non-dimensional parameter of Bouc-Wen model
γ_0	Shear strain amplitude
γ	Shear Strain
$\dot{\gamma}(t)$	Shear strain rate
δ	Phase or loss angle
η	Viscosity
ρ	Density
τ	Shear stress

Table of contents

List of Figures	vii
List of Tables	x
Chapter 1: Introduction, Literature Review and Objectives	1
1.1 Introduction	1
1.2 Magnetorheological elastomers (MREs)	2
1.2.1 Physics of MREs	2
1.2.2 Applications of MREs	4
1.3 Fabrication of MREs	6
1.3.1 Fabrication methods	6
1.3.2 Factors affecting properties of MREs	9
1.4 Mechanical properties of MREs	10
1.4.1 Methods of characterization	11
1.4.2 Static properties of MREs	14
1.4.3 Dynamic properties of MREs	15
1.5 Models for predicting dynamic behavior of MREs	20
1.5.1 Differential equation-based phenomenological models	21
1.5.2 Operator-based phenomenological models	24
1.6 Scope and objectives	26
1.7 Organization of the dissertation	27
Chapter 2: Fabrication of MREs	28
2.1 Introduction	28
2.2 Selection of materials for fabrication of MREs	29
2.2.1 Non-magnetic elastomeric matrix	29
2.2.2 Micron-sized ferromagnetic particles	30
2.2.3 Additives	30

2.3	Design of experiment and fabrication procedure	31
2.3.1	Fabrication design	31
2.3.2	Fabrication procedure	34
2.4	Physical properties of fabricated MREs.....	35
2.5	Summary	36
Chapter 3:	Magneto-Mechanical Characterization of MREs	37
3.1	Introduction.....	37
3.2	Standards for static and dynamic characterization of rubbers	37
3.3	Experimental setup and proposed test procedures	45
3.3.1	Test procedure for static characteristics of MREs	54
3.3.2	Test procedure for dynamic characteristics of MREs	54
3.4	Static properties	55
3.5	Dynamic properties	62
3.5.1	Effects of excitation frequency	62
3.5.2	Effects of strain amplitude.....	62
3.5.3	Effects of magnetic field intensity.....	63
3.5.4	Storage (Elastic) and Loss Moduli of the MREs	63
3.5.4.1	Effects of excitation frequency	66
3.5.4.2	Effects of strain amplitude.....	69
3.5.4.3	Effects of magnetic field intensity.....	70
3.6	Discussion on factors influencing static and dynamic properties	72
3.7	Summary	75
Chapter 4:	Modeling of Dynamic Properties of MREs	76
4.1	Introduction.....	76
4.2	Classical Prandtl-Ishlinskii model	77
4.2.1	A Stop hysteresis operator.....	77
4.2.2	Classical Prandtl-Ishlinskii model.....	78

4.3	Classical Prandtl-Ishlinskii model for characterizing hysteresis in MREs.....	80
4.3.1	Model parameter identification	81
4.4	Model verification	83
4.5	Formulation of a generalized Prandtl-Ishlinskii model	88
4.6	Simulation results.....	92
4.7	Summary	94
Chapter 5:	Conclusions and Recommendation for Future Studies	95
5.1	Major contributions.....	95
5.2	Major conclusions	96
5.3	Recommendations for future work	97
Appendix	98
A	Material properties.....	98
References	104

Chapter 1: Introduction, Literature Review and Objectives

1.1 Introduction

Magnetorheological elastomers (MREs) are an emerging class of smart materials that can change their properties in a reversible manner under the application of an external magnetic field [1-3]. MREs consist of micron-sized iron particles arranged or suspended within an elastomer matrix. The magnetic interaction between the particles within the matrix leads to controllable variations in mechanical properties such as stiffness and damping coefficients. The elastic modulus of this flexible composite varies rapidly in response to a relatively low externally applied magnetic field. Since the particles are locked in the matrix and have no time to arrange while an external magnetic field is applied, the response time of MREs is extremely quick (a few milliseconds) [4]. Additionally, the shape and the electrical properties of MREs can be altered by the external stimuli. The possibility of controlling the mechanical and electrical properties of MREs in real time has made them an excellent choice to be utilized in a wide range of engineering applications. MREs are ideal candidates for application in vibration absorbers and vibration isolators for civil and mechanical engineering applications [5, 6], sensing devices [7], actuators to control the flow [8] and adaptive beam structures [9]. The responses of MRE, however, are highly complex due to strong coupled dependence on the loading conditions and the magnetic field intensity. Although, the properties of MREs have been widely studied during the past decade using experimental and analytical methods [10-12], standardized methodologies for characterization and modeling of MREs do not yet exist.

This dissertation research focuses in fabrication, experimental characterization of static and dynamic properties, and modeling of MREs. Six different samples of MREs were fabricated in the laboratory with varying volume fractions of the iron particles. The static and dynamic properties of MREs are measured in the laboratory under wide ranges of strain amplitude, strain rate (frequency) and magnetic field intensity. The data are analyzed to quantify the MR effect of the samples. The stop operator-based Prandtl-Ishlinskii models are subsequently formulated for predicting the static and dynamic properties of MREs. The validity of the model is demonstrated under wide ranges of strain deformation, strain rate and magnetic field intensity.

In this chapter, the physics of MRE is briefly summarized in section 1.2 and various engineering applications of this smart composite are described in section 1.3. Next, the fabrication methods of MRE together with factors affecting the magneto-mechanical properties of MRE, such

as the size and content of iron particles, are discussed in details in section 1.4. The reported experimental methods for static and dynamic characterization of MREs are reviewed in section 1.5 together with the effects of loading conditions and magnetic field intensity. The reported phenomenological models for predicting nonlinear dynamic behavior of MREs are reviewed in section 1.6. The scope and objectives of the dissertation are finally presented in section 1.7.

1.2 Magnetorheological elastomers (MREs)

1.2.1 Physics of MREs

Magnetorheological elastomers (MREs) are a class of smart materials that can sense changes in their environment and respond to it in an efficient and controlled manner. The MR effect was first discovered on Magnetorheological fluids by Rabinow [13] in 1948. It was not until 1983, when Rigbi and Jilken [14] conducted preliminary tests to demonstrate the MR effect in magnetorheological elastomers. Jolly et al. [15, 16] conducted the first comprehensive study on MR elastomers in 1996, and reported that such elastomer composites offer considerable performance in variable stiffness devices and adaptive structures. Following the studies of Jolly et al. [15, 16], there has been growing interest in understanding the potential properties for wide ranges of engineering applications.

MREs are composed of three fundamental components: ferromagnetic particles, elastomeric matrix and the additives. The main features of the particles can be addressed as: a) high saturation magnetization; b) low remnant magnetization; and c) high permeability. Polarizable particles with such properties will increase the MR effect and also improve the mechanical properties of the composite [1]. High saturation magnetization of the particles permits enhancement of the total magnetic field by the MRE ferromagnetic particles even in higher magnitudes of the externally applied magnetic field. Permeability accounts for the degree of magnetization that a material obtains in response to an applied magnetic field. High permeability intensifies the magnetic network between the particles. Ferromagnetic particles with low remanence magnetization are a promising candidate for achieving reversible MR effect since the residual magnetization in particles can disturb the control process of the MR effect in real time. Carbonyl iron particles (CIP) with the average size of $5\mu\text{m}$ are the most common type of fillers that have been most widely used for MRE fabrication in the recent years. Additionally, nano-sized irregularly shaped (about $200\mu\text{m}$ diameter) particles such as magnetite have been utilized in MRE fabrication. Different types of matrix materials have been used for MRE fabrication such as

silicone rubber, natural rubber, thermoplastic elastomers, and polyurethane. Soft Silicone rubbers are the most common matrix material. Furthermore, additives are generally used to increase the fluidity of the matrix [17]. Silicone oil is the most common additive in MRE fabrication, which works as a diluting agent and decreases the modulus of elastomeric matrix. Additives also prevent the agglomeration of ferromagnetic particles and increase the compatibility of the matrix with the particles [18]. Such added ingredients thus help achieve more uniform distribution of internal stress in the material, which makes the material properties more stable [17].

From the fabrication point of view, MREs can be classified into two types: isotropic and anisotropic. If an external magnetic field is applied while the MRE is being cured, some specific anisotropic properties can be achieved. In this case, particles are mixed with the fluid-like polymer but remain locked up within the cross-linked network of the cured elastomer. It has been observed that these chain-like structures make the MRE anisotropic in terms of mechanical, magnetic, electrical and thermal properties [19]. On the other hand, isotropic MREs are cured in the absence of any external magnetic field. The particles thus remain dispersed within the cured elastomer. Figure 1.1 illustrates the procedure of MRE fabrication. Initially, the primary three components (silicone rubber, iron particles and silicone oil), are thoroughly mixed. The mixture is then vacuumed in order to extract the air bubbles. Depending on the MRE type, the mixture is permitted to cure in absence or presence of a Magnetic field. A strong magnetic field, normally up to 1 T, is applied to realize anisotropic properties. While some silicone rubbers can be cured at room temperature, a constant temperature generally above 100 °C has been suggested to speed up the curing process.

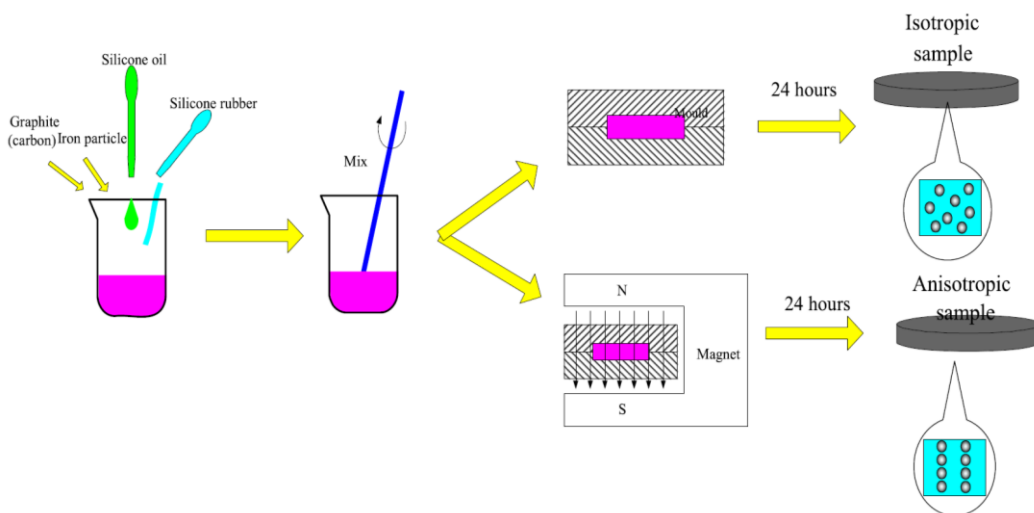


Figure 1.1: MRE fabrication process [20].

The MR effect of MREs can be realized in three fundamental modes: shear mode, squeeze mode and field-active mode, as illustrated in figure 1.2 [17]. The field-active mode is related to the magnetostriction property of the MRE that causes changes in shape or dimensions of the MRE during the process of magnetization [21]. Various types of actuators are designed based on this operational mode of the MRE [8]. The MREs employed in vibration absorbers [6, 22-30], vibration mounts [31] and vibration isolators [2, 5, 32-34] may operate in either the squeeze mode or the shear mode.

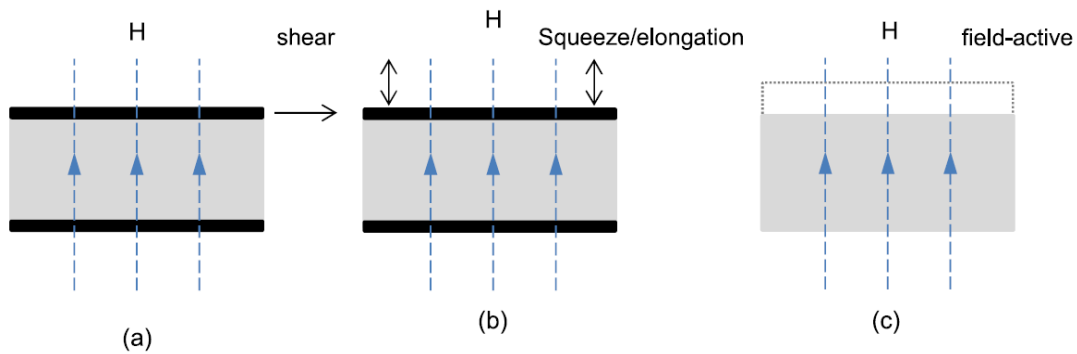


Figure 1.2: Operational modes of MREs: (a) shear mode; (b) squeeze mode; and (c) field-active mode [17].

1.2.2 Applications of MREs

MREs exhibit variable stiffness and damping properties when subjected to a magnetic field. MREs are thus considered as ideal for developing controllable vibration absorbers, vibration isolators and smart sandwich structures. Tuned Vibration Absorber (TVA) based on MRE is one of the applications that has attracted a significant attention in the recent years. Ginder et al. [29] first proposed a design of a tuned vibration absorber using the MREs, where the absorber frequency could vary from 500 to 610 Hz under the application of 560 mT magnetic field intensity. Similarly, Deng et al. [27] developed an adaptive tuned vibration absorber with frequency shift capability of 45% under the application of 900 mT flux. Deng and Gong [26] further proposed an alternate compact design of a tuned vibration absorber without the additional oscillator, which revealed variations in the natural frequency from 27.5 to 40Hz. Dong et al. [28] proposed a novel configuration of an adaptive TVA shown in Figure 1.3 (d), where the motion of the piston causes the shear deformation in the MRE. The magnetic field applied perpendicular to the motion of the piston provided controllable variations in the shear modulus of the MRE and thereby the elastic

force of the absorber. The schematic diagrams of all the above mentioned adaptive TVAs are shown in Figure 1.3.

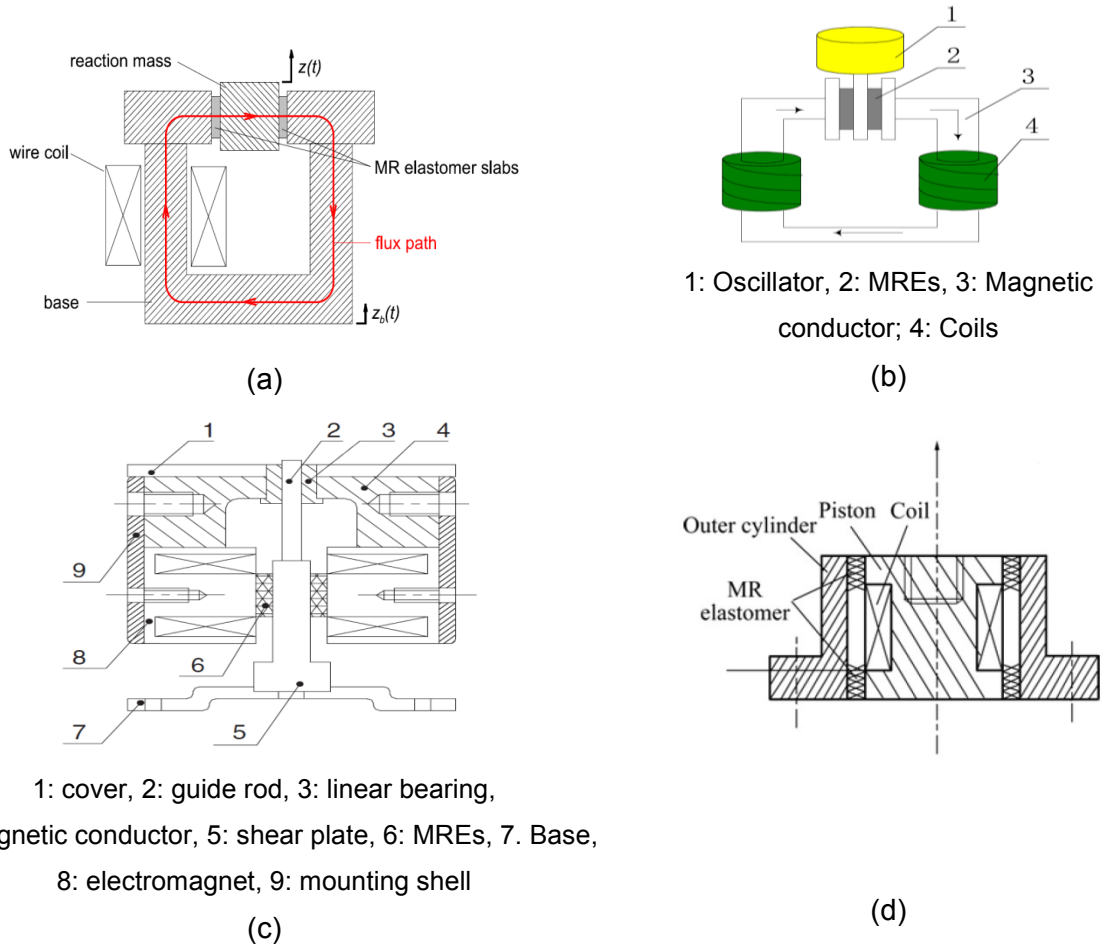


Figure 1.3: Different configurations of the Adaptive tuned vibration absorbers based on MR, proposed by: (a) Ginder et al. [29]; (b) Deng et al. [27]; (c) Deng and Gong [26]; and (d) Dong et al. [28].

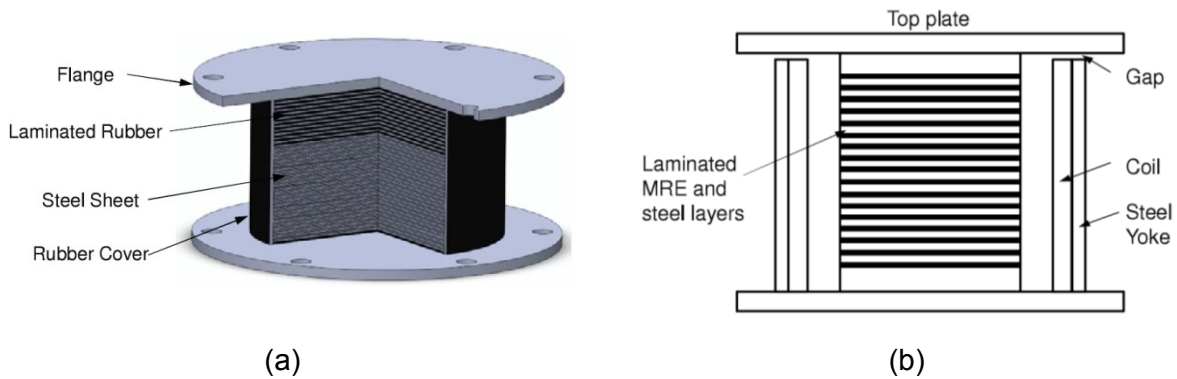


Figure 1.4: (a) Typical laminated rubber bearing/isolator and (b) Cross-section of the MRE base isolator by Li et al. [33].

Multilayered base isolators based on MREs are another promising application of the MREs, which has attracted the attention of many researchers in the last few years. The laminated structure of the traditional passive base isolator consists of two steel endplates and a number of sandwiched thin steel and rubber layers, shown in Figure 1.4 (a). MREs are incorporated in this type of design to overcome the drawbacks of the traditional base isolator originating from its inherent passive feature. As an example, the structural design of a new MRE base isolator proposed by Li et al. [33] is shown in Figure 1.4 (b). The isolator consists of 26 layers of 1 mm thick steel sheets and 25 layers of 1 mm thick MRE sheets. The laminated structure is placed inside a solenoid, which provides uniform magnetic field through the MRE layers. The laboratory measurements of the proposed isolator showed remarkable adaptive capability with nearly 1473% gain in the force and 1630% increase in stiffness, when the applied current changed from 0 to 3 A.

1.3 Fabrication of MREs

The reported studies have employed similar methods for fabrication of MREs, while these have applied different matrix, ferromagnetic particles and additive materials. A few studies have also investigated the factors affecting the properties of MRE such as content and size of ferromagnetic particles, and elastic property of the matrix material. The reported fabrication methods and the factors affecting the properties of the MREs are briefly described in the following subsections.

1.3.1 Fabrication methods

In 1996, Jolly et al. [15, 16] fabricated the MRE samples in three different volume fractions 10, 20 and 30% of iron particles with the mean diameter in the 3-4 μm range. The mixture was permitted to cure for one hour at 140°C, followed by two hours of post curing at 165°C in the presence of a magnetic field ($0.8 \times 10^6 \text{ A/m}$). The reported studies in the subsequent years (until 1999) generally employed similar soft silicone rubbers or gels [15, 16, 35]. Ginder et al. [36] employed natural rubber, a relatively stiffer matrix material. In these studies, the MRE samples were manufactured in the presence of a magnetic field. Lokander and Stenberg [37] suggested that curing with a magnetic field may pose some challenges. The study reported manufacturing of MR solids made from four different nitrile rubbers with dissimilar acrylonitrile (ACN) contents. They utilized two different polarizable particles: a) large and irregular shaped pure iron particles in three different sizes (60 μm , 180 μm and 200 μm); and b) spherical carbonyl iron powder with

particles of size ranging from 3.9 to 5 μm . Sulphur were used to facilitate vulcanization of the rubber, which resulted in modifying of the polymer by forming cross-links (bridges) between individual polymer chains. All materials were vulcanized at 150°C for 30 minutes under pressure of approximately 12 MPa. Gong et al. [38] fabricated MRE samples without applying an external magnetic field in the curing process. The samples used spherical carbonyl iron particles (CIPs) with mean diameter in the range of 3 μm . The CIPs were immersed in silicone oil with viscosity of 0.1 PaS and the blend was mixed with RTV room temperature vulcanized silicone rubber. The ingredients were stirred for 5 minutes and placed at room temperature in a vacuum chamber to remove the air bubbles. The mixture was subsequently cured for 24 hours at room temperature in an open mold without applying any magnetic field. The study fabricated 8 different samples with varying percentages of CIPs, silicone oil and silicone rubber. Table 1.1 summarizes the compositions of different samples manufactured in their work.

Table 1.1: Composition of different samples fabricated by gong et al. [38].

Sample No.	CIPs (mass %)	Silicone oil (mass %)	Silicone rubber (mass %)	Sample No.	CIPs (mass %)	Silicone oil (mass %)	Silicone rubber (mass %)
1	60	0	40	5	20	20	60
2	60	10	30	6	40	20	40
3	60	20	20	7	60	20	20
4	60	30	10	8	70	20	10

During the past two decades, the studies have reported MRE fabrication procedure with varying CIP fractions and different matrix materials. Table 1.2 summarizes the different matrix materials, CIP fractions and particle size used in the reported studies in a chronological order. Following are deduced from the review of these studies:

- The blend of silicone rubber and silicone oil is the most commonly used matrix compound;
- CIPs are the most commonly used as the polarizable particles with an average size ranging from 1 to 10 μm ;
- The isotropic MREs have become the widespread type of MRE since these do not require magnetic field during the curing process.

Table 1.2: A summary of constituents of the reported fabricated MRE samples.

Researcher	Matrix	Particles	Particle content	Type of MRE
Shiga [35], 1995	Silicone Gel	Iron (100 μ m)	Up to 28 Vol%	Anisotropic
Jolly et al. [16], 1996	Silicone oil	CIP (3-4 μ m)	10 to 30 Vol%	Anisotropic
Ginder et al. [21], 2000	Natural Rubber	CIP (1-3 μ m)	30 to 45 Vol%	Anisotropic
Bellan et al. [39], 2002	Silicone rubber; Silicone oil	CIP (2 μ m) Nickel particles	5 to 25 Vol%	Anisotropic
Lokander et al. [37], 2003	Nitrile rubbers acrylonitrile (ACN)	large and irregular shaped pure iron particles (60,180, 200 μ m); and CIP (3.9-5 μ m)	-	Isotropic
Farshad et al. [40], 2004	Silicone rubber	CIP (3.8 μ m)	27 Vol%	Anisotropic
Kallio et al. [1], 2005	Natural rubber Silicone rubber Thermoplastics	CIP (4 μ m); and Irregular iron particles (up to 200 μ m)	-	Anisotropic
Gong et al. [38], 2005	Silicone Rubber; Silicone oil	CIP (3 μ m)	20 to 70 Weight%	Isotropic
Lockette et al. [41], 2006	Silicone rubber	combination of 40 μ m and 10 μ m iron particles	Up to 32 Vol%	Anisotropic
Lerner et al. [22], 2007	Silicone rubber	CIP (6-9 μ m)	Up to 35 Vol%	Anisotropic
Böse et al. [11], 2009	Silicone rubber	CIP (5 μ m) CIP (40 μ m)	0 to 35 Vol%	Isotropic Anisotropic
Li et al. [32], 2013	RTV Silicone Rubber	5 μ m	30 Vol %	Anisotropic
Li et al. [33], 2013	Silicone Rubber; Silicone Oil	CIP (3-5 μ m)	23 Vol%	Isotropic
Agirre-Olabide et al. [42], 2014	Silicone rubber; Vulcanizer	CIP (1.25 \pm 0.55 μ m)	10 to 30 Vol%	Isotropic Anisotropic
Sun et al. [24, 25, 30], 2015	Silicone Rubber; Silicone oil	CIP (3-5 μ m)	75 to 80 weight %	Isotropic
Norouzi et al. [4], 2015	Silicone rubber; Silicone oil	CIP (3-5 μ m)	70 Weight%	Isotropic
Yu et al. [34], 2016	Silicone rubber; Silicone Rubber	CIP (3-5 μ m)	23 Vol%	Isotropic
Vatandoost et al. [18], 2017	Silicone rubber; Silicone oil	CIP (3-5 μ m)	70 Weight%	Isotropic

1.3.2 Factors affecting properties of MREs

The behavior of a MRE in the absence of the magnetic field is basically determined by the characteristics of the composite material. Under the application of an external magnetic field, the forced developed between the polarizable particles affect the viscoelastic properties of the MR elastomer, which may be influenced by the fabrication-related factors. The studied have mostly reported the effect of the matrix material and the polarizable particles on the properties of MREs. For the purpose of quantifying the effects of these factors, the rheology of the MRE is often defined in term of the magnetorheological (MR) effect. The MR effect has been defined as the absolute or relative change in the shear modulus of a MRE under application of a magnetic field [37]. The absolute MR effect is the difference between the maximum value of the shear modulus G_{max} achieved under a magnetic field, and that obtained without a magnetic field G_0 . The absolute MR effect is thus expressed by change in shear modulus, ΔG , as:

$$\Delta G = G_{max} - G_0 \quad (1.1)$$

The relative MR effect, ΔG_r , is the ratio of the absolute MR effect to modulus G_0 , which generally expressed by the percent change, as:

$$\Delta G_r = \frac{\Delta G}{G_0} \times 100\% \quad (1.2)$$

Various types of matrix materials such as natural and synthetic rubber, silicone rubber, polyurethane, thermoplastic and polyvinyl alcohol have been used in the MREs. Apart from the rheological properties, the magnetic permeability of the matrix material is the most significant factor that influences the mechanical properties of the MRE. The magnetic permeability of the matrix must be as low as possible; since the matrix material magnetization could adversely affect polarization of the particles and thereby the MR effect. Fabricating the MRE with magnetically active fillers could also decrease the MR effect [37, 43]. Lokander and Stenberg [37, 44] reported that the absolute MR effect is independent of the matrix material, while the relative MR effect depends on the stiffness. A low stiffness matrix showed higher relative MR effect, while the zero field modulus and thus the stiffness of the matrix could be decreased by adding plasticizers or softer matrix materials [44].

Compared to the MR fluids, relatively larger sizes of polarizable particles could be used in MREs since the particles sedimentation is not a concern on MREs [19]. The reported studies have

employed widely different sizes of CIP, ranging from 1 μ m to 200 μ m. In order to achieve a higher MR effect, the particles must be large enough to support at least several magnetic domains.

Böse et al. [11] investigated the viscoelastic properties of isotropic and anisotropic MRE composites containing various concentrations of iron particles ranging from 0% to 35% volume fraction in two different sizes (5 μ m and 40 μ m) blended in the silicone rubber matrix. The isotropic MRE samples with larger iron particles showed considerably higher increases in the storage and the loss moduli when compared to those of the MRE with smaller particles. Furthermore, the zero field moduli of the samples with even very low particle contents was observed to be lower than the storage modulus of the pure silicone rubber samples without the iron particles. This suggests that the crosslinking of the silicone is affected by the particle size and increasing the particle size yields reduced elasticity of the MRE [11]. It has been shown that the anisotropic MREs with small size particles can provide higher storage modulus similar to the isotropic MRE with larger size particles but with significantly higher zero field modulus.

The “apparent density” of the iron powder is much less than the density of solid iron particles, which is due to the air entrapped between the iron particles. In case of MREs, the air gap between the particles is filled by rubber. When the rubber is filled with a critical amount of iron particles, the particles are in physical contact with each other [44]. At particle concentrations close to the critical, the distances between the particles cannot be decreased, which contributes to the relatively higher stiffness of the composite. The MREs thus exhibit the maximum relative MR effect around the critical concentration [37].

In order to achieve substantial MR effect from an isotropic MRE, the iron particle concentration has to be close to the critical particle volume concentration (CPVC), where the inter-particle distances are minimal. The pre-cure orientation of the particles in this case will not affect the absolute MR effect [44]. However, the composite with such high iron particle concentrations exhibit high zero-field modulus, thus which yield low relative MR effect. The softening of the matrix thus constitutes one of the challenges in MRE fabrication in order to achieve higher relative MR effect.

1.4 Mechanical properties of MREs

The MREs are viscoelastic materials similar to polymers and polymer-based composites, MREs can be characterized by viscoelastic properties. Viscoelastic materials combine the features of elastic solids and viscous liquids, and their mechanical behavior lies between that of

an ideal solid described by Hooke's law, and the Newtonian fluid, defined by Newton's law of viscosity. For an ideal solid the stress is directly proportional to the strain and independent of strain rate, while for a viscous liquid stress is proportional to the strain rate. Viscoelastic materials behave more like an elastic material under rapid change in the applied deformation, and like a Newtonian fluid under slow deformations [45].

1.4.1 Methods of characterization

Reported studies have employed widely different methods and experimental conditions for characterizing the mechanical properties of MREs. The studies may be classified into two groups. The first group of studies aimed at characterization of MRE samples alone [1, 3, 4, 11, 12, 18, 20, 21, 35-40, 46-49], while the second group of studies focused on characterization of MRE-based devices such as vibration absorber and isolators [3, 6, 18, 23-25, 27, 28, 30, 32-34, 50]. The studies involving experimental characterization may be further categorized into two groups based on the deformation mode: a) uniaxial tension or compression; b) simple shear. The majority of the studies, however, have focused on the MRE operating in the shear mode. Lokander et al. [37, 44, 48] evaluated the MR effect by measuring the dynamic shear modulus with and without an applied magnetic field of double lap shear specimen, using the Instron 8032 dynamic testing machine equipped with an electromagnet, as shown in Figure 1.5. The MRE specimens were approximately $50 \times 15 \times 2 \text{ mm}^3$, which were sandwiched between the brass and steel plates. The composites were fixed to the plates with a special adhesive, Mega Bond Plus. The strain amplitude was 2.5 % at 1 Hz, which was decreased with increasing frequency, down to 0.6 % at 21 Hz. It was shown that the steel plates could induce relatively stronger magnetic field through the MRE samples. The behavior of a relatively thick MRE was experimentally investigated by Gordaninejad et al. [12] using a lap-shear experimental setup shown in Figure 1.6. In the experiment, the MRE specimens ($22.45 \times 12.70 \text{ mm}^2$) with four different thicknesses ranging from 6.35 to 25.40 mm were sandwiched between three thin steel bars. Shear force was applied on the MRE samples by pushing the central steel bar. The study concluded that the shear modulus is independent of the sample thickness. Norouzi et al. [4] designed an alternate test fixture to perform double lap shear tests on MREs (Figure 1.7). The fixture consisted of two steel plates that were fixed together with specific distance between them using four stainless steel screws and bushings. The MRE layers with dimensions of $50 \times 12 \times 9.5 \text{ mm}^3$ were sandwiched between the three steel plates, while permanent magnets were used to apply magnetic field perpendicular to the shear direction. The field intensity was changing by varying the number of magnets. The MRE samples were subject to different strain amplitudes ranging from 2-16%, and frequencies

(0.1, 0.3, 0.5, 1, 3, 5 and 8 Hz) using a servo-hydraulic material testing machine. Different magnetic field intensities (100, 180, 230, and 272 mT) were considered and data were acquired to determine the field-, frequency- and displacement-dependency of the MRE properties.

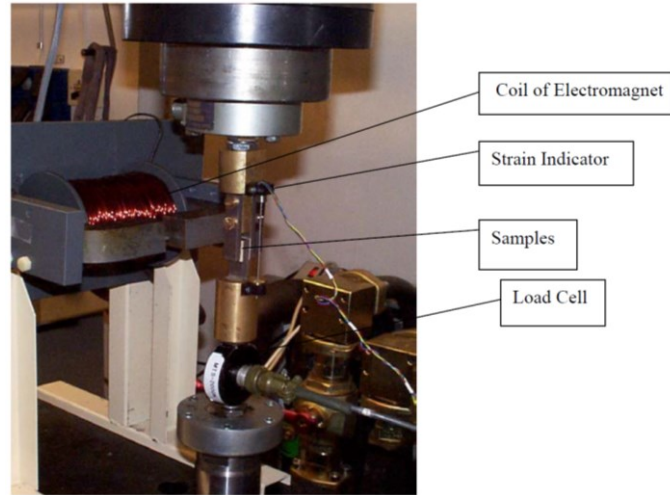
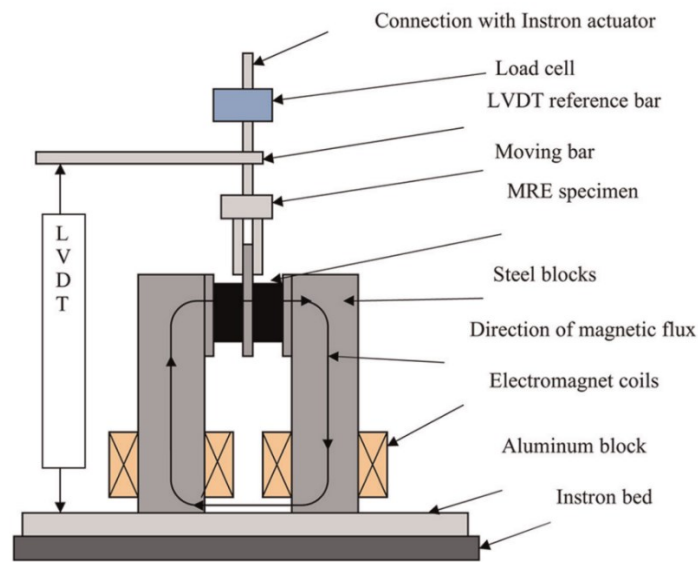
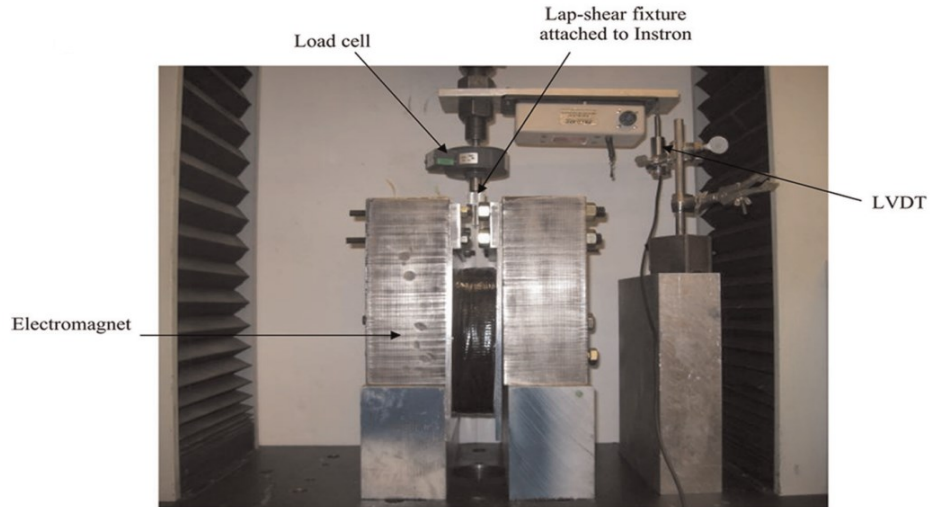


Figure 1.5: Experimental setup designed by Lokander et al. [48] for measurement of MR effect in the shear mode.



(a)



(b)

Figure 1.6: (a) Schematic of the double lap-shear test setup; and (b) experimental setup for double lap-shear testing designed by Gordaninejad et al. [12] (LVDT: linear variable differential transformer).

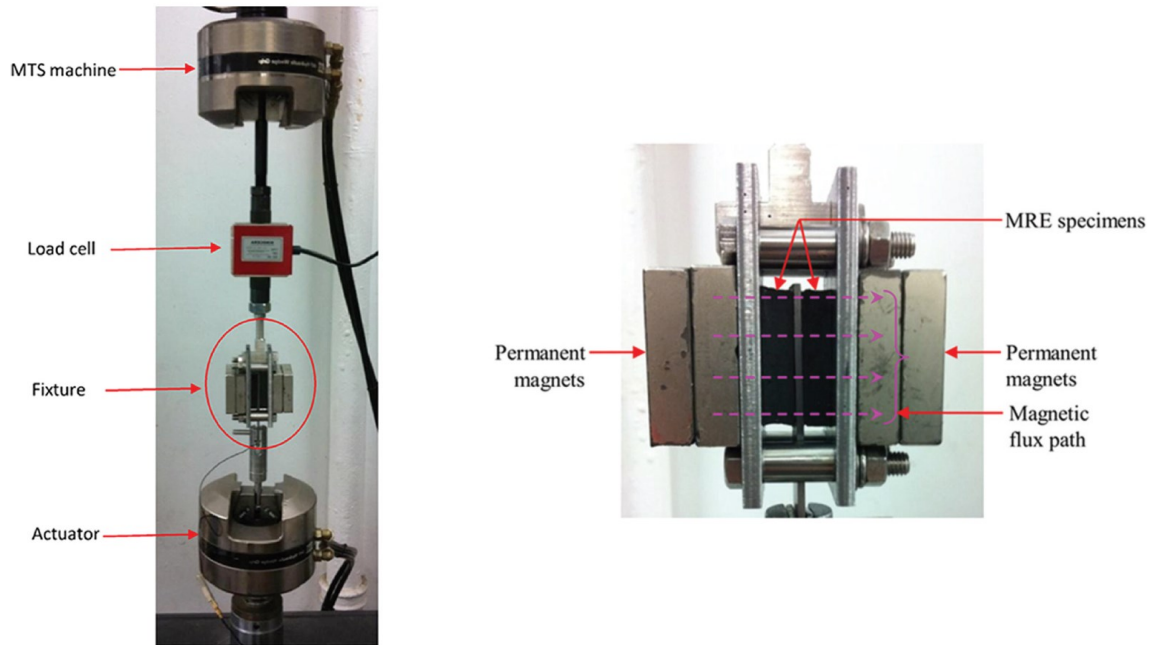


Figure 1.7: Experimental setup employed for characterizations of the MRE specimens with permanent magnets by Norouzi et al. [4].

A number of studies have concentrated on characterization of adaptive devices integrating the MREs [3, 6, 18, 23-25, 27, 28, 30, 32-34, 50]. Yu et al. [34] prototyped a MRE base isolator consisting of 25 layers of 1mm thick MRE sheets and 25 layers of steel plates. An electromagnet was positioned around the layered isolator to generate a uniform magnetic field, and the isolator was subject to horizontal quasi-static and dynamic displacement excitations, as shown in Figure 1.8. The dynamic characterization was performed under sinusoidal excitations of three different amplitudes (2, 4 and 8mm) at four different frequencies (0.1, 1, 2 and 4 Hz) and magnetic field intensities ranging from 0 to 500 mT.

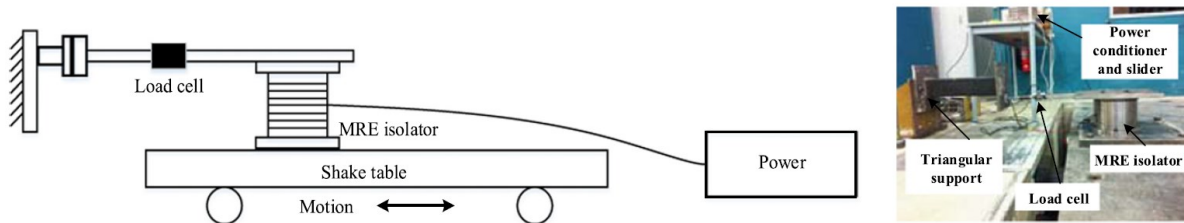


Figure 1.8: Schematic diagram and experiment setup designed by Yu et al. [34] for characterization of a multi-layered MRE vibration isolator.

1.4.2 Static properties of MREs

Effects of magnetic field on the static properties of MREs can be evaluated by measuring the strain-stress or force-displacement properties of a sample in the presence or absence of an external magnetic field. Figure 1.9 illustrates the strain-stress curve of a typical MRE at different magnetic field intensities, ranging from 0 mT to 440 mT [20]. The slope of the stress-strain curve represents the shear modulus of the MRE. The results suggest that the shear modulus of the MRE increases when the magnetic flux is enhanced. The relationship between the shear stress and shear strain may be considered linear up to about 10% strain, which suggests that the composite behaves like a linear viscoelastic material in this strain range. The shear modulus, however, tends to either saturate or decrease under higher strain amplitude [20]. In another study, Li et al. [32] reported the stress-strain behavior of a large capacity MRE-based adaptive seismic isolator suitable for civil engineering applications (Figure 1.10). The measured properties revealed nearly linear viscoelastic behavior of the MRE isolator up to 20% shear strain, while the shear modulus of the isolator increased with increasing magnetic field intensity.

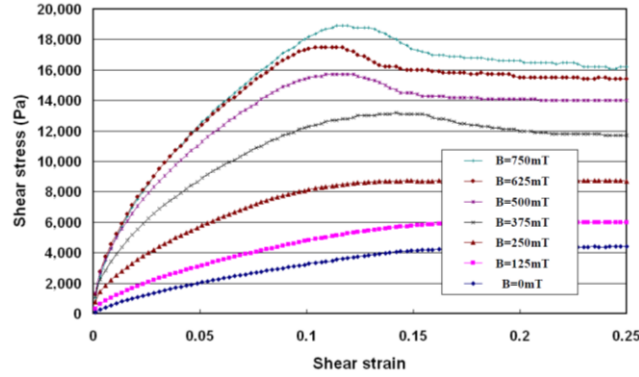


Figure 1.9: Shear stress versus shear strain of a MRE sample under different magnetic fields [20].

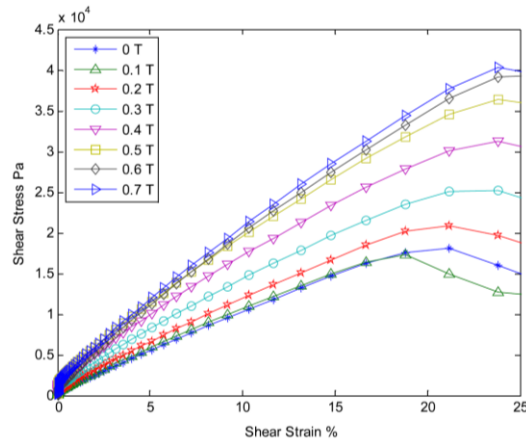


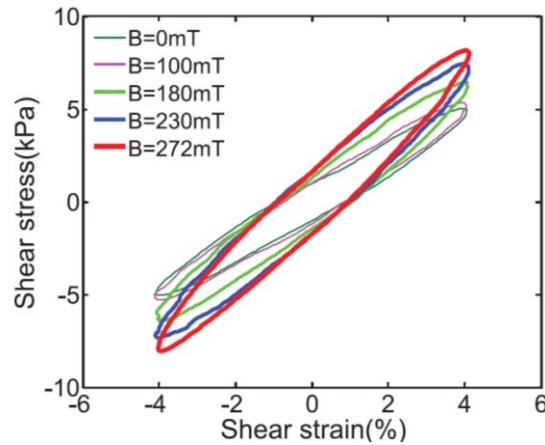
Figure 1.10: Shear stress - shear strain characteristics of a large capacity MRE-based seismic isolator [32].

1.4.3 Dynamic properties of MREs

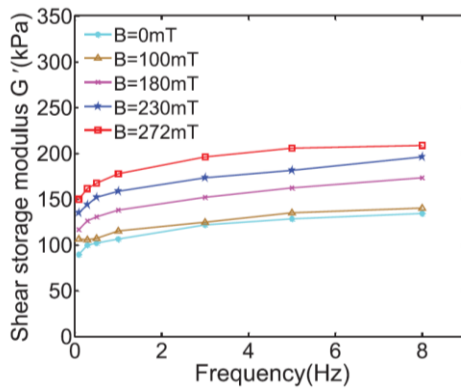
A number of studies have experimentally investigated dynamic properties of the MREs in terms of storage modulus, loss factor and hysteresis in the stress-strain curves under different loading and magnetic field intensities. These have generally focused on characterization of the effects of magnetic field intensity, loading frequency and loading amplitude on the MRE dynamic properties of the MREs.

Norouzi et al. [4] investigated the dynamic behavior of MRE in simple shear mode under different harmonic excitations. The stress-strain responses of the MRE revealed strong dependence on the strain amplitude, strain rate and magnetic field intensity. An increase in the magnetic flux resulting in increase in the slope of the curve (stiffness) and enclosed area of the hysteresis loops (Figure 1.11(a)). The shear storage modulus also increased nearly quadratically

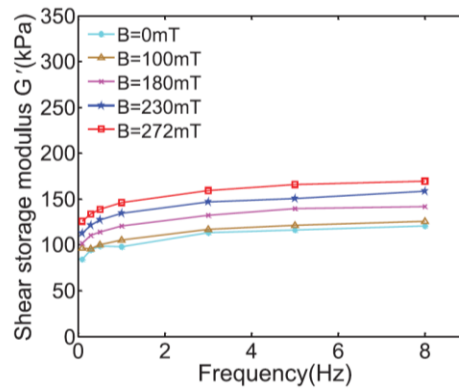
with the magnetic flux, irrespective of the shear strain amplitude and frequency, as seen in Figure 1.11 (b) and 1.11 (c) for 4% and 16% shear strains, respectively. The study concluded that the loss factor increases almost linearly with the magnetic flux density and this increment was more obvious under large shear strains (Figure 1.12). Yu et al. [34] reported similar dynamic characteristics of a MRE-based isolator. Both the slope and the width of the hysteresis loops in the stress-strain curve increased with increasing flux density.



(a)



(b)



(c)

Figure 1.11: (a) shear stress-strain responses of the MRE under different magnetic field intensities ($\gamma = 4\%$); (b) variations in the shear storage modulus with frequency ($\gamma = 4\%$); and (c) variations in the shear storage modulus with frequency ($\gamma = 16\%$) [4].

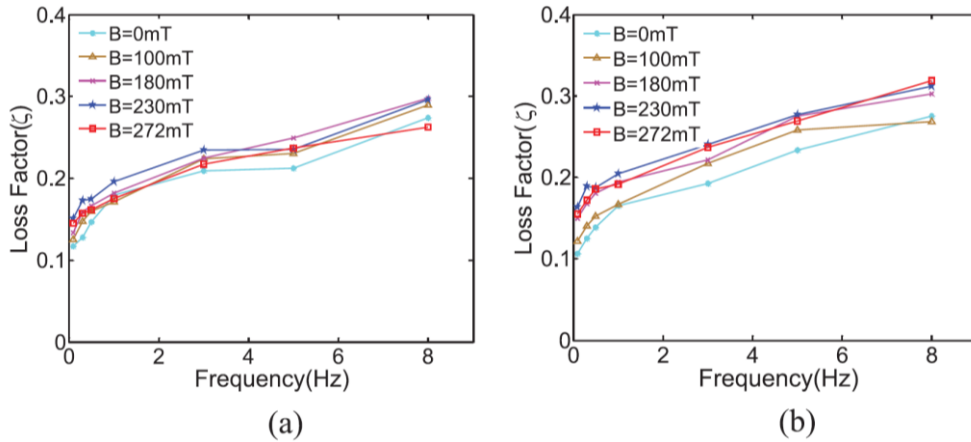


Figure 1.12: Loss factor versus frequency for different magnetic flux densities: (a) $\gamma = 4\%$ and (b) $\gamma = 16\%$ [4].

Lokander et al. [48] conducted a comprehensive experimental study to characterize the influence of excitation frequency on the MR effect over a broad range of excitation frequencies. It was shown that the absolute and relative MR effects increase considerably with increasing frequency and approach saturation above 800 Hz and 500 Hz, respectively (Figure 1.13). The MR effect also increased with the magnetic flux intensity, as reported in [4], while a magnetic saturation was observed at about 0.5 T. The loss factor, however, was observed to be independent of both the frequency and the applied magnetic field (Figure 1.14), contrary to the trend reported in [4] for low frequency excitations. The loss angle ($\tan \delta$) increased only slightly in the low frequency range (1-21 Hz) when the field intensity was increased (Figure 1.15), as reported by Jolly et al. [15].

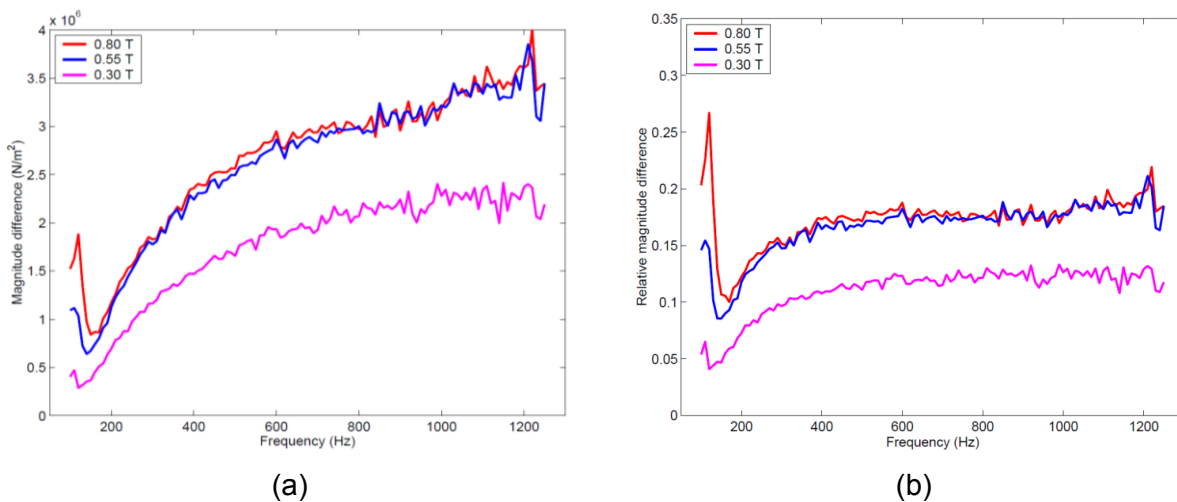


Figure 1.13: (a) Absolute and (b) relative MR effect versus frequency at high frequencies ranging from 100 to 1250 Hz with different applied magnetic fields [48].

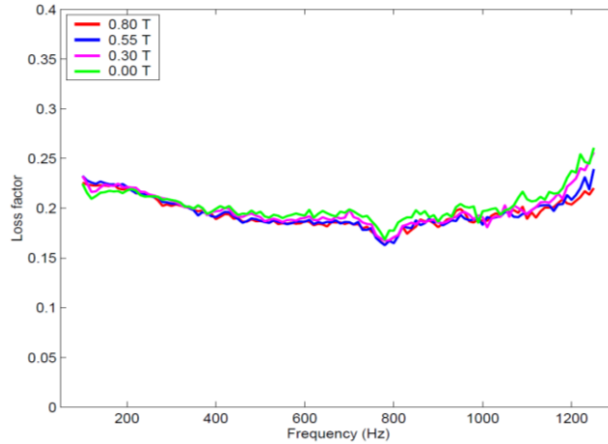


Figure 1.14: Loss factor versus frequency under higher frequency excitations, ranging from 100 to 1250 Hz under different magnetic fields intensities [48].

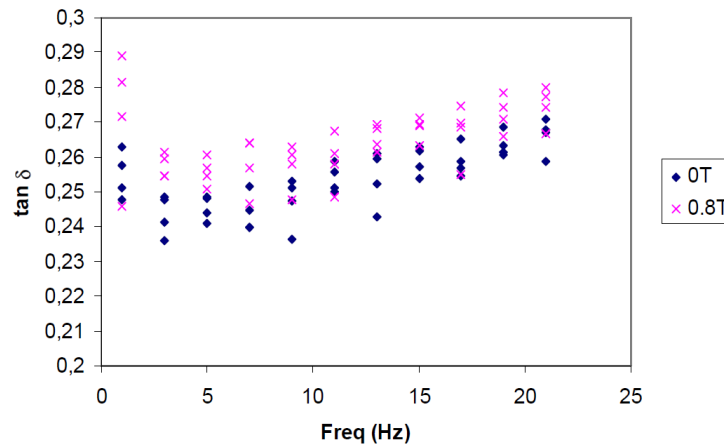


Figure 1.15: Variations in the loss angle ($\tan \delta$) in the lower frequency range (1 to 21 Hz) under different magnetic field intensities [48].

Norouzi et al. [4] further investigated frequency dependency of the MRE dynamic behavior measured in terms of the shear stress - shear strain hysteresis loops. The measured data were used to assess change in the stiffness and the dissipated energy per cycle as a function of excitation frequency. Both the slope (stiffness) and dissipated energy increased with increasing frequency up to 8 Hz (Figure 1.16). The modulus also increased nearly linearly with increasing frequency beyond 1 Hz. Similar tendency of the shear modulus was also reported in earlier studies by Gong et al. [38], Kallio et al. [51] Lokander et al. [37] Norouzi et al. [52]. Similar to the shear modulus, a positive linear relationship was also observed between the shear loss and the frequency.

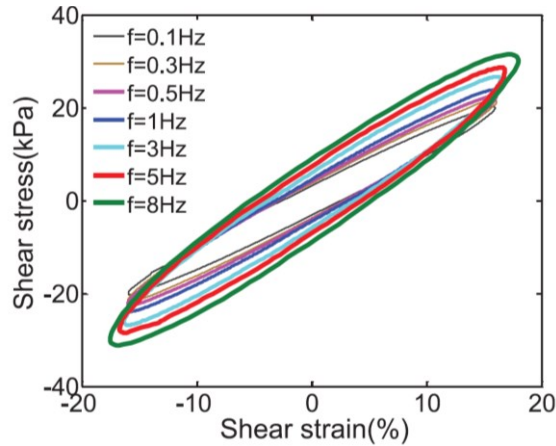


Figure 1.16: Shear strain- shear stress hysteresis loops obtained at different frequencies with 16% strain and magnetic flux density of 272 mT [4].

The measured shear stress – shear strain characteristics show viscoelastic property of the MREs similar to rubbers, often referred to as the Fletcher-Gent effect [52] or the Payne effect [53]. This effect is perceived under cyclic loading conditions with small strain amplitudes and is manifest as a dependence of the storage modulus on the amplitude of applied strain. For rubbers, the storage modulus decreases rapidly with increase in the strain amplitude above 0.1% and approaches its lower bound at strains exceeding 20%. Physically, the Payne effect is caused by the deformation-induced changes in the material's microstructure, i.e. breakage and recovery of weak physical bonds linking adjacent filler clusters [52, 53]. In case of MREs, increasing the strain amplitude leads to higher distances between the ferromagnetic particles, which results in decrease in the magnetic force between the polarizable particles and thereby intensifies the shear modulus decrement. Norouzi et al. [4] investigated the effect of the amplitude of applied dynamic loading on the shear modulus and loss factor of the MREs under different intensities of the magnetic field. Figures 1.17 and 1.18 show the effect of strain on shear modulus and loss factor of MREs under different applied magnetic field intensities. These results presented for 0.1 and 3 Hz deformations suggest that the shear modulus decreases with increase in the shear strain at both the frequencies. As expected, the reduction in shear modulus is more notable under higher magnetic field intensities. The study further concluded that the loss factor is independent of the strain level.

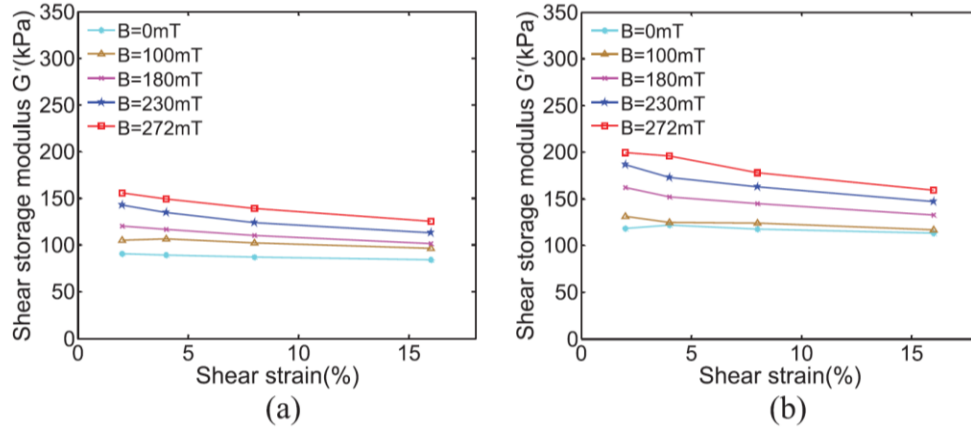


Figure 1.17: Variations in the storage modulus with shear strain applied at different frequencies under different magnetic flux intensities: (a) $f = 0.1$ Hz; and (b) $f = 3$ Hz [4].

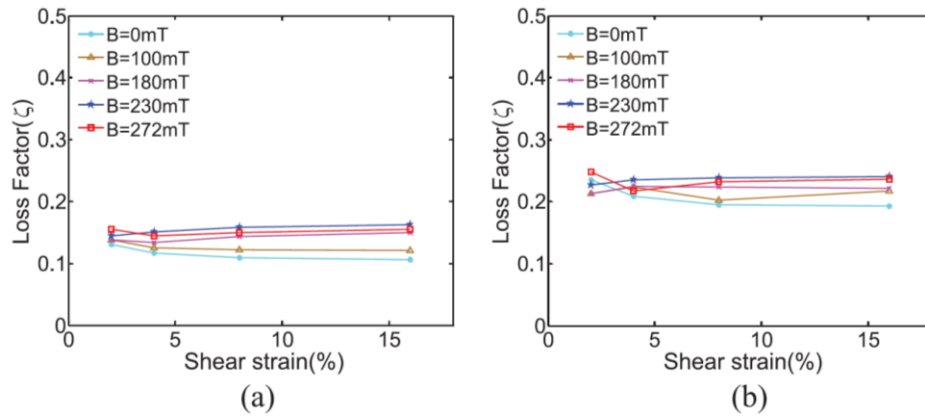


Figure 1.18: Variations in the loss factor with shear strain applied at different frequencies under different magnetic flux intensities: (a) $f = 0.1$ Hz; and (b) $f = 3$ Hz [4].

1.5 Models for predicting dynamic behavior of MREs

A number of studies have proposed models for predicting properties and dynamic responses of MREs and MRE-based devices. The reported modeling efforts address two different viewpoints; micro and macro aspects of the MREs [4]. The models focusing on the micro aspect are generally physic-based models, which may be further classified into two different branches. The first type of modeling is based on the continuum mechanics theory, employing finite strain theory to study the coupled mechanical and magnetic behavior of MREs. The effect of shape, orientation, distribution, chain-like structures and the size of ferromagnetic particles on the stress components is typically considered in this type of modeling [46, 54]. The second branch of physics-based models focuses on studying the field dependency of MRE modulus as well as MR

effect, which is based on exploring the interaction of dipole ferromagnetic particles. The reported models, invariably, employ simplifying assumptions with regard to the local strain and magnetic field [10, 55]. The macro aspects of MREs are dealt in models focusing on properties of the MREs. These are also known as phenomenological models aimed at predictions of force-displacement or stress-strain relationships for the MRE-based mechanisms [4]. Such model are known to be effective in predicting properties of specific MRE or MRE-device, while the physical aspects of MRE are ignored [56]. The reported studies have mostly described the phenomenological models using polynomial functions [4, 18] or Bouc-Wen formulation [2, 3].

Owing to the viscoelastic nature, the MREs exhibit hysteresis-like stress-strain characteristics. The stress-strain or force-displacement hysteresis strongly depends on the input frequency, strain amplitude as well as applied magnetic field intensity [2, 18, 57]. The reported physic-based models [10, 55] are generally independent of the strain rate, and do not yield accurate predictions of dynamic properties of MREs over ranges of strain amplitudes and frequencies. Furthermore, the generalization of a physics-based models for application to different MREs has not yet been proven [56]. A number of phenomenological models have been proposed for predicting hysteresis effect in the MREs [2-4, 18, 33, 34, 47, 57-59]. These are mostly based on differential equation-based Bouc-Wen formulations. Alternatively, operator-based phenomenological models such as Prandtl-Ishlinskii and Preisach models, have been widely reported for modeling of hysteresis in smart material actuators employing piezoceramics, magnetostrictive materials and smart memory alloys [56, 60, 61]. These have provided reasonably accurate predictions of the hysteresis behavior over wide ranges of amplitudes and rates of the applied input. Such operator-based models, however, have not yet been attempted for characterizing hysteretic stress-strain properties of the MREs. The reported models are briefly summarized in the following subsections.

1.5.1 Differential equation-based phenomenological models

A number of differential equation-based phenomenological models have been proposed to characterize the hysteresis effects of the MREs in the shear mode [2-4, 34, 47, 57, 59]. One of the most well-known models in modeling the hysteresis nonlinearities is the Bouc-Wen model introduced by Wen [62] in 1976. Yang et al. [3] proposed a model consisting of a Bouc-Wen component for describing hysteresis in parallel with a Voigt element for the solid-material behavior of a seismic isolator (Figure 1.19 (a)). The Bouc-Wen component is generally defined with an evolutionary variable z , which represents a function of the time history of the displacement. The

isolator integrated a MRE in the shear mode. The force obtained from the mode was expressed as:

$$F = \alpha K_0 x + (1 - \alpha) K_0 z + C_0 \dot{x} \quad (1.3)$$

Where z is the evolutionary variable, given by:

$$\dot{z} = A\dot{x} - \beta|\dot{x}||z|^{n-1}z - \gamma\dot{x}|z|^n \quad (1.4)$$

In the above relations, K_0 is the stiffness coefficient and C_0 represents the viscous coefficient indicating the damping capacity of the system. A, n, β and γ are non-dimensional parameters related to the shape and the size of the hysteresis loops. The predicted peak force was most sensitive to parameter A , while constant n was recognized to control the transition from linear to the nonlinear range. The study further established linear dependence of parameters A, α, C_0 and K_0 on the applied current. The model involved identification of 10 different from the measured data and was designed to predict the dynamic behavior under strain amplitude range 8 – 32 % in the 0.1 – 4 Hz range. Behrooz et al. [2] modified the Bouc–Wen model by introducing a standard three-element solid model (Figure 1.19 (b)) for predicting the behavior of a variable damping and stiffness isolator employed a MRE in the shear mode. The model involved 9 different parameters similar to that proposed by Yang et al. [3], and showed applicability in the strain amplitude range of 8-32% at a single frequency of 0.1 Hz. Identification of relatively large number of parameters from the measured data, however, may impose considerable computational demand. Apart from this, the strain and magnetic field dependency of the parameters could not be described.

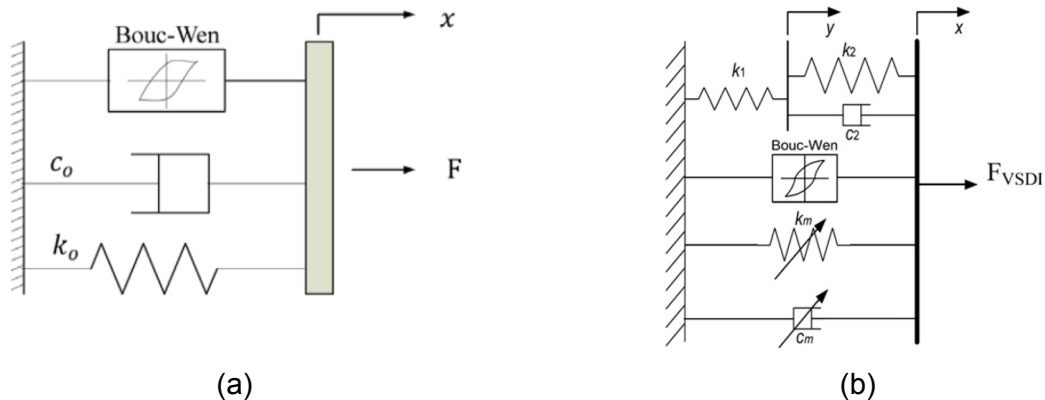


Figure 1.19: Schematic diagram of the phenomenological models incorporating Bouc–Wen element (a) in parallel with a Voigt element proposed by Yang et al. [3] for a seismic isolator; (b) proposed by Behrooz et al. [2] for a variable stiffness and damping isolator.

Norouzi et al. [4] generalized the Kelvin-Voigt viscoelastic model to define the MRE stress-strain relationship in the shear mode, as shown in Figure 1.20. The shear stress $\tau(t)$ is the response of the model under a harmonic shear strain input $\gamma(t) = \gamma_0 \sin(2\pi ft)$, was related to both the strain amplitude and the strain rate as:

$$\tau(t) = G(f, \gamma_0, B) \gamma(t) + \eta(f, B) \dot{\gamma}(t) \quad (1.5)$$

Where G is the shear modulus dependent on the frequency f , strain amplitude γ_0 and magnetic field intensity B , η is the viscosity dependent on the frequency and magnetic field intensity. The frequency dependence of the stiffness and damping properties, and strain dependency of the MRE stiffness was represented by a power function, while the damping was shown to have a steady behavior under strain variations. The magnetic field dependency of the MRE stiffness and damping properties was further defined by polynomial functions. Overall, the model involved 10 constants and provided reasonably good predictions of the hysteretic properties of the MRE regardless under variations in the magnetic field intensity (0-272 mT), excitation frequency (0.1-5 Hz) and strain amplitude (0-272 mT). The measured stress-strain hysteresis loops of the MRE, however, revealed nearly perfectly elliptical curves under the entire range of the loading conditions, which suggested nearly linear behavior. These contradicted measured responses reported in vast majority of the studies, which show nonlinear behavior under increasing strain amplitude, frequency or magnetic field intensity [2, 3, 11, 12, 32, 34]. The proposed model thus expected to yield error under strain stiffening or strain softening conditions, which are commonly reported for typical MREs. Yu et al. [34] introduced a strain-stiffening element in parallel with the Kelvin-Voigt model to characterize the nonlinear hysteresis of an MRE-based adaptive base isolator (Figure 1.20 (b)). The hysteresis loops in the stress-strain data for the MRE-based isolator were described using two main features: a) viscoelasticity, b) strain-stiffening. The model force developed by isolator model was expressed as:

$$F = K_0 x + C_0 \dot{x} + \alpha |x| x^3 + F_0 \quad (1.6)$$

Where K_0 , C_0 , α and F_0 are the parameters of the model to be identified using the measured data of the base isolator. The data acquired under strain amplitudes ranging from 8-32% in the 1-4 Hz range, 0-3 amp applied current were considered for identification of the model parameters. The model parameters showed strong dependence on the loading frequency and applied current. The model involving 12 different parameters demonstrated accurate predictions of the hysteresis nonlinearities of the MRE-based isolator over the range of loading conditions considered, while the excitation frequency was limited to a narrow range (1 to 4 Hz).

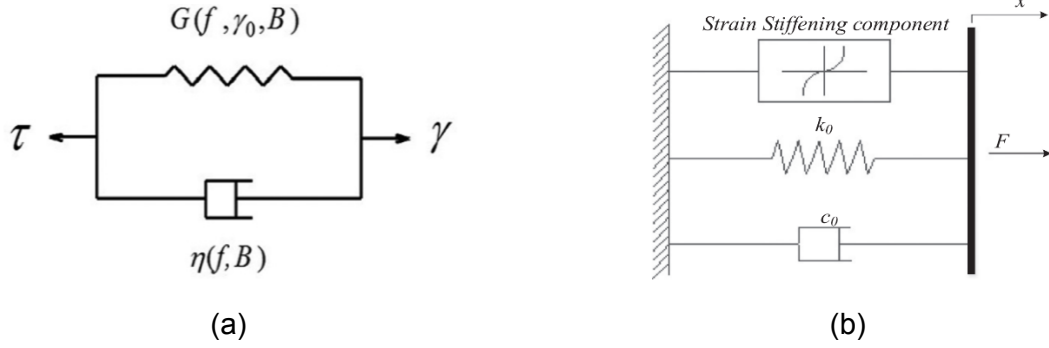


Figure 1.20: (a) Modified viscoelastic Kelvin-Voigt model proposed by Norouzi et al. [4]; and (b) Schematic of the phenomenological model proposed by Yu et al. 2016 [34].

1.5.2 Operator-based phenomenological models

Various Operator-based phenomenological models have been proposed to capture the hysteresis in ferromagnetic materials and smart actuators [61, 63-65]. The key advantage of these models is their suitability for the design of control algorithms. The applicability of such operator-based phenomenological models, however, has not yet been explored for describing the hysteresis nonlinearities in MREs and MRE-based devices. Preisach [66], Prandtl-Ishlinskii [67] and Krasnosel'skii-Pokrovskii [68] have been most commonly used operator-based phenomenological models in modeling the hysteresis phenomena of smart materials actuators, such as piezoceramics, magnetostrictive and smart material alloy micro-positioning devices [56, 60, 61, 69]. It has been reported that the Prandtl-Ishlinskii model, owing to its analytical invertibility, is better suited for design of controllers.

Prandtl-Ishlinskii (PI) model integrates on either play or stop operators continuous hysteresis operators describing the input $v(t)$ and the threshold r . The stop operator was initially proposed to describe the elastic-plastic behavior in continuum mechanics [67]. The input-output descriptions of the play stop and play operators are elucidated in Figure 1.21. In accordance with the Hook's law, the linear stress-strain relationship when the stress is below the yield stress r (denoted as the threshold), is depicted in Figure 1.21 (a). Let the partition $C_m[0, T]$ represents the space of piecewise monotone continuous functions. The output of the stop operator $E_r[v](t)$ for an input $v(t) \in C_m[0, T]$ is expressed as:

$$w(0) = e_r(v(0))$$

$$w(t) = e_r(v(t) - v(t_i) + w(t_i)); t_i \leq t \leq t_{i+1} \text{ and } 0 \leq i \leq N - 1 \quad (1.7)$$

$$E_r[v](t) = w(t)$$

Where $t_0 = 0 < t_1 < \dots < t_N = T$ are the partitions of $[0, T]$, and:

$$e_r(v) = \min(r, \max(-r, v)) \quad (1.8)$$

The play hysteresis operator was first proposed to describe the backlash phenomena that exists in the backlash in a gear mechanism [70]. In this case, input v described the motion of center of a driving gear tooth, while the motion of the mating gear was considered as u . The threshold r represented the backlash. The output of the play operator $F_r[v](t)$ for any input $v(t) \in C_m[0, T]$ is defined as:

$$\begin{aligned} u(0) &= f_r(v(0), 0), \\ u(t) &= f_r(v(t), u(t_i)); t_i \leq t \leq t_{i+1} \text{ and } 0 \leq i \leq N - 1 \\ F_r[v](t) &= u(t) \end{aligned} \quad (1.9)$$

Where $t_0 = 0 < t_1 < \dots < t_N = T$, and:

$$f_r(v, u) = \min(v - r, \min(v + r, u)) \quad (1.10)$$

Where $t_i \in [0, T]$ such that the function v is monotone on each of the sub-intervals $[t_i, t_{i+1}]$. It should be remarked that the play and stop operators are both continuous in space and time [56].

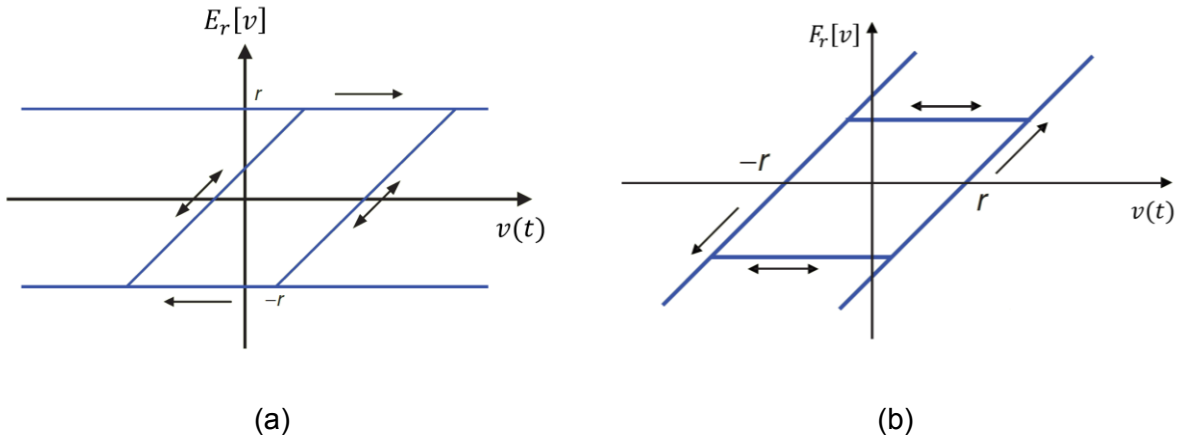


Figure 1.21: The (a) stop and (b) Play Hysteresis operators [70].

Utilizing the stop operator $E_r[v](t)$, the output of the Prandtl-Ishlinskii model is expressed through integration of the operators, as [67]:

$$\Omega[v](t) = \int_0^R p(r)E_r[v](t)dr \quad (1.11)$$

Where $\Omega[v](t)$ is the output of the Prandtl-Ishlinskii model and $p(r)$ is an integrable density function satisfying $p(r) \geq 0$, which is generally identified from the experimental data. The output of Prandtl-Ishlinskii model can also be defined using the play operator $F_r[v](t)$, as [67]:

$$\Pi[v](t) = qv(t) + \int_0^R p(r)F_r[v](t)dr \quad (1.12)$$

Considering the unity slope of the stop and play operators, it can be concluded that under Lipschitz continuous inputs, the outputs of Prandtl-Ishlinskii model in both definitions (1.13) and (1.14) are Lipschitz continuous. The choice of $R = \infty$ as the upper limit of integration is generally used in the literature as a matter of convenience, since the density function $p(r) \geq 0$ vanishes for large values of r .

1.6 Scope and objectives

The overall goal of the dissertation research is to characterize the behavior of MREs with a major focus on their coupled magneto-mechanical properties under wide ranges of strain amplitudes, excitation frequencies and magnetic field intensities. The specific objectives of the study included:

- (a) Fabricate isotropic MREs using a repeatable and reliable process using different iron particle contents and the matrix material.
- (b) Characterize the static stress-strain response of the fabricated MREs in the shear mode, considering different MRE components including matrix, polarizable particles and additives.
- (c) Characterize of hysteresis properties of MRE subjected to wide ranges of inputs involving variations in strain amplitude, frequency and magnetic field intensity, and analyze the measured data to identify the hysteresis nonlinearities of MREs and effects of strain amplitude, strain rate and magnetic field intensity on the MR effect.
- (d) Formulate a stop operator based Prandtl-Ishlinskii model for predicting nonlinear stress-strain properties of the MREs, and propose a generalized model to describe dynamic behavior of the MRE under harmonic excitations and varying loading conditions.

1.7 Organization of the dissertation

This dissertation research is organized in five chapters describing the research effects and outcomes in a systematic manner. The studies reporting fabrications and characterizations of MREs have been summarized in chapter 1.

Chapter 2 describes the methods of fabrication of the MRE samples, including the material selection, fabrication design and procedure for the isotropic MREs and some of the physical properties of the samples.

The design of experiments for characterizing the static and dynamic properties of MRE samples is presented in chapter 3. A comprehensive review of the standardized methods available for characterization of rubbers is presented for formulating the experiment design. A double-lap shear test setup is designed for measurements of shear stress – shear strain properties of selected samples under different static and dynamic strains and magnetic field intensities. The measured static properties are analyzed in terms of magneto-mechanical properties. The data acquired under harmonic strains inputs are used to describe nonlinear stress-strain hysteresis loops along with the effects of loading conditions and magnetic field intensity on the elastic and dissipative properties of MRE. Finally, physical interpretations of the measured dynamic and static properties are attempted to acquire in-depth understanding of the nonlinear behavior of the MREs.

Subsequently, stop operator-based classical Prandtl-Ishlinskii model is formulated for characterization of MRE hysteresis nonlinearities in chapter 4. The parameters of the proposed model is identified using the laboratory-measured data acquired under different loading conditions and applied magnetic field intensities. A generalized model is further proposed for predicting the hysteresis effects of MRE over the range of loading conditions, and the effectiveness of the generalized model is demonstrated using the measured data. In Chapter 5, the major findings of the study are summarized in chapter 5 together with some suggestions for possible future works.

Chapter 2: Fabrication of MREs

2.1 Introduction

Magnetorheological elastomer is a type of smart composite material commonly made of micron-sized iron particles dispersed or prearranged in an elastomeric matrix. The matrix can have different levels of hardness from extra soft to medium hard. Softer elastomers are commonly preferred in MRE fabrication since a higher relative change in the material stiffness (relative MR effect) can be achieved by the application of an external magnetic field. Elastomers in their uncured state are viscous fluids and based on the elastomer type, crosslinking (bridges) between their macromolecular chains can be created by adding different catalyzers such as platinum, sulfur, etc. This process (also called vulcanization) can occur at room temperature or may require heating depending on the type of elastomers. As mentioned in Chapter 1 (section 1.2.1), the magneto-elasticity of MRE is achieved by dispersing micron-sized ferromagnetic particles (typically carbonyl iron particles due to its high magnetic saturation limit) into an elastic nonmagnetic polymeric medium [20, 22, 34]. The size of iron particles, which have generally spherical shapes may range from 0.5 to 200 μm . To fabricate MREs, the ferromagnetic particles are initially added to the uncured elastomer; the blend is then completely mixed, de-aired using vacuum chamber, and then poured into the desired mold to cure under room or elevated temperature in the oven. Applying uniform magnetic field during the vulcanization leads to formation of particles in a chain-like form in the structures. Therefore, MREs could be manufactured in either anisotropic or isotropic samples in the presence or absence of an external magnetic field, respectively.

Investigating the effects of matrix material and volume fraction of iron particles on the magneto-mechanical properties of MREs is one of the primary objectives of the present research study. Considering this, various types of MRE samples with different matrix material and volume fractions of iron particles are fabricated. The fabricated MRE samples will then be characterized to investigate their static and dynamic characteristics.

This chapter addresses the critical steps in fabrication of MRE samples including selection of MRE ingredient materials, design matrix and fabrication procedure. At the end, some of the physical properties of fabricated MREs will be presented. Experimental test set-up and static and dynamic characterization of the fabricated MRE samples will be investigated in the Chapter 3.

2.2 Selection of materials for fabrication of MREs

Three important ingredients required to fabricate MRE samples are elastomeric matrix, filler (ferromagnetic particles) and additives. In the following, these materials and selection criteria are described.

2.2.1 Non-magnetic elastomeric matrix

Various types of elastomers such as natural rubber, silicone rubber, thermo-plastic elastomers, etc., has been utilized as a host polymeric matrix in MRE fabrication. Elastomer is a type of polymer having both viscosity and elasticity generally with low young's modulus and high failure strain compared to other materials [71]. This kind of polymer is formed by linked monomers usually made of carbon, hydrogen, oxygen and silicon. Among all elastomers, silicone rubber has been widely used, mainly due to its unique features. Being non-reactive and stable, easy manufacturing and shaping and resistant to extreme environments and temperatures from -55 °C to +300 °C while still keeping its desirable properties are the main distinctive features of silicone rubbers. In addition, silicon rubbers are available in different level of viscosity and hardness making them an excellent choice to be used in not only MRE fabrication but also vast variety of engineering applications. Silicone rubber in its uncured state is like a highly adhesive liquid and it must be cured or vulcanized in order to transform to solid state. In fact, silicone rubbers are classified into two main families based on the method of vulcanization. The first group is tin-based silicone rubbers also known as “condensation cure system” and the second is platinum-based silicone rubbers also called “addition cure system”. In platinum based silicone rubbers, polymerization is done by the reaction between the monomers with multiple bonds, where a saturated polymer is formed by joining these monomers. As a matter of fact, with platinum as catalyst, two different chemical groups, a silicone hydride and a vinyl, react which leads to formation of ethyl bridges between the two. While in condensation system, functional group of two monomers react together and release a small molecule which will form a polymer.

Three key factors are generally considered for the selection of a proper silicone rubber to fabricate MREs. The first criteria is viscosity. Clearly, low viscosity silicone rubber is required in order to be able to thoroughly mix it with the ferromagnetic iron particles. The second factor is related to the pot life, which is defined as the time it takes for an initial mixed viscosity to be doubled at room temperature (quadruple for lower viscosity materials - less than 1000 cps). At least 10 minutes of pot life was required for mixing and degassing the blend of silicone rubber,

iron particles and additives. The last factor is capability of silicone rubber to be mixed with the other additives such as silicone oil and silicone thinner. It was reported by the silicone rubber manufacturer (Smooth-On Company) that only platinum based silicone rubbers are mixable with silicone oil and silicone thinner provided by the company. Considering all these factors, Ecoflex 00-20 from Smooth-On Company, USA which is platinum based silicone rubber is selected (See Appendix A.1 for the detailed specification). The product consists of the rubber component (A) and the catalyst component (B): these parts should be mixed together with the ratio of A1 : B1. The compound can then be cured at room temperature within 4 hours, but the curing rate can be increased by application of mild heat based on the manufacturer recommendation. Table 2.1 provide the technical properties of Ecoflex 00-20.

Table 2.1: Technical properties of Ecoflex 00-20, extra soft silicone rubber.

Mixed Viscosity	Specific Gravity	Pot Life	Cure Time	Shore Hardness	Tensile Strength
3000 cps	1.07 g/ml	30 min	4 hours	00-20	160 psi

2.2.2 Micron-sized ferromagnetic particles

Iron has one of the largest saturation magnetization among metallic elements with genetic saturation around $M_s = 2.1 \text{ Testa}$ [1]. High permeability and low remnant magnetization and also low cost are the other features of this material which makes it an ideal choice to be used as the filler for MRE fabrication. The filler is selected to be BASF SQ - carbonyl iron powder (CIP) provided by BASF SE, Ludwigshafen, Deutschland. The powder is composed of spherical carbonyl iron particles with diameter ranging from 3.9 to 5 μm . No coating has been used on the particles and the minimum iron content is 99.5 g/100 g.

2.2.3 Additives

Two kinds of additives namely “Slacker” and “Silicon thinner” are offered by the Smooth-On Company (silicone rubber manufacturer). These additives enable to change the viscosity and ultimate stiffness of silicone rubber. The additive “slacker” is a translucent clear fluid that is added to the host platinum-based silicones to make it softer (See Appendix A.2 for detail specification). The advantage of this softener is that it will not exude silicone oil which is a potential problem with the other softening methods. Table 2.2 provided by the manufacturer can be used as a reference to achieve the desired effect. It is worth mentioning that mixing can be done by weight or volume.

Table 2.2: The effects slacker on the softness of the silicone rubber.

1 Part A + 1 Part B + 1 Part Slacker Result : "Tacky"	1 Part A + 1 Part B + 2 Parts Slacker Result : "Very Tacky"
1 Part A + 1 Part B + 3 Parts Slacker Result : "Extremely Tacky / Gel-like"	1 Part A + 1 Part B + 4 Parts Slacker Result : "Super Soft Tacky Silicone Gel"

The additive "silicone thinner" is basically a silicone rubber thinning fluid (see Appendix A.3 for the detail specification). Silicone thinner will make the vacuuming process faster and easier since it reduces the mixed viscosity. It is noted that the lower viscosity causes the mixed rubber to flow better. Based on the manufacturer report, silicone thinner will also increase the pot life of the mixture as well. The main disadvantage of the silicon thinner is that it reduces the ultimate tensile strength of the fabricated MRE. It is recommended by the manufacturer not to exceed 10% silicone thinner by weight of the total system. Table 2.3 presents the test data offered by the manufacturer as an example of the effects of silicone thinner on mold max 30 silicone rubber.

Table 2.3: The Effects of silicone thinner on the properties of mold max 30 silicone rubber.

Value	Mold Max® 30 0% Silicone Thinner	Mold Max® 30 5% Silicone Thinner	Mold Max® 30 10% Silicone Thinner
Mixed Viscosity (A+B)	25,000 cps	19,000 cps	13,800 cps
Shore Hardness	30 A	26 A	23 A
Tensile Strength	400 psi	350 psi	330 psi

2.3 Design of experiment and fabrication procedure

In this section, design matrix including the percentage of the MRE ingredients (silicon rubber, carbonyl iron particles and additives) to fabricate different MRE types is provided. This is followed by the description of the equipment and procedure for MRE fabrication.

2.3.1 Fabrication design

Six different types of MRE are fabricated to fundamentally investigate the effects of volume fraction of iron particles as well as the additives on the magneto-mechanical properties of MREs. The volume fraction of components for each of the designed MREs are presented in Table 2.4.

In the first three types (MRE types 1-3), no additives have been used during the fabrication process while MRE types 4 and 5 includes one type of additive (slacker) and MRE type 6 includes both types of additives (slacker and silicon thinner). It should be noted that in higher contents of iron particles (MRE type 6), silicone thinner should be added to reduce the viscosity of mixture. Particularly, in a mixture with 40% volume fraction of iron particles and higher, the viscosity of the mixture becomes too high that the presence of silicone thinner to decrease the viscosity of the mixture is inevitable.

Table 2.4: The volume fraction of each component in fabricated MREs.

MRE type	Carbonyl iron particles (Vol%)	Silicone rubber (Vol%)	Slacker (Vol%)	Silicone thinner (Vol%)
1	12.5	87.5	-	-
2	17.5	82.5	-	-
3	25	75	-	-
4	25	60	15	-
5	30	50	20	-
6	40	40	10	10

The weight of each component is calculated based on its density. The bulk or apparent density of carbonyl iron particles (BASF SQ – CIP) is reported to be 2.3 g/mL [1] while the true density of iron (solid metal) is around 7.874 g/mL. The difference between apparent and true density is that in apparent density the volume of inter-particles voids is included in the total volume. The reported density that has been taken for weight calculation of iron particles in the literature is the iron's true density. Considering this, when the MRE is composed of for instance 40 Vol% iron particles, it means that 40% of the total volume is made of solid metal not the particles with voids between them. The inter-particles voids between the particles will be covered by the elastomeric matrix. Thus, the apparent density becomes irrelevant while calculating the weight of the iron particles in the MRE fabrication. The density of MRE components used for weight calculation are presented in Table 2.5. In the following, a simple example is provided to explain the mass calculation of each component of MRE type 6 based on their volume percentage.

Table 2.5: The density of MRE components.

Carbonyl iron particles (True density)	Silicone rubber	Slacker	Silicone thinner
7.874 g/mL	1.04 g/mL	0.94 – 1 g/mL	1 g/mL

Example 2.1: assume the MRE sample product has the volume of 100 ml. Then, the weight of each component can be calculated as:

- **Carbonyl ion particles (CIP):**

$$m_{\text{CIP}} = V_{\text{CIP}} \times \rho_{\text{CIP}} \quad (2.1)$$

$$m_{\text{CIP}} = \left(100 \times \frac{40}{100}\right) \times 7.874$$

$$m_{\text{CIP}} = 314.96 \text{ g}$$

- **Silicone rubber:**

$$m_{\text{silicone rubber}} = V_{\text{silicone rubber}} \times \rho_{\text{silicone rubber}} \quad (2.2)$$

$$m_{\text{silicone rubber}} = \left(100 \times \frac{40}{100}\right) \times 1.04$$

$$m_{\text{silicone rubber}} = 41.6 \text{ g}$$

- **Slacker:**

$$m_{\text{slacker}} = V_{\text{slacker}} \times \rho_{\text{slacker}} \quad (2.3)$$

$$m_{\text{slacker}} = \left(100 \times \frac{10}{100}\right) \times 0.97$$

$$m_{\text{slacker}} = 9.7 \text{ g}$$

- **Silicone thinner:**

$$m_{\text{silicone thinner}} = V_{\text{silicone thinner}} \times \rho_{\text{silicone thinner}} \quad (2.4)$$

$$m_{\text{silicone thinner}} = \left(100 \times \frac{10}{100}\right) \times 1$$

$$m_{\text{silicone thinner}} = 10 \text{ g}$$

It should be noted that different sample shapes and dimensions have been used for magneto-mechanical characterization of MREs in the literature. Here in this present study, a comprehensive investigation based on the international standards available for characterization of rubbers (will be presented in the experimental setup and method - section 3.2) has been conducted to find appropriate dimensions for fabrication. These dimensions are then used to design required molds to hold MREs.

2.3.2 Fabrication procedure

To begin the Fabrication, the desired amount (mass) of each component is accurately measured and prepared in separate beakers. Then, the two parts of silicone rubber (Part A and Part B) are mixed well enough with a wooden stick by hand. If required, slacker and silicone thinner are also added and mixed thoroughly. Afterwards, carbonyl iron powder is slowly added to the mixture, and blended initially with wooden stick to achieve a dark grey mixture. After that, the blend is mixed using an electrical blender (Oster kitchen Immersion blender-10000 rpm) for almost 5 minutes. Next, the beaker containing a homogenous dark grey oil-like mixture is put into the vacuum chamber for 5 minutes to be degassed. The mixture should be vacuumed under around 29 in-Hg. The vacuum chamber and pump is provided by Best Value Vacs, USA (see Appendix A.4). Subsequently, the beaker containing the degassed mixture is removed from the vacuum chamber. The mixture is poured into the desired mold, and then placed into the kitchen oven at temperature around 150 °F for 20 minutes to cure. The whole fabrication set-up is shown in Figure 2.1. By experience, the whole process before curing takes 15 minutes which is less than the pot life (30 minutes) of the silicone rubber. It is observed that adding iron powder to silicone rubber drastically increase the viscosity of mixture and decreases the pot life and cure time. Molds contain MRE samples are finally allowed to rest in room temperature after curing for about 4 hours. Figure 2.2 shows the fabricated samples of MRE type 3 in and out of the circular shape molds.



Figure 2.1: MRE Fabrication set-up.

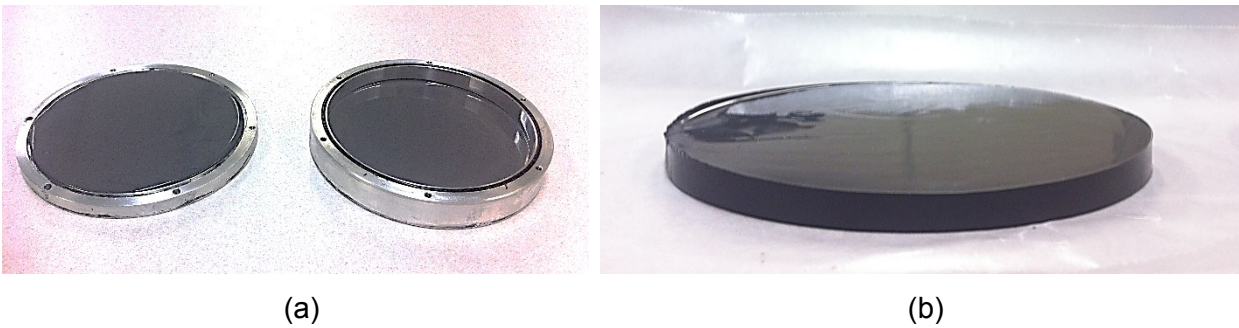


Figure 2.2: Fabricated MRE – type 3 (a) in and (b) out of the designed circular molds.

2.4 Physical properties of fabricated MREs

Beside the volume fraction (φ_i), Mass fraction (w_i) of iron particles is another factor that is used in the literature to represent the content of iron particles in the MRE. Mass fraction of carbonyl iron particles in MRE can be calculated as:

$$w_{CIP} = \frac{m_{CIP}}{m_{total}} = \frac{m_{CIP}}{m_{CIP} + m_{silicone\ rubber} + m_{slacker} + m_{silicone\ thinner}} \quad (2.5)$$

Calculating the required mass for each component of the MREs (Table 2.4) based on their volume fraction (see for an example, Eqs. 2.1-2.4 for MRE type 6), and then using the Eq. (2.5), the mass fraction of iron particles are calculated and provided in table 2.6. The Manufactured MREs have the same color of dark grey with noticeable difference in their densities. To measure the density

of different types of MREs, a sample block with dimension (25×20×5 mm³) was cut from all the six types of MRE and its density was measured. On the other hand, theoretically, the density of MREs was calculated as:

$$\rho_{MRE} = \frac{m_{total}}{V_{total}} = \frac{m_{CIP} + m_{silicone\ rubber} + m_{slacker} + m_{silicone\ thinner}}{V_{CIP} + V_{silicone\ rubber} + V_{slacker} + V_{silicone\ thinner}} \quad (2.6)$$

Table 2.6 represents the measured and calculated densities of fabricated MREs. Results shows that there is a perfect agreement between experimental measurements and calculations.

Table 2.6: The Physical properties of fabricated MREs.

MRE type	Volume fraction (%)	Mass Fraction (%)	calculated density of MRE (g/mL)	Measured density of MRE (g/mL)
1	12.5	55	1.928	1.984
2	17.5	62.5	2.23	2.24
3	25	70	2.69	2.82
4	25	70	2.67	2.54
5	30	80	3.23	3.305
6	40	85	3.94	4.069

2.5 Summary

Six types of magnetorheological elastomers are designed and manufactured. The first three types of MREs are made of silicone rubber and different contents of micron sized carbonyl iron particles. While increasing the volume percentage of iron particles for the 4th and 5th types of MREs, slacker (silicone tactile mutator) is also added to increase softness of the smart composite. In higher contents of iron particles, it is required to reduce the viscosity of the uncured blend for mixing and degassing. Thus, silicone thinner is added and a novel MRE with 85% weight fraction iron particles (MRE type 6) is manufactured. The density of fabricated MREs is measured and compared with those of calculated theoretically. Results shows ideal agreement between the measured and the expected theoretical densities.

Chapter 3: Magneto-Mechanical Characterization of MREs

3.1 Introduction

MREs possess combined characteristics of elastic solid and viscous liquid. Therefore, similar to many of polymers and their composites, they are described with viscoelastic properties. To effectively utilize MREs in the design of MRE-based adaptive devices or structures, it is of paramount importance to fundamentally investigate and characterize their static and dynamic behavior in wider range of frequency and excitation amplitudes. While there are a number of studies on dynamic characterization of MREs [1, 3-5, 12, 25, 33, 34, 38, 42, 55, 72], they are mostly limited to limited range of frequency and amplitude of excitation. Moreover, no standard procedure has been followed in previous works reported on characterization of MREs

Here in this research study, due to the similar viscoelastic behavior of MR elastomers to rubbers, a similar standard procedure available for testing the rubbers has been utilized to characterize MREs under wide range of excitation frequencies and amplitude as well as applied magnetic field. MREs have shown highly rate, strain and magnetic field dependent dynamic properties. As mentioned above, in majority of previous studies, MREs have been mainly characterized in a narrow range of excitation frequency and strain amplitude and also applied magnetic field intensity. In this research work, an experimental setup based on the standards available for determination of dynamic and static properties of rubbers has been designed to characterize different types of fabricated MREs in a wide range of strain amplitudes, frequencies and magnetic field intensities. The designed experimental setup, characterization test methods, measured static and dynamic properties as well as discussion on the nonlinear magnetic field, strain and rate dependent behavior of fabricated MREs are described in the following sections.

3.2 Standards for static and dynamic characterization of rubbers

In this study, the test arrangement, shape and size of MRE samples, static and dynamic test procedures and expression of results are all in accordance with the two ISO standards: ISO 1827 [73] and ISO 4664 [74] available for rubbery materials. Here, a summary of these two ISO standards as well as pertinent ASTM and British standards are first presented to clarify and justify the proposed test arrangement, experimental design and test procedures, which will be presented and discussed thereafter.

ISO 1827 - Rubber, vulcanized or thermoplastic - Determination of shear modulus and adhesion to rigid plates - Quadruple-shear methods:

Standard ISO 1827 provides the test procedure to measure the shear modulus of rubbery materials according to the following guidelines:

a) **Terms and definitions:**

Shear Modulus (G): This is basically the ratio of the “applied shear stress (calculated with respect to the bonded areas of the rubber in a test piece), divided by the resultant shear strain in the direction of application of the stress.”

b) **Apparatus:**

Test instrument should be able to measure the deformation of the rubber test samples to an accuracy of 0.02 mm .

c) **Test pieces:**

The samples shall be rectangular parallelepiped elements with the size of $4\text{mm} \pm 1\text{mm}$ thick, $20\text{mm} \pm 5\text{mm}$ wide, $25\text{mm} \pm 5\text{mm}$ long.

d) **Arrangement:**

A typical test arrangement is shown in Figure 3.1.

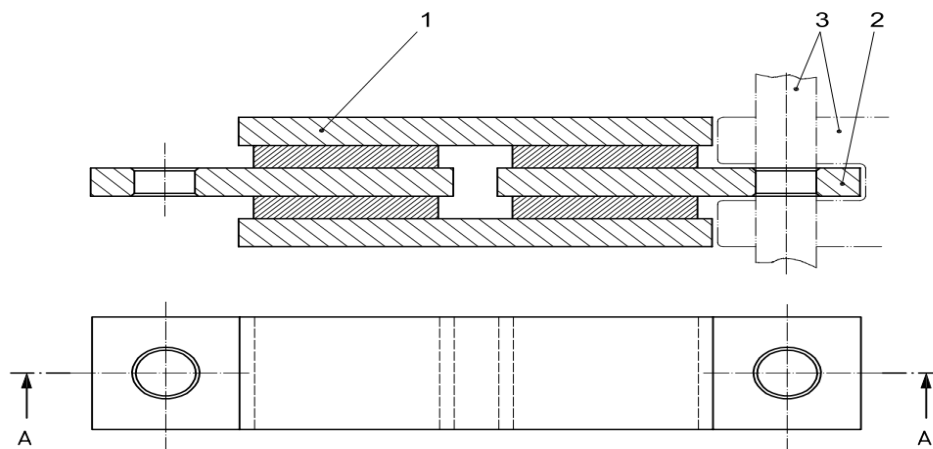


Figure 3.1: Typical test piece arrangement – ISO 1827 (1: two external plates, 2: two internal plates, 3: pin and fixture for tensile loading) [73].

e) **Bonding:**

The samples shall be bonded to the rigid plates using an adhesive system providing a high modulus bond.

f) **Conditioning:**

The test pieces shall be kept at the laboratory condition with the standards temperature for at least 3 *h* before the test.

g) **Procedure:**

Shear-loading cycle from 0% to 30% should be applied at a rate of 5mm/min ± 1mm/min while recording the force/deformation curve.

h) **Expression of results:**

The shear modulus is calculated at 25% shear strain. Shear strain is given by:

$$\gamma = \frac{d}{2c} \quad (3.1)$$

Where

d is the deformation of the test pieces in millimetres and *c* is the thickness of one rubber element in millimetres. Shear stress can be calculated from the equation:

$$\tau = \frac{F}{2A} \quad (3.2)$$

Where

F is the force in newtons and *A* is the bonded area of one face of one test sample in square millimetres. Finally, the shear modulus (*G*) in N/mm² is calculated as:

$$G = \frac{\tau_{25\%}}{\gamma_{25\%}} = \frac{\tau_{25\%}}{0.25} \quad (3.3)$$

ISO 4664-1 - Rubber, vulcanized or thermoplastic - Determination of dynamic properties - Part 1: General guidance[74]

Standard ISO 4664-1 provides guidelines and test procedure to characterize the dynamic properties of rubbery materials. In the following, definition of relative terms, sample dimensions, test procedure and other pertinent information are briefly described.

a) Terms and definitions:

Complex shear modulus (G^*): the ratio of shear stress to shear strain. Each of shear stress and shear strain are a vector; thus, the term can be represented by a complex number such that:

$$G^* = G' + iG'' \quad (3.4)$$

Loss angle (δ): It is a phase angle between the strain and stress expressed in rad.

Elastic shear modulus (G'): This is a component of the shear stress divided by the shear strain which is in the same phase with the applied shear strain:

$$G' = |G^*| \cos\delta \quad (3.5)$$

Loss shear modulus (G''): This is a component of the shear stress divided by the shear strain which is in quadrature with the applied shear strain:

$$G'' = |G^*| \sin\delta \quad (3.6)$$

Tangent of loss angle ($\tan\delta$): This is a ratio of the loss modulus to the elastic modulus which is commonly known as the loss factor:

$$\tan\delta = \frac{G''}{G'} \quad (3.7)$$

b) Dynamic motion:

The response of rubbers to dynamic stressing is a combination of elastic and viscous response. Let us to describe the motion with sinusoidal strain as:

$$\gamma = \gamma_0 \sin \omega t \quad (3.8)$$

Due to the energy loss, the stress will not be in the same phase with the strain and it can be considered that there is a phase angle difference of δ between them as shown in Figure 3.2. Thus:

$$\tau = \tau_0 \sin(\omega t + \delta) \quad (3.9)$$

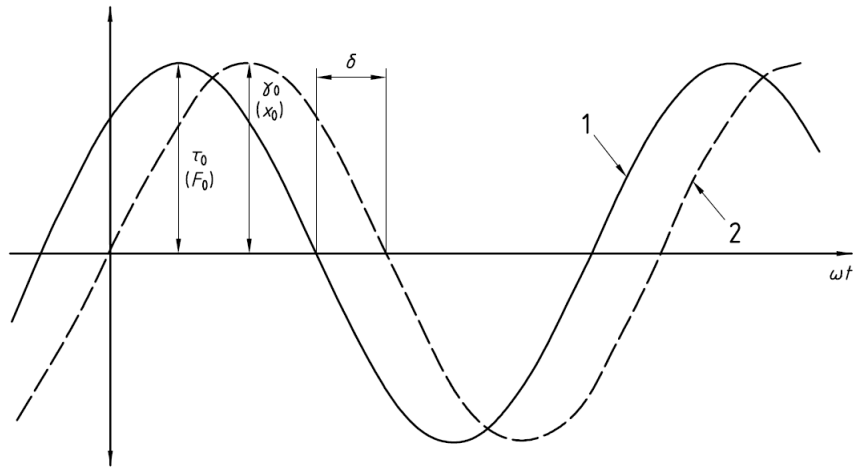


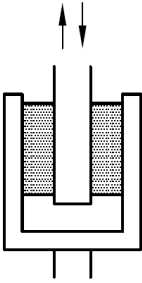
Figure 3.2: Typical stress-strain response of viscoelastic materials under sinusoidal deformation [74].

c) Test conditions and test pieces

Test pieces preparation: The samples can be molded or cut from prepared sheets. The samples can be bonded to metal plates during molding or after with a thin layer of adhesive.

Test piece dimensions: In accordance with the deformation mode, type of test machine and its capacity, different sample shape and dimensions are proposed in this standard. For instance for shear mode deformation and small-sized test apparatus, two options for shape and dimension are suggested, which are given in table 3.1.

Table 3.1: Shear test conditions for small-sized apparatus [74].

Arrangement in Shear mode	Shape and dimension	
	Cylinder	Rectangular column
	<p>d = diameter</p> <p>h = height</p> <p>$h: d = 1: 4$</p> <p>$h \leq 12mm$</p>	<p>d = side×side</p> <p>h = height</p> <p>$h: d = 1: 4$</p>

d) Test Procedure

- It might be better to start the measurements from the least severe condition meaning lower amplitudes and frequencies.
- In order to measure the data close to the steady-state condition, it is recommended that the measurement begins after applying at least six cycles in higher amplitudes and frequencies, there is an increasing danger of heat generation which may substantially affect the data; thus, the test duration should be as short as possible.

e) Expression of results

The elastic and loss shear moduli are normally required. These parameters can be derived from the load-deflection hysteresis loop. In rubbers containing fillers and at higher amplitudes, the hysteresis loops might deviate from perfect ellipse. A presentative of load-deflection hysteresis loop acquired from double-lap dynamic shear test is shown in Figure 3.3. A perfect ellipse shows that the rubber behavior is linear.

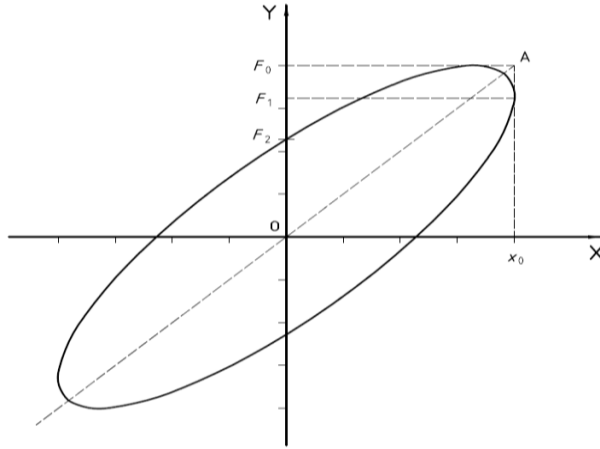


Figure 3.3: Load deflection hysteresis loop (X: deflection, Y: load) [74].

The absolute value of the complex shear modulus is given by:

$$|G^*| = \frac{F_0 h}{2Ax_0} \quad (3.10)$$

Where F_0 and x_0 are the maximum load amplitude and maximum deflection amplitude, respectively. A is the cross-section area of the test piece and h is its thickness of one test piece. The loss angle is also given by:

$$\sin\delta = \frac{\text{Area of ellipse}}{\pi F_0 x_0} \quad (3.11)$$

The in-phase and out-of-phase moduli can then calculated using Eqs. (3.5) and (3.6), respectively.

ASTM D5992 – 96, Standard Guide for Dynamic Testing of Vulcanized Rubber and Rubber-Like Materials Using Vibratory Methods

Standard ASTM D5992-96 [74] is a ASTM standard which provide similar test procedure as that of ISO 4664-1 for dynamic characterization of rubbery type materials considering the following guidelines.

a) Specimen Geometry

A typical double-lap shear specimen is illustrated in Figure 3.4.

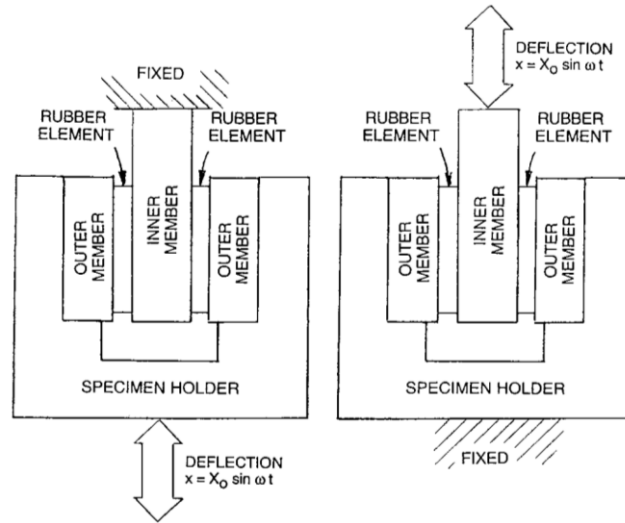


Figure 3.4: Double lap shear test arrangement [75].

b) Test Sample shape and dimensions

The height to thickness ratio of eight is recommended in order to place the vast majority of elastomer in shear instead of bending. Three specimen design of rectangular, square and circular are illustrated in Figure 3.5. The recommended dimensions of specimens are presented in table 3.2.

BS 903-5:2004 – Physical testing of rubber – Part 5: Guide to the application of rubber testing to finite element analysis This British standard also provides similar guidelines for dynamic characterization of rubber type material with following additional guidelines for double-lap shear test and recommended dimensions for test samples.

Section 6.4.4.6 – simple shear test:

The thickness of each test specimen should not exceed one quarter of its width or diameter as to avoid bending of elastomers in shear or quadruple shear test pieces.

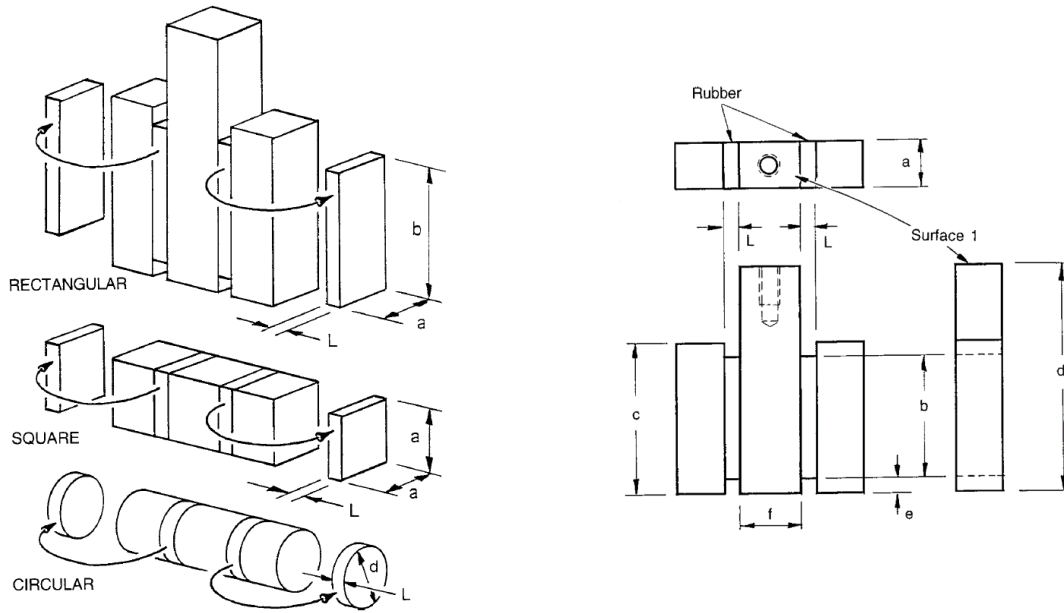


Figure 3.5: Double lap shear test specimens design[75].

Table 3.2: Recommended dimensions for double lap shear test specimens[75].

Dimensions							
	CRITICAL			CONVINIENT			
	L	a	b	c	d	r	F
mm	5.00	16.00	40.00	50.0	75.0	5.0	20.0
inches	0.200	0.625	1.600	2.00	3.00	0.20	0.75

3.3 Experimental setup and proposed test procedures

An experimental test setup is designed to characterize the force-displacement characteristics of magnetorheological elastomer in shear mode. The experiments are conducted using Bose ElectroForce 3200 Series which is a versatile table-top test instrument for static and dynamic characterization of rubbery materials and small components. The equipment and its specifications are shown in Figure 3.6 and Table 3.3, respectively. Considering the ISO 1827 recommendations for shape and dimensions of test pieces, rectangular MRE samples are carefully cut from the prepared circular panels with the dimensions of $25\text{mm} \times 20\text{mm} \times 5\text{mm}$. The test fixture arrangement for performing double lap shear test is designed in accordance with the prepared MRE samples and test equipment. The inner and outer components of the fixture are then manufactured by 3D printing technology using polymeric material (see Appendix A.4 for the material properties). It should be noted that the main reason for selection of polymeric material

for fixture components is that it does not react or interfere with the applied magnetic field. The MRE samples are then bonded to inner and outer components of the fixture using the super glue (Armor Coat Single-use Super Glue Adhesive). The 3D designed assembly, manufactured fixture components together with the MRE samples and the actual arrangement (MREs bonded between the inner and outer fixture components) are shown in Figure 3.7.

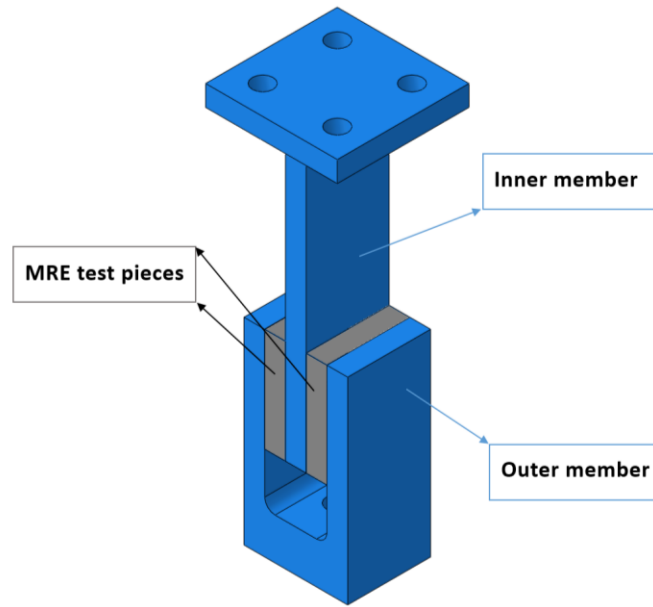


Figure 3.6: ElectroForce 3200 test instrument – Axial Configuration.

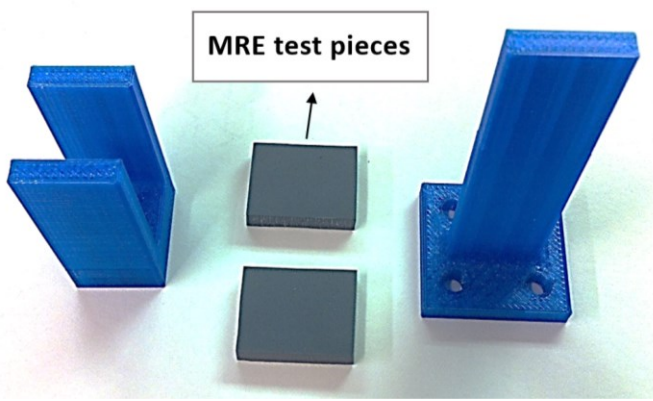
Table 3.3: Specifications of Bose - ElectroForce 3200.

Linear Motor	
Standard	
Peak/Max Sine	± 225 N
Static or RMS (continuous)	± 160 N
High Force Option	
Peak/Max Sine	± 450 N
Static or RMS (continuous)	± 320 N
Displacement	13 mm
Extended Stroke Option	150 mm
Linear Velocity	0.0065 $\mu\text{m/s}$ – 3.2 m/s
Frequency	0.00001 Hz – 200 Hz
Torsional Motor	
Standard	
Peak/Max	± 5.6 N-m
Static or RMS (continuous)	± 5.6 N-m
High Torque Option	
Peak/Max	—
Static or RMS (continuous)	—
Rotation	Multi-turn (± 10 revolutions Standard)

Neodymium permanent magnets are used to apply the desired magnetic field intensity on the MRE samples sandwiched between inner and outer members of the fixture. Two sets of permanent magnets each consisting of 3 attached rectangular blocks with dimensions of $50\text{mm} \times 50\text{mm} \times 10\text{mm}$ are placed symmetrically at a distance along the central axis of the test arrangement using a proper fixture as shown in Figure 3.8. The fixture holding permanent magnets is designed in such manner as to allow the distance between the magnets to be adjusted using bolts and screws. Therefore, different magnetic field intensities can be achieved by changing the distance between the magnets. As shown in F3.9, the test arrangement is placed in between the magnets using 2 shafts made of non-magnetic materials. Shaft number 1 connects the inner component to the actuator and shaft number 2 connects the outer component of the fixture to the load cell. These non-magnetic shafts are considered to make sure that the magnetic field does not affect the load cell and actuator.



(a)



(b)



(c)

Figure 3.7: (a) 3D designed test arrangement, (b) manufactured test specimens and MRE samples and (c) actual test arrangement.

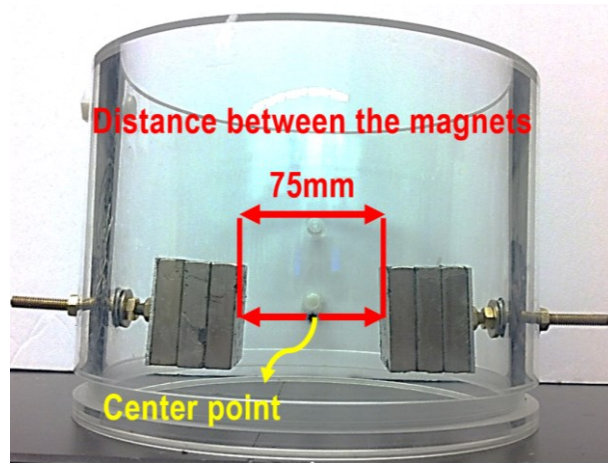


Figure 3.8: Experimental set-up designed for applying magnetic field on the test arrangement.

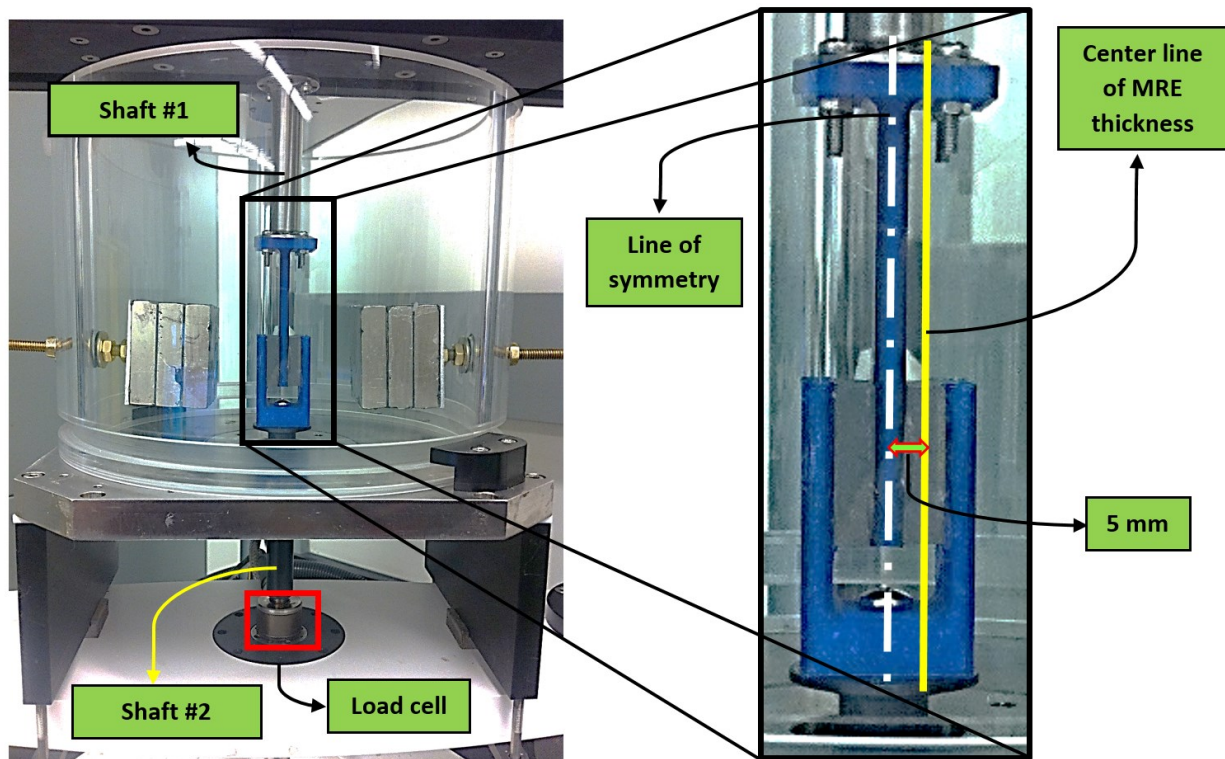


Figure 3.9: Simple shear test set-up placed between the two sets of permanent magnets.

The magnetic field density is measured using a Gauss-meter at the center of MRE sample's thickness, which has distance of about 5mm from the test set-up center point (see Figure 3.9). The measurement is performed under six different conditions in which the distance between the magnets is varied from 75mm to 25mm. It is noted that 75mm is the maximum distance due

to the fixture limitations and the 25mm corresponds to the minimum distance between the magnets due to the 25mm width of outer component of the fixture. Figure 3.10 demonstrates the measured magnetic field density variation with respect to the distance between the permanent magnets. Results show that the magnetic field intensity decreases nearly exponentially by increasing the distance between the magnets. Therefore, an exponential function is suggested to curve fit on the measured data, expressed as:

$$B(x) = a_1 * \exp(-a_2x) \quad (3.12)$$

Where $B(x)$ is the magnetic field intensity at 5mm from the center point between the magnets (see Figure 3.9) in mT , x is the distance between the magnets in mm and a_1 and a_2 are the positive constant parameters to be found. The constant parameter vector $X = \{a_1, a_2\}$ of the function $B(x)$ was then identified to minimize the error between the predicted and measured magnetic field densities. The error function $J(X)$ can be expressed as:

$$J(X) = \sum_{i=1}^n R_i^2 = \sum_{i=1}^n (B_{measured} - B(x))^2 \quad (3.13)$$

Where n is the number of measured data and R_i is the error between the measured and predicted value at each measured point i . This is an unconstrained nonlinear optimization problem which can be easily solved using Least-Squares (model fitting) algorithms available in MATLAB optimization toolbox. Command "lsqcurvefit" in MATLAB is particularly useful for nonlinear curve-fitting problems in the least-square form in which either of Trust-region-reflective or Levenberg-Marquardt algorithms is utilized to solve the optimization problem. The optimal constant parameters using the Trust-region-reflective are found to be $a_1 = 790.4, a_2 = 0.023$. The measured magnetic field densities at 6 conditions and the proposed curve-fitted exponential function are presented in Figure 3.10. The coefficient of determination, R^2 , is a term in statistics which provides information about the suitability of the fit of a model and varies between 0 and 1 in which 1 represents the perfect fit. For the proposed exponential model, it is found that $R^2 = 0.9948$.

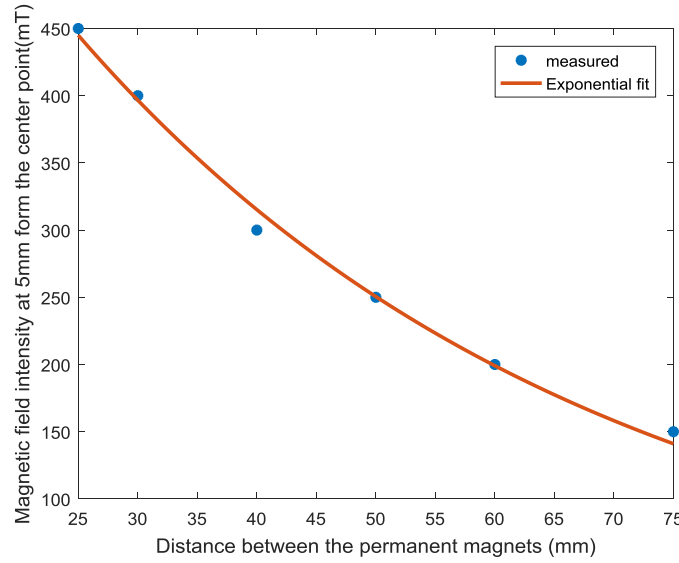


Figure 3.10: Magnetic field intensity at 5mm from center point versus distance between the permanent magnets.

The measured magnetic field intensities are validated using an analytical method, which predicts the magnetic field density (B) around a rectangular permanent magnet [76, 77]. The analytical method approximates the magnetic field density on the central axis at a distance x from a rectangular magnet (see Figure 3.11(a)), which can be expressed as:

$$B = \frac{B_r}{\pi} \left[\tan^{-1} \left[\frac{W.L}{2x \cdot [4x^2 + W^2 + L^2]^{1/2}} \right] - \tan^{-1} \left[\frac{W.L}{2(x+T) \cdot [4(x+T)^2 + W^2 + L^2]^{1/2}} \right] \right] \quad (3.14)$$

Where B_r is the remanence magnetism and W , L and T are the width, length and thickness of rectangular magnet, respectively. Using the principle of superposition, the magnetic field density between two rectangular magnets is then predicted as:

$$B = B_1 + B_2 \quad (3.15)$$

Where B_1 is the field density on the central axis for a rectangular block at a distance $x_1 = \left(\frac{d}{2} + x\right)$, B_2 is the field density on the central axis for a rectangular block at a distance $x_2 = \left(\frac{d}{2} - x\right)$ and d is the total distance between the magnets as shown in Figure 3.11. Thus, the total magnetic field on the central axis is expressed as:

$$B = \frac{B_r}{\pi} \left[\tan^{-1} \left[\frac{W.L}{2x_1 \cdot [4x_1^2 + W^2 + L^2]^{1/2}} \right] - \tan^{-1} \left[\frac{W.L}{2(x_1+T) \cdot [4(x_1+T)^2 + W^2 + L^2]^{1/2}} \right] \right] + \frac{B_r}{\pi} \left[\tan^{-1} \left[\frac{W.L}{2x_2 \cdot [4x_2^2 + W^2 + L^2]^{1/2}} \right] - \tan^{-1} \left[\frac{W.L}{2(x_2+T) \cdot [4(x_2+T)^2 + W^2 + L^2]^{1/2}} \right] \right] \quad (3.16)$$

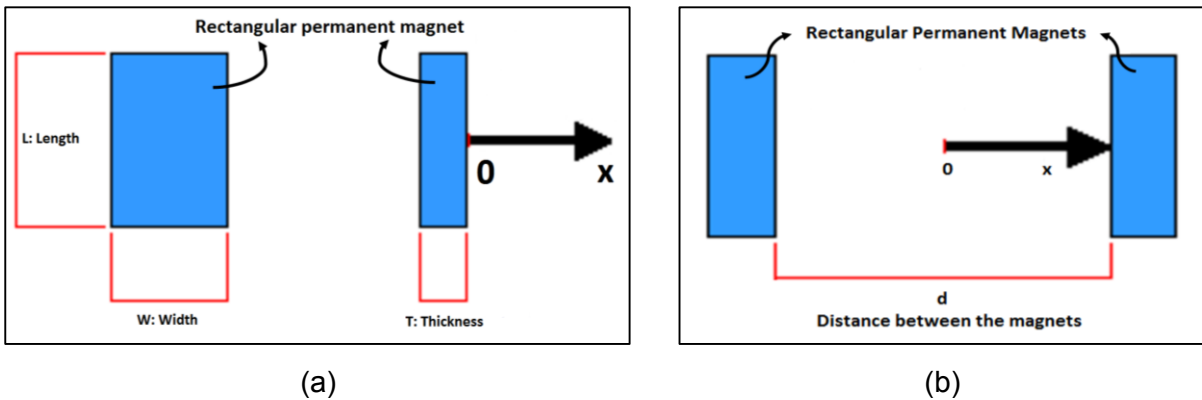


Figure 3.11: Schematic diagram for calculating the magnetic field on the central axis (a) of a rectangular block at a distance x and (b) between the two rectangular magnet at a distance x from the center point.

Magnetic remanence (B_r) for neodymium – N35 magnet ranges between 1170 mT to 1220 mT . Figure 3.12 compares the measured and analytically calculated magnetic field density at centerline of MRE which is 5 mm from the center line of test set-up for different values of distance between permanent magnets and also magnetic remanence. It can be realized that the predicted magnetic field densities using analytical approach follow the same trend and decrease almost exponentially as the distance between permanent magnet increases. Excellent agreement between the analytical magnetic field densities and those measured exist once the distance between the permanent magnet increases beyond 60 mm irrespective of the value of the remnance. However, the difference between the measured and analytical values increases by decreasing the distance between the magnets which is around maximum 11% at distance of 25 mm . Considering underlying assumptions in derivation of the analytical equation (Eq. 3.16) such as uniformity of the magnetic field and neglecting the effect of leakage and interference, this level of accuracy is generally acceptable.

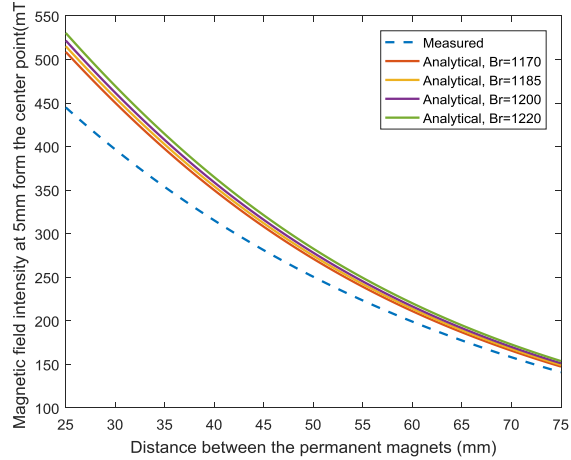


Figure 3.12: Comparison between the measured and analytical magnetic field intensities at 5 mm from the center point for varying values of magnetic remanence.

To investigate the uniformity of the magnetic field around the center point between the magnets, the magnetic field density along the central x axis was calculated using the analytical method at three different distances between permanent magnets 75mm , 40mm and 25mm , in which the magnetic field density evaluated at 5mm from the center point was found to be 150mT , 300mT and 450mT , respectively as shown in Figure 3.10. Figure 3.13 depicts the distribution of magnetic field intensity throughout the central x axis between the magnets at three different cases of distance between the magnets. It can be observed that within 2.5mm to 7.5mm from the center point (corresponding to MRE element thickness) the value of magnetic field intensity varies less than 5%, which verifies the assumption made on the uniformity of magnetic field distribution along the thickness of the MRE elements.

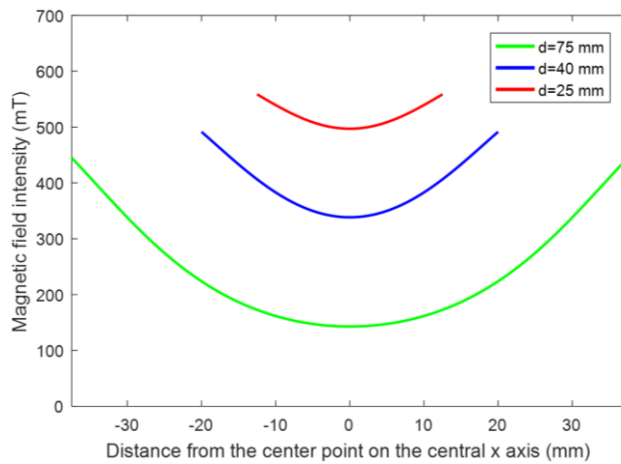


Figure 3.13: Distribution of magnetic field intensity between two permanent magnets along the central x axis in different distances between the magnets.

3.3.1 Test procedure for static characteristics of MREs

Static tests are performed on samples from each of the MRE types (type 1 to type 6) in accordance with ISO 1827. Deformation is applied on the inner member of test arrangement up to 30% shear strain by the very small rate of 5mm/min. Considering the 5mm thickness of MRE elements, 1.5 mm is the maximum deformation applied to achieve 30% shear strain. The force is recorded by the load cell through the shaft number 2 (Figure 3.9) connecting the load cell and the outer component of the fixture. The test equipment is capable of recording data by the maximum sampling rate of 5000 point/second. For static tests, the force and deformation data is recorded by the sampling rate of 2000 point/sec. For each MRE type, first the test is conducted in the absence of the magnetic field. Then the experiment is conducted under different applied magnetic field densities of $150mT$, $300mT$ and $450mT$ on the center of MRE elements' thickness, which are generated by changing distances between the permanent magnets to 75mm, 40mm and 25mm, respectively.. It should be noted that each test is repeated 4 times; two times in upward direction and two times in downward direction. Due to the symmetric structure of the test arrangement, there is no noticeable difference between the tests in upward and downward directions. Yet, performing the tests in opposite directions is helpful to verify that the MREs in the initial state are in unreformed configurations. This is due to the fact that, a minute pre-deformation due to the misalignment can lead to difference between the data obtained from tests performed in opposite directions. In each test, the average from the 4 tests is evaluated which will be then used to evaluate the shear modulus at 25% shear strain according the standard.

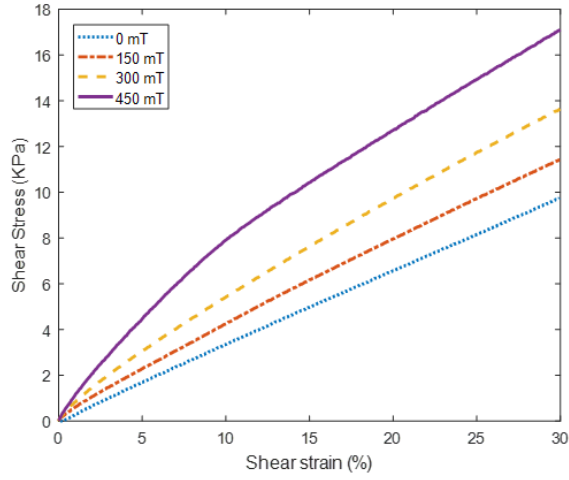
3.3.2 Test procedure for dynamic characteristics of MREs

To acquire in-depth understanding of dynamic behavior of MREs, it is required to accurately investigate the stress (output)-strain (input) characteristics of MRE over a wide range of excitation frequencies and amplitudes as well as applied magnetic field intensities. In this study, extensive experimental tests are performed on the MRE type 6 containing 40% volume fraction iron particles in simple shear mode to measure its hysteresis nonlinearities under harmonic excitations. The hysteresis loop of MRE is amplitude, rate and magnetic field dependent. Thus, wide ranges of strain amplitudes, frequencies and magnetic field intensities should be considered as the loading conditions in the experiment. The response characteristics of MRE are measured at discrete strain amplitudes in the range of 2.5 — 20%, discrete frequencies in the range of 0.1 — 50 Hz and discrete magnetic field intensities in the range of 0 — 450 mT . The measurement are carried out under harmonic strain amplitudes of 2.5%, 5%, 10% and 20% at

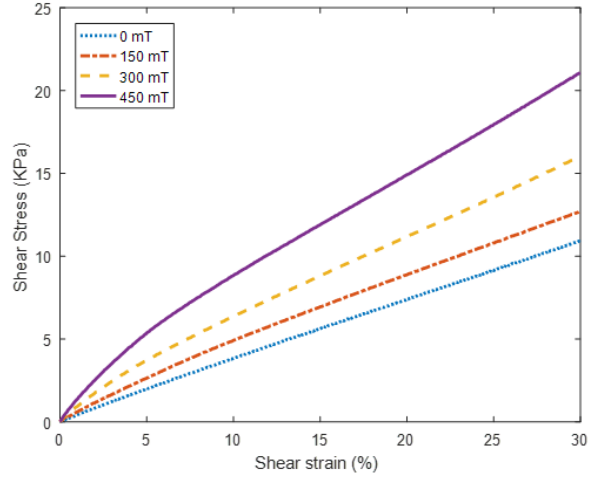
different frequencies of 0.1 Hz, 1 Hz, 10 Hz, 50 Hz. Each test is then performed at four different magnetic field intensities of 0mT, 150 mT, 300mT and 450mT. Thus, in total 64 tests ($4 \times 4 \times 4$) at different loading conditions and magnetic field intensities are carried out and the force-displacement response of MRE is recorded for each test. The sampling rate is adjusted in a way to record 100 data points for each cycle. Thus, at each frequency the sampling rate is different. For instance, the sampling rate for the test at the frequency of 10 Hz, is adjusted to 100 points / 0.1 second (1000 point/sec) where the 0.1 second is the period when the excitation frequency is 10 Hz. The measurements are carried out in displacement control mode by applying the displacement to the inner component of the fixture as shown in Figure 3.9. The relationship that are utilized to covert the displacement to shear strain and the force to shear stress are presented in section 3.2, Eqs. 3.1 and 3.2.

3.4 Static properties

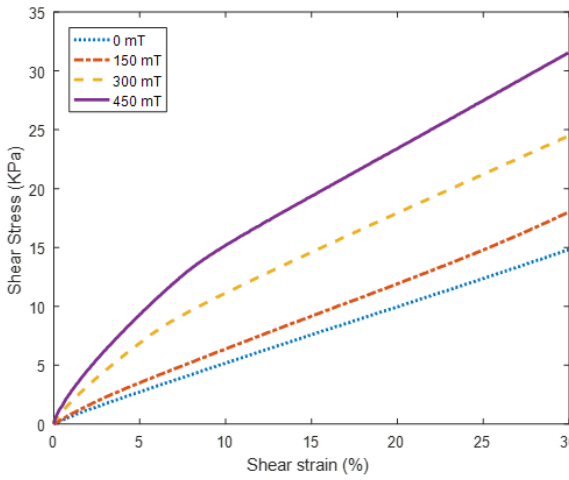
Figure 3.14 presents the stress-strain curves of each fabricated MRE (types 1 to 6) at 4 different magnetic field intensities. The shear modulus of MREs at 25% shear strain are then calculated using the method recommended by ISO 1827. Figure 3.15 represents the shear modulus of all fabricated MREs at varying magnetic field densities ranging between 0 mT to 450mT. Smoothing-spline method provided by the MATLAB Curve fitting toolbox is utilized to demonstrate the trend of shear modulus versus applied magnetic field intensity between the measured data points.



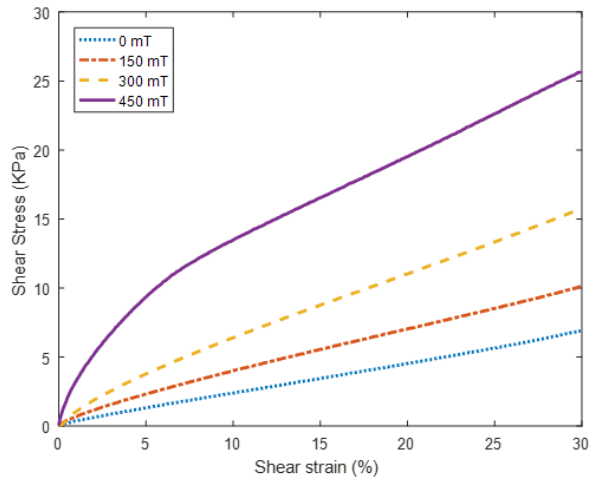
(a)



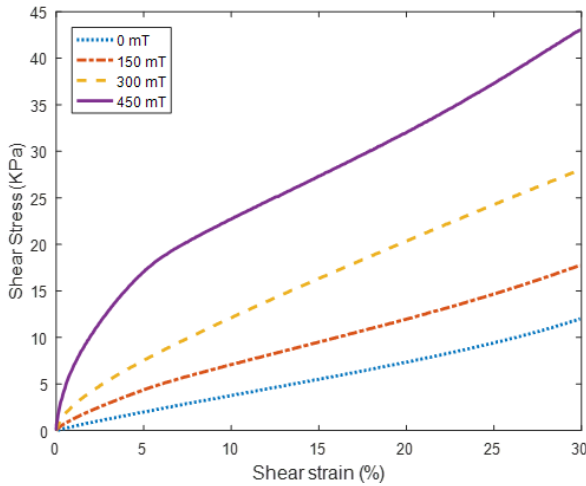
(b)



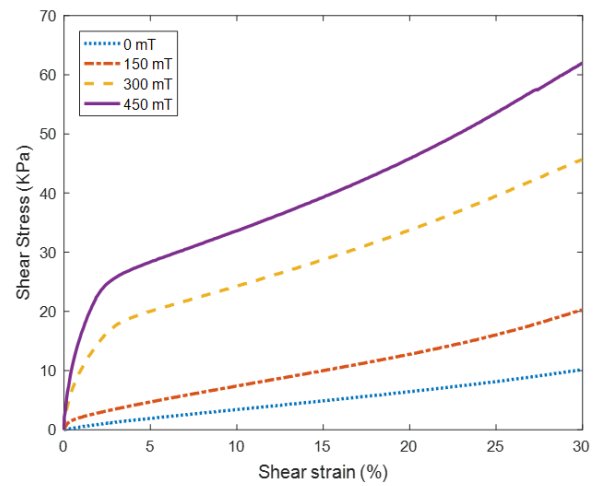
(c)



(d)

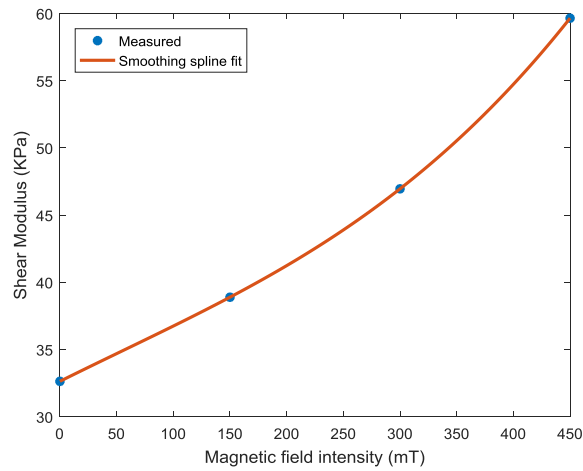


(e)

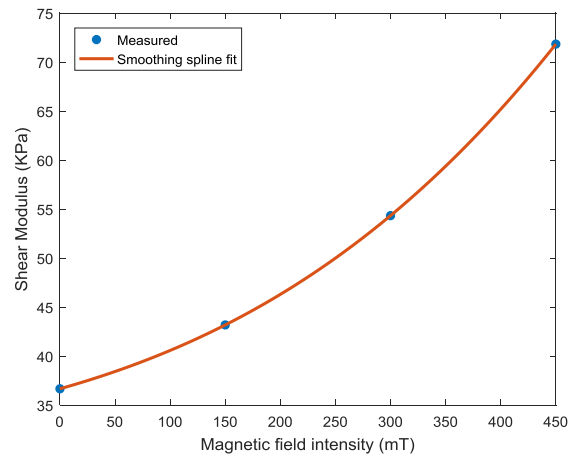


(f)

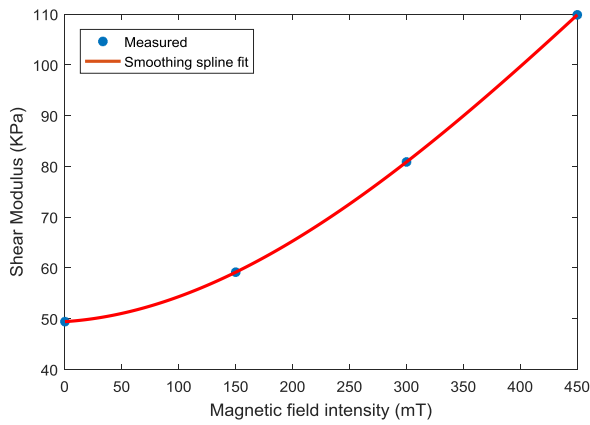
Figure 3.14: Stress-strain curve of fabricated MREs (a) type1, (b) type2, (c) type3, (d) type4, (e) type5, (f) type6, at 4 different magnetic field intensities.



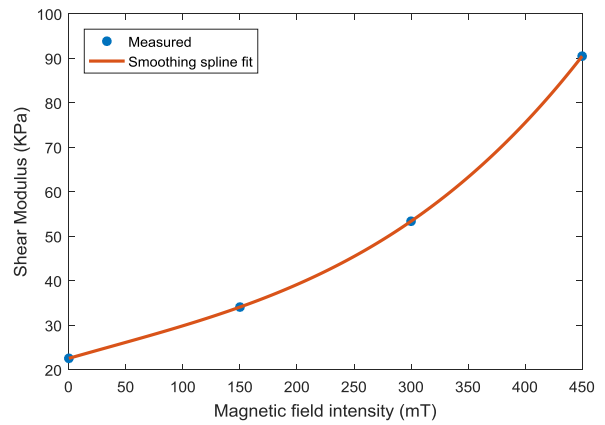
(a)



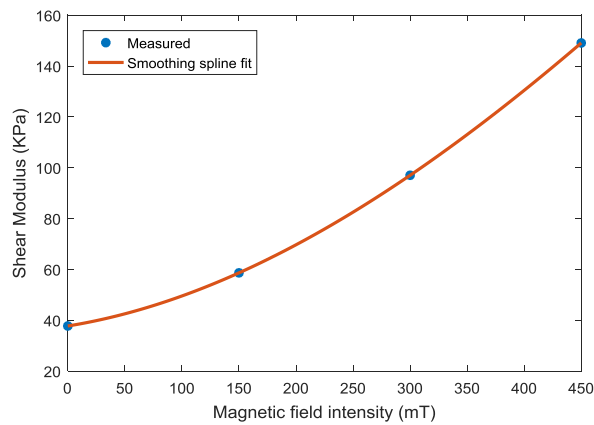
(b)



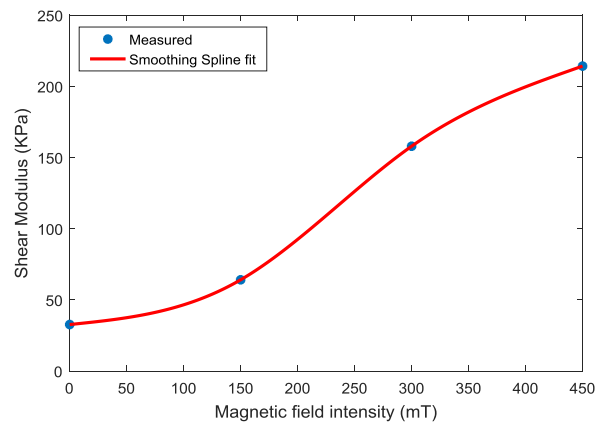
(c)



(d)



(e)



(f)

Figure 3.15: Shear modulus versus magnetic field intensity for MRE (a) type1, (b) type2, (c) type3, (d) type4, (e) type5, (f) type6.

Examination of results in Figures 3.14 and 3.15 clearly shows the applied magnetic field has significant effect on shear stress-shear strain behavior and thus shear modulus of MREs irrespective of their types, although the effect is more intense for MRE types with higher volume fraction of iron particles (MREs types 5 and 6). As the level of iron particles volume fraction increases, the saturation phenomenon at high level of applied magnetic field is noticeable as shown in Figure 3.15 (f). It is also important to note that the effect of nonlinearity increases by increasing the applied magnetic field and shear strain rate. The nonlinearity effect is further compounded by increasing the volume fraction of iron particles which increases from 12.5% in MRE type 1 to 40% in MRE type 6.

To further compare the magneto-mechanical properties of fabricated MREs, the effects of magnetic field intensity on the shear modulus are presented for all the MRE types in Figure 3.16. As it can be realized, MRE type 6 covers the largest range of shear modulus by the application of 450 *mT* magnetic field intensity compared to all other fabricated MREs. The Zero-field shear modulus, shear modulus at maximum magnetic field intensity, relative and absolute MR effect are major properties of MRE that should be evaluated for each MRE types. It should be noted that here the absolute MR effect is the absolute increase in the shear modulus when the applied magnetic field is increased from zero to the maximum value of 450 *mT* while relative MR effect is the percentage increase with respect to the zero field condition. Table 3.4 compares all the aforementioned magneto-mechanical properties of MREs. Figure 3.17 is the bar graph representation of table 3.4 for a more convenient comparison between the magneto mechanical properties.

First, let us compare the first three types of MRE where the only variable is content of iron particles. As discussed in Chapter 2, MRE types 1, 2 and 3 contain 12.5%, 17.5% and 25% volume fraction of iron particles, respectively. Results show that increasing the volume fraction of iron powder (filler) content has caused the MRE to have higher zero-field shear modulus due to the higher amount of filler material which is stiffer compared to the matrix material. Higher amount of iron particles has also led to establishment of stronger dipoles network that will increase more the shear modulus of MREs under the applied magnetic field, thus yielding to higher absolute and relative MR effects.

The main purpose of fabricating MRE type 4 was to compare its properties with MRE type 3 where the volume fraction of iron particles is the same (25%) while 15 Vol % slacker (playing the role of silicone oil) is added to the matrix by decreasing the silicon rubber volume percentage to 60% from 75% in MRE type 3. Silicone oil is commonly used to prevent agglomeration and to

enhance the compatibility within the silicone blend [18]. This additive also works as a diluting agent to decrease the modulus of silicone elastomer by facilitating frictional sliding at the interface between the matrix and the particles [18]. This is the main reason why the zero field shear modulus of MRE type 4 is less than half of that in MRE type 3. As it is expected, MRE type 4 shows greater relative MRE effect compared to MRE type 3 due to its lower zero-field shear modulus while there is no noticeable difference between the absolute MR effect of these two types of MREs which can be attributed to the same volume percentage of iron particles.

MRE type 5 contains 30 Vol% iron particles close to the critical particles volume concentration (CPVC: see section 1.3.3.2) of BASF SQ - carbonyl iron powder which is reported to be 29.1% [1]. In volume fractions close to CPVC, it is expected to observe the maximum relative MR effect [1]. It is observed that MRE type 5 with 5% more volume content of iron particles than MRE type 4 exhibits 111.34 KPa absolute MR effect showing considerable increase compared to 67.93 KPa for MRE type 4. However, there is no difference between the relative MR effect of MRE type 4 and type 5 due to lower zero-field shear modulus associated with MRE type 4. In fact, there is no specific percentage of iron particles in which the maximum relative MR effect can be achieved. This is attributed to the fact that the relative MR effect is dependent to the matrix material's stiffness at zero-field, so as the matrix is softened using diluting agents such as silicone oil or silicone thinner, the zero-field shear modulus of MRE will decrease, yielding to the higher relative MR effect. For instance, if we increase the volume content of slacker in MRE type 5, the zero-field shear modulus will decrease and then higher relative MR effect can be achieved compared with MRE type 4 with lower content of filler. However, the absolute MR effect is significantly dependent on the content of iron particles, and increases by increasing the content of iron particles regardless of the matrix material as it can be observed from Table 3.4

Finally, MRE type 6 composed of 40 Vol% iron particles, 40 Vol% silicone rubber, 10 Vol% slacker and 10 Vol% silicone thinner exhibit a very low zero-field shear modulus of 32.66 KPa which increases to 214.21 KPa by the application of 450 mT magnetic field density. This is associated with 181.54 KPa absolute MR effect and 555.74% relative MR effect which are the highest among all MRE types investigated here. It is interesting to note that the zero-field shear modulus of MRE type 6 is the lowest among all instigated MREs

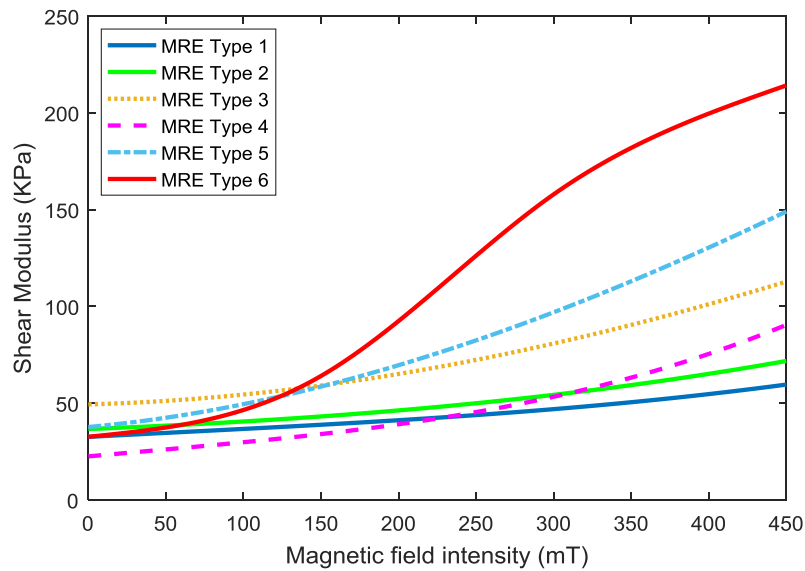


Figure 3.16: Effects of magnetic field intensity on the shear modulus of fabricated MREs obtained from static tests.

Table 3.4: Comparison between the magneto-mechanical properties of fabricated MREs.

MRE type	Zero field shear Modulus (KPa)	Shear Modulus at 450 mT(KPa)	Absolute MR effect (KPa)	Relative MR effect (%)
1	32.62	59.64	27.01	82.80
2	36.67	71.83	35.16	95.90
3	49.40	109.84	60.43	122.31
4	22.53	90.47	67.93	301.41
5	37.72	149.07	111.34	295.15
6	32.66	214.21	181.54	555.74

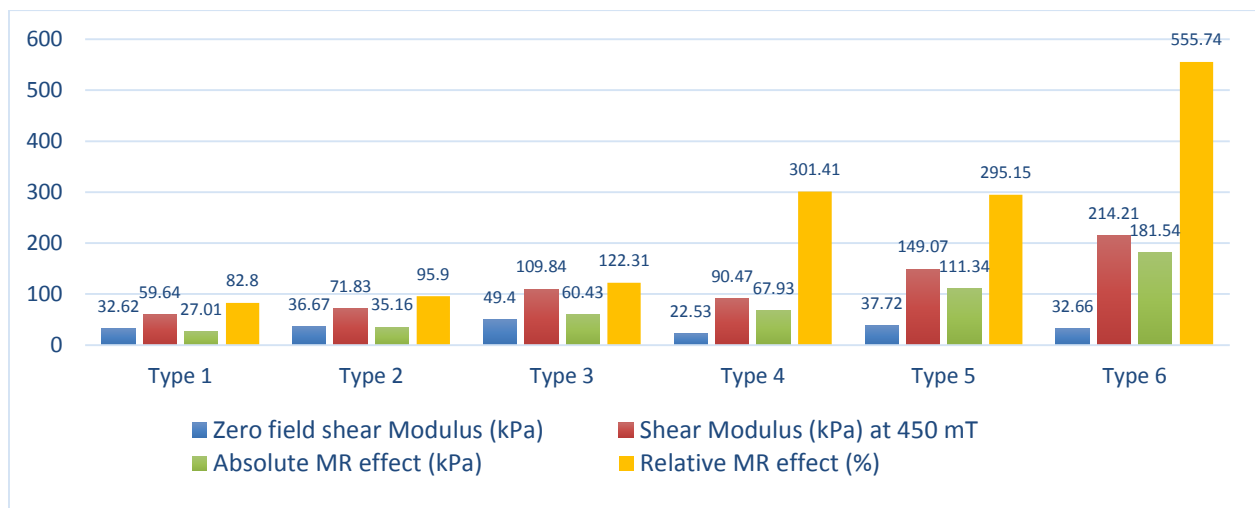


Figure 3.17: Bar graph representation of magneto-mechanical properties of MREs.

The relationship between the magnetic field density and the shear modulus of MRE type 6 obtained from static tests can be derived based on the measured data. For MRE type 6, since the trend of shear modulus versus magnetic field intensity as shown in Figure 3.16 is similar to that of tangent hyperbolic function, thus a tangent hyperbolic function with four constant parameters is used to curve fit on the measured data, expressed as:

$$G(B) = m_1 * \tanh(m_2 * B + m_3) + m_4 \quad (3.17)$$

Where G is the shear modulus of MRE in KPa and the B is the magnetic field intensity in mT . m_1, m_2, m_3, m_4 are the constants to be identified. The parameter vector $Y = \{m_1, m_2, m_3, m_4\}$ of the function $G(B)$ is identified by minimization of the error function $J(Y)$, given by:

$$J(Y) = \sum_{i=1}^n (G_{measured} - G_{model})^2 \quad (3.18)$$

Where n is the number of measured data. The minimization problem is again solved using the least square algorithm for nonlinear curve-fitting problems available in MATLAB optimization toolbox. The optimal results for the constant coefficients were found to be $m_1 = 99.03, m_2 = 0.007138, m_3 = -1.813, m_4 = 126.6$ and the coefficient of determination is calculated to be $R^2 = 1$. Figure 3.18 shows the shear modulus of MRE type 6 at different magnetic field intensities predicted by the proposed model and the measured data.

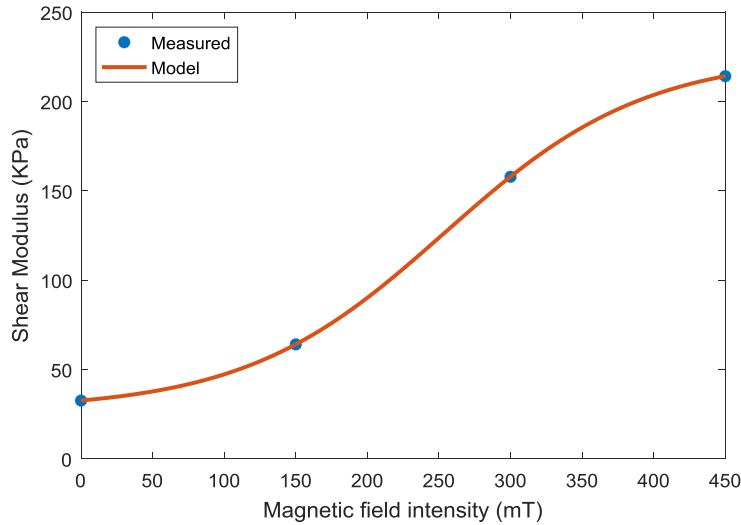


Figure 3.18: Proposed model of shear modulus at different magnetic field densities and the measured data.

3.5 Dynamic properties

As it was mentioned in section 3.2.2, for dynamic characterization, total number of 64 tests were carried out on MRE type 6 (containing 40% volume fraction iron particles) in simple shear mode to capture stress-strain hysteresis loops under various harmonic excitations. The effects of rate, amplitude and magnetic field intensity on the hysteresis loops of MRE are investigated and results are presented in the following subsection.

3.5.1 Effects of excitation frequency

The captured hysteresis loops of MREs in simple shear mode under 10% shear strain amplitude at different magnetic field densities and excitation frequencies are illustrated in Figure 3.19. It can be observed that at lower magnetic field intensities, the excitation frequency has considerable effect on the stiffness or storage modulus (slope of the hysteresis loop) and damping or loss modulus (the area enclosed by the hysteresis loop) characteristics of the MRE. Results show that increasing the excitation frequency at lower magnetic field intensities substantially increases the slope and the area enclosed by the hysteresis loop while at higher magnetic field intensities (especially at 450 mT), the frequency effect considerably diminishes. Also, it can be realized that while the shear strain is constant in all the hysteresis loops shown in Figure 3.19, the shape of hysteresis is changing by enhancement of the applied magnetic field. It can be noticed that the hysteresis shape is transforming from perfectly elliptical at lower magnetic field intensities to non-perfectly elliptical (nonlinear hysteresis) at higher magnetic field intensities. This is attributed to the fact that the effect of nonlinearity as also observed in static testing increases by increasing the applied magnetic field intensity. In other words, at low magnetic field intensities, MREs behave nearly like a linear viscoelastic materials while their behavior follows those of nonlinear viscoelastic materials at elevated magnetic field intensities.

3.5.2 Effects of strain amplitude

Figure 3.20 illustrates the effects of strain amplitude on the hysteresis nonlinearities at excitation frequency of 10 Hz and different magnetic field intensities. It can be observed that the slope of the major axis of hysteresis representative of storage modulus of MRE is dependent to the strain amplitude and this dependency is intensifying by the enhancement of magnetic field intensity. It can also be noted that slope of the major axis of the hysteresis is descending by increasing the strain amplitude confirming the softening effect at higher strain amplitudes. Moreover, in the absence of the applied magnetic field y , the hysteresis shape gradually changes

from perfectly elliptical shape at low strain amplitudes (up to nearly 10%) to non-elliptical non-linear hysteresis shape at high strain amplitudes. This basically confirms that MRE behaves like nonlinear viscoelastic materials at high strain amplitudes regardless of the applied excitation frequency and magnetic field intensity.

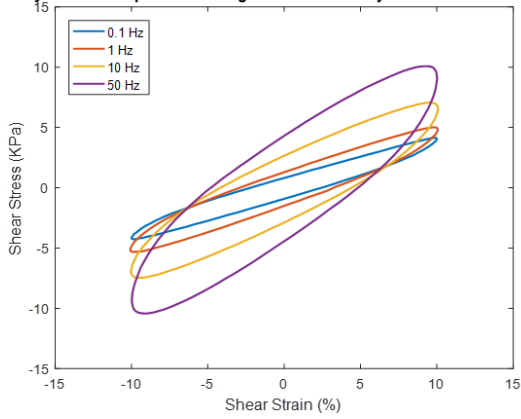
3.5.3 Effects of magnetic field intensity

Magnetic field intensity is the major factor that affects the dynamic behavior of MREs. Figure 3.21 presents the effects of magnetic field intensity on the hysteresis behavior of MREs at excitation frequency of 10 Hz and different strain amplitudes. High dependency of enclosed area (loss modulus) and the slope of the major axis of the hysteresis loop (storage modulus) on the applied magnetic field can be clearly observed in Figure 3.21. In fact, both storage and loss modulus of MREs are substantially increasing by magnifying the magnetic field densities. This observation, completely verifies the strong adaptability of MREs to change their dynamic characteristics by varying the applied magnetic field. This provides a unique opportunity to use these smart materials to control vibration and noise in wide range of applications.

3.5.4 Storage (Elastic) and Loss Moduli of the MREs

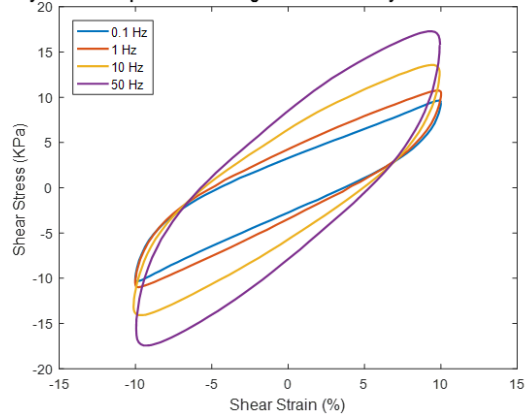
As it was mentioned in section 3.2 – BS ISO 6446, the absolute value of complex shear modulus and the phase angle between the stress and strain can be calculated using the stress-strain hysteresis loop and Eqs. (3.10) and (3.11). These values can then be effectively utilized to evaluate the storage and loss moduli using Eqs. (3.5) and (3.6), respectively. Here the value of absolute complex modulus and sine of phase angle have been evaluated for each of the 64 captured hysteresis loops and then they are subsequently used to evaluate the storage and loss moduli of the MREs. Similar to the hysteresis nonlinear loops, the effects of rate, amplitude and magnetic field intensity on the storage and loss moduli of MREs have been thoroughly investigated. The results are presented in the following.

Hysteresis Loops at: 0mT Magnetic field intensity & 10% Shear Strain



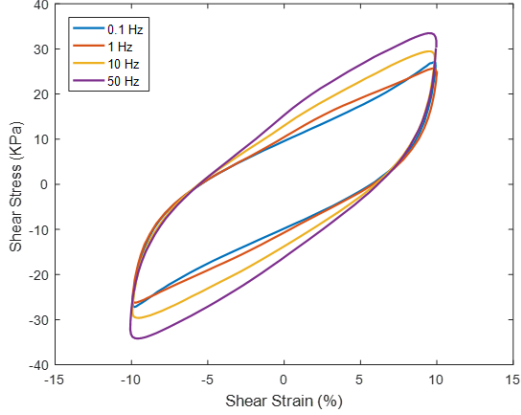
(a)

Hysteresis Loops at: 150mT Magnetic field intensity & 10% Shear Strain



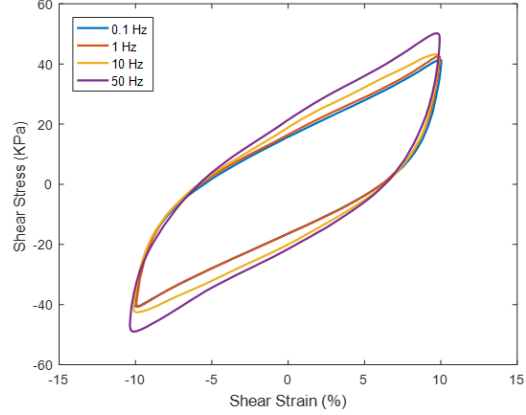
(b)

Hysteresis Loops at: 300mT Magnetic field intensity & 10% Shear Strain



(c)

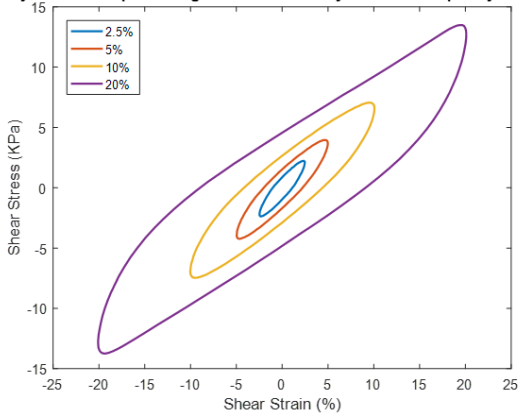
Hysteresis Loops at: 450mT Magnetic field intensity & 10% Shear Strain



(d)

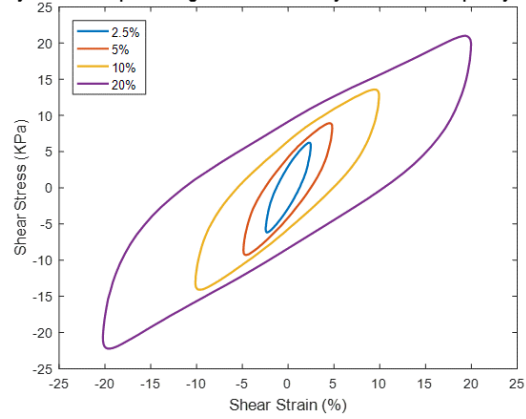
Figure 3.19: Measured hysteresis nonlinearities of MRE in simple shear mode under different frequencies with 10% shear strain and (a) magnetic field intensity: 0mT, (b) magnetic field intensity: 150mT, (c) magnetic field intensity: 300mT, (d) magnetic field intensity: 450mT.

Hysteresis Loops at: Magnetic field intensity = 0mT & Frequency = 10Hz



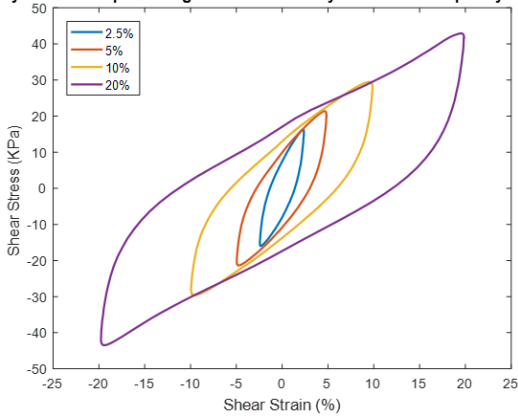
(a)

Hysteresis Loops at: Magnetic field intensity = 150mT & Frequency = 10Hz



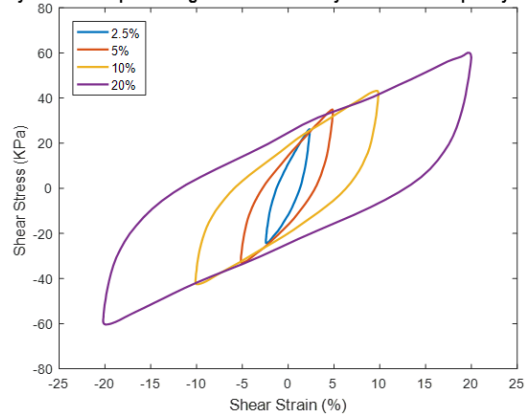
(b)

Hysteresis Loops at: Magnetic field intensity = 300mT & Frequency = 10Hz



(c)

Hysteresis Loops at: Magnetic field intensity = 450mT & Frequency = 10Hz



(d)

Figure 3.20: Measured hysteresis nonlinearities of MRE in simple shear mode under different strain amplitudes at 10 Hz and (a) magnetic field intensity: 0mT, (b) magnetic field intensity: 150mT, (c) magnetic field intensity: 300mT, (d) magnetic field intensity: 450mT.

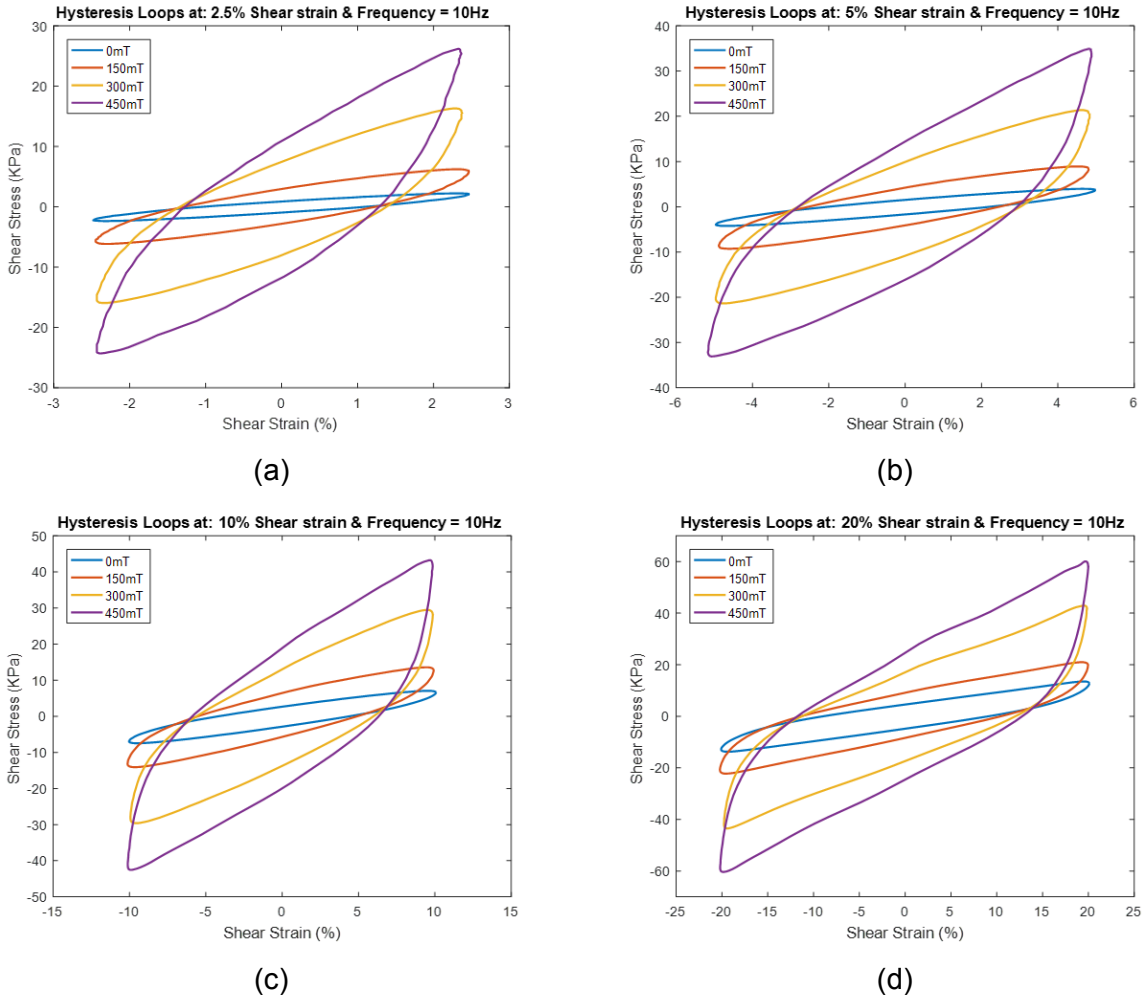


Figure 3.21: Measured hysteresis nonlinearities of MRE in simple shear mode at different magnetic field intensities under excitation frequency of 10 Hz and (a) shear strain amplitude: 2.5%, (b) shear strain amplitude: 5%, (c) shear strain amplitude: 10%, (d) shear strain amplitude: 20%.

3.5.4.1 Effects of excitation frequency

The variation of elastic shear modulus versus excitation frequency for different strain amplitudes and magnetic field densities are shown in Figure 3.22. It can be realized that the elastic shear modulus is increasing by increasing the excitation frequency demonstrating the strain-rate stiffening effect. In the absence of the magnetic field intensity, the elastic modulus is showing exponential increase by increasing the excitation frequency while its dependency on the frequency significantly diminishes by increasing the magnetic field intensity so that it is nearly constant (specially at low strain amplitudes) over the considered frequency range.

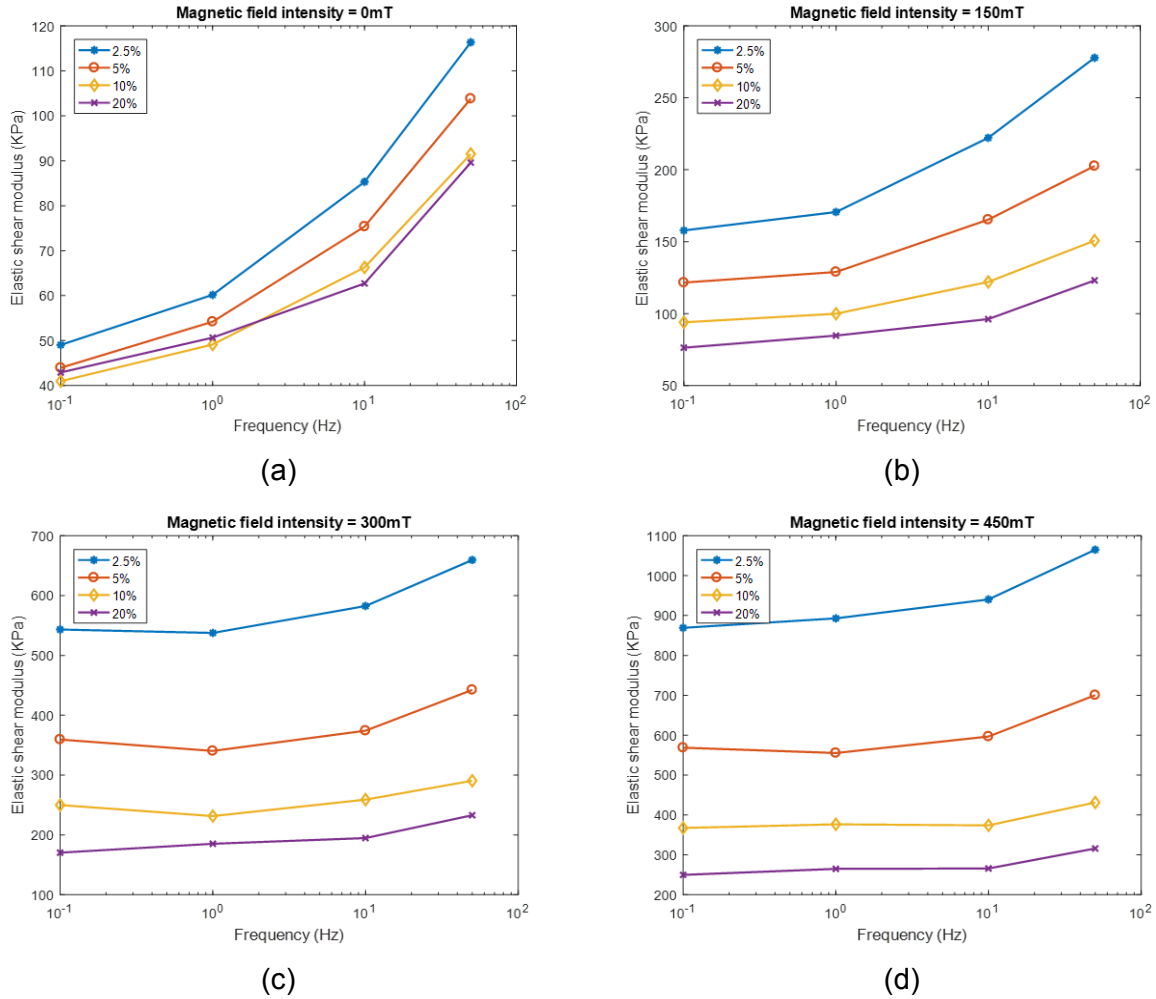


Figure 3.22: Effects of excitation frequency on the elastic shear modulus of MRE at different strain amplitudes and (a) magnetic field intensity: 0mT, (b) magnetic field intensity: 150mT, (c) magnetic field intensity: 300mT, (d) magnetic field intensity: 450mT.

Similar to the storage modulus, the loss shear modulus of the MREs is also strongly dependent on the loading frequency especially at low applied magnetic field densities. Figure 3.23 shows the effects of excitation frequency on the loss shear modulus of the MREs in different strain amplitudes and magnetic field intensities. Results clearly show that increasing the excitation frequency will lead to the higher loss shear modulus values while the relative increase in the value of loss shear modulus is higher in lower magnetic field intensities. It is noted, the relative increase in loss shear modulus in higher applied magnetic field is more noticeable compared with that of storage modulus. For instance, in the absence of the applied magnetic field intensity, the value of loss shear modulus at 2.5 % shear strain amplitude shows relative increase of 408.37% (11.95 kPa to 60.75 kPa) in the frequency range of 0 to 50 Hz while at 450mT magnetic field

intensity, the relative increase is around 33.74% (392.7 KPa to 525.2 KPa) which is still considerable. It should also be noted that the absolute increase in the loss shear modulus is 48.8 KPa and 132.5 KPa at 0mT and 450 mT magnetic field densities confirming that in high magnetic field intensities, still the loss shear modulus is quite dependent upon the excitation frequency. Finally, it can be realized that similar to the storage modulus, the loss modulus decreases by increasing the strain amplitude regardless of the applied magnetic field intensities.

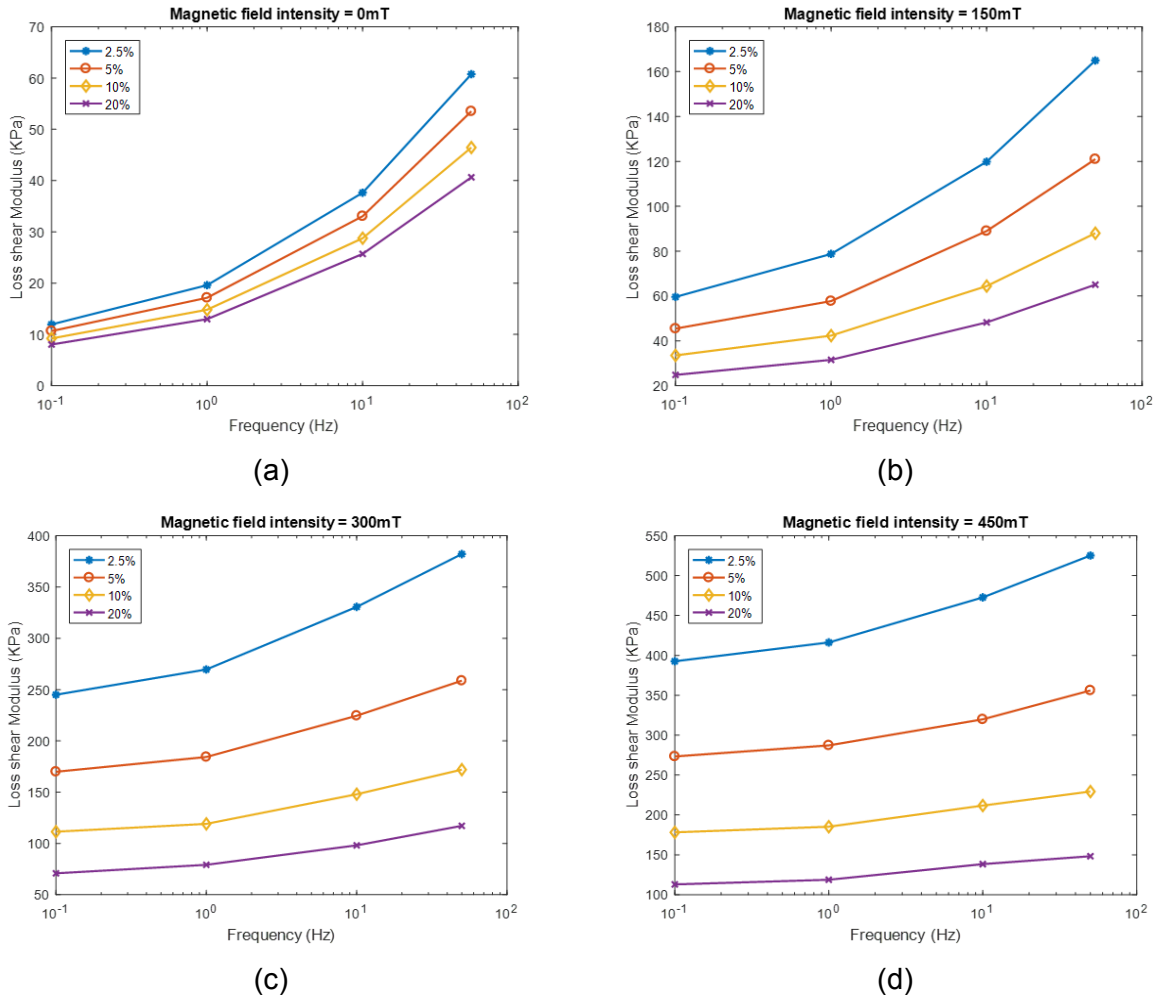


Figure 3.23: Effects of excitation frequency on the loss shear modulus of MRE at different strain amplitudes and (a) magnetic field intensity: 0mT, (b) magnetic field intensity: 150mT, (c) magnetic field intensity: 300mT, (d) magnetic field intensity: 450mT.

3.5.4.2 Effects of strain amplitude

Figure 3.24 shows the dependency of elastic shear modulus on the amplitude of excitation in different frequencies and magnetic field densities. It is observed that the elastic shear modulus decreases by increasing the amplitude of excitation, however the rate of decrease substantially declines for strain amplitudes beyond 10%. It is also interesting to note that strain dependency of elastic shear modulus of MRE increases by enhancement of the magnetic field intensity.

Similar behavior is also observed on the effect of loading strain amplitude on the loss shear modulus of MRE as shown in Figure 3.25. Similar to the storage modulus, the loss modulus decreases substantially at low strain amplitude while the rate of decrease declines at higher strain amplitudes. Also the dependency of the loss modulus on the strain amplitude is more pronounced for higher applied magnetic field.

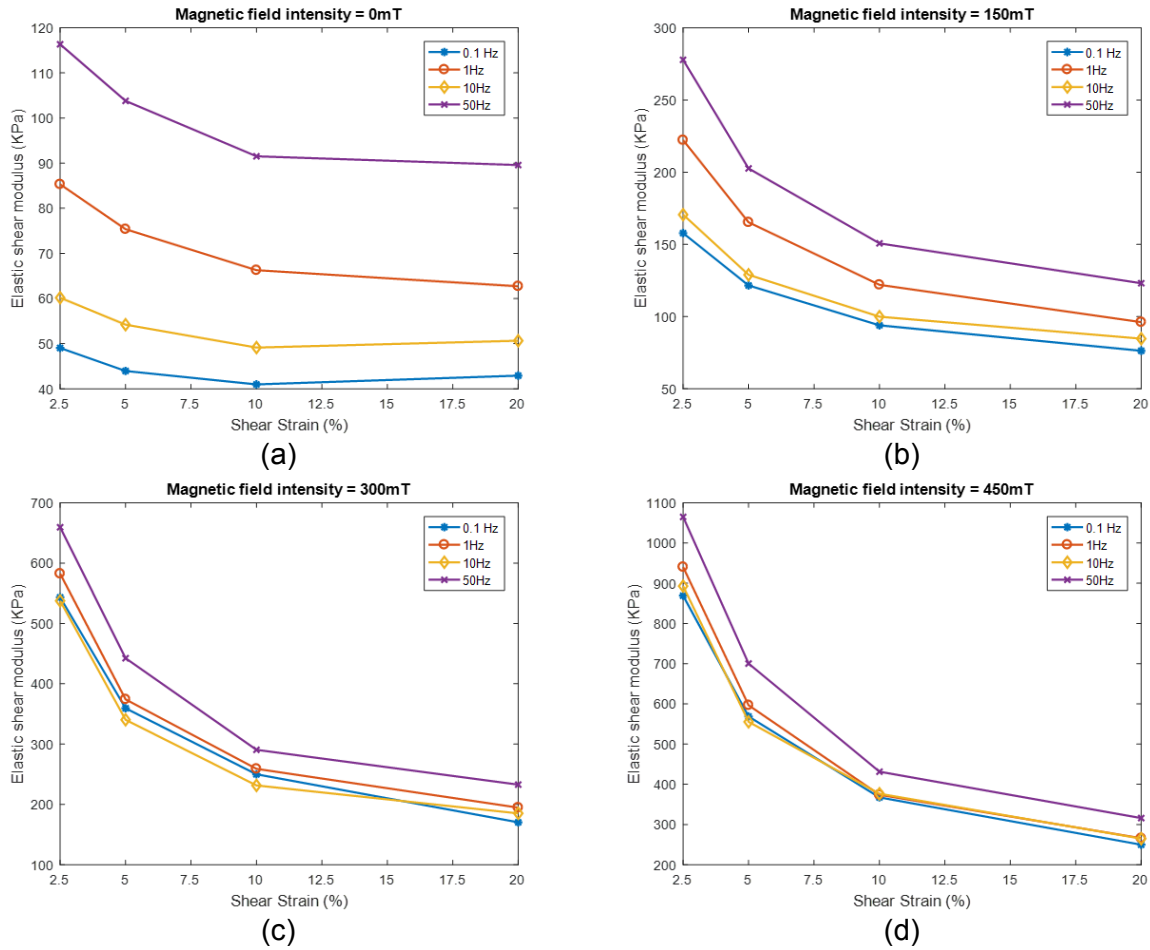


Figure 3.24: Effects of strain amplitude on the elastic shear modulus of MRE at different excitation frequencies and (a) magnetic field intensity: 0mT, (b) magnetic field intensity: 150mT, (c) magnetic field intensity: 300mT, (d) magnetic field intensity: 450mT

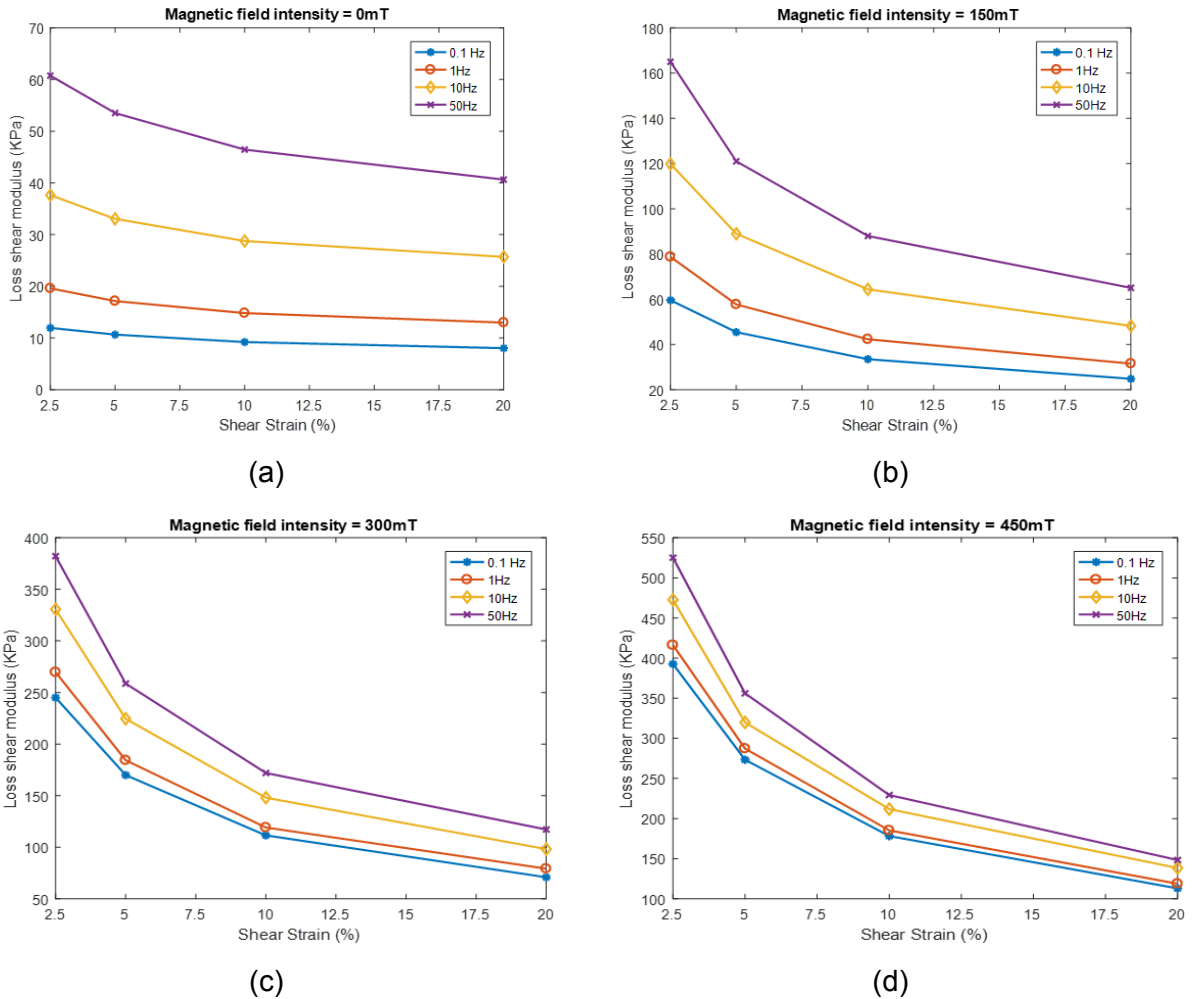


Figure 3.25: Effects of strain amplitude on the loss shear modulus of MRE at different excitation frequencies and (a) magnetic field intensity: 0mT, (b) magnetic field intensity: 150mT, (c) magnetic field intensity: 300mT, (d) magnetic field intensity: 450mT.

3.5.4.3 Effects of magnetic field intensity

Effects of frequency and strain amplitude on the dynamic behavior of MREs is mainly related to the viscoelastic nature of these smart materials. However what is turning this unique composites into smart materials is the magnetic field dependency of their elastic and loss moduli. The field dependency of storage and loss moduli of MRE at different frequencies and strain amplitudes are shown in Figures 3.26 and 3.27, respectively. As it can be realized, both the elastic and loss shear moduli of MREs are increasing exponentially by enhancement of the magnetic field, regardless of the excitation frequencies and strain amplitudes while the saturation phenomenon can be observed at high strain amplitude of 20%. In other words, at 2.5%, 5% and 10% strain amplitudes, both elastic and loss shear moduli tend to increase by enhancement of

the magnetic field up to 450mT without observing the saturation while at 20% shear strain amplitude, it can be seen that the slope of the line connecting the data points at 300mT to 450mT is decreased compared to the line connecting the data points at 150mT to 300 mT which shows possible saturation in higher magnetic field intensities.

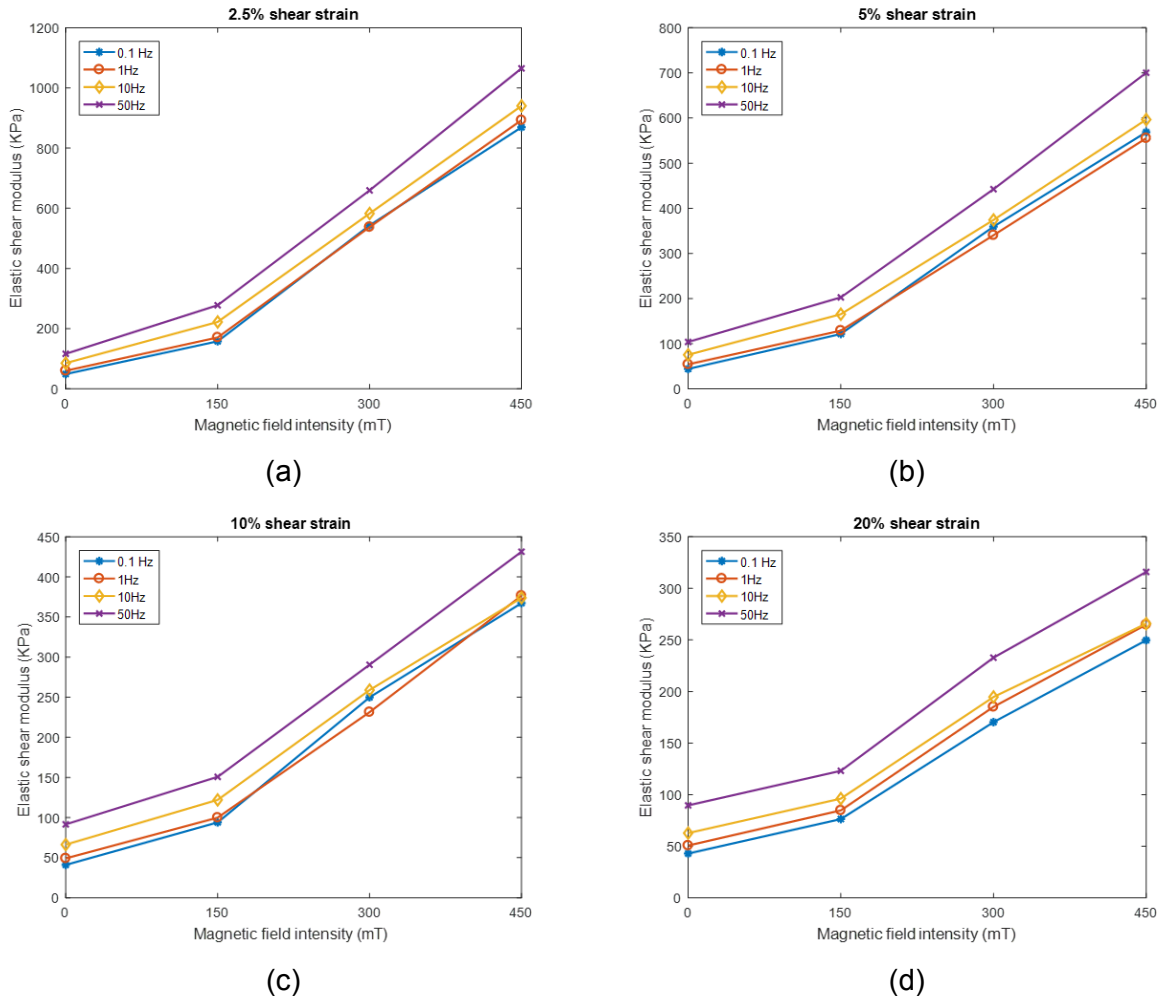


Figure 3.26: Effects of magnetic field intensity on the elastic shear modulus of MRE at different excitation frequencies and (a) shear strain amplitude: 2.5%, (b) shear strain amplitude: 5%, (c) shear strain amplitude: 10%, (d) shear strain amplitude: 20%.

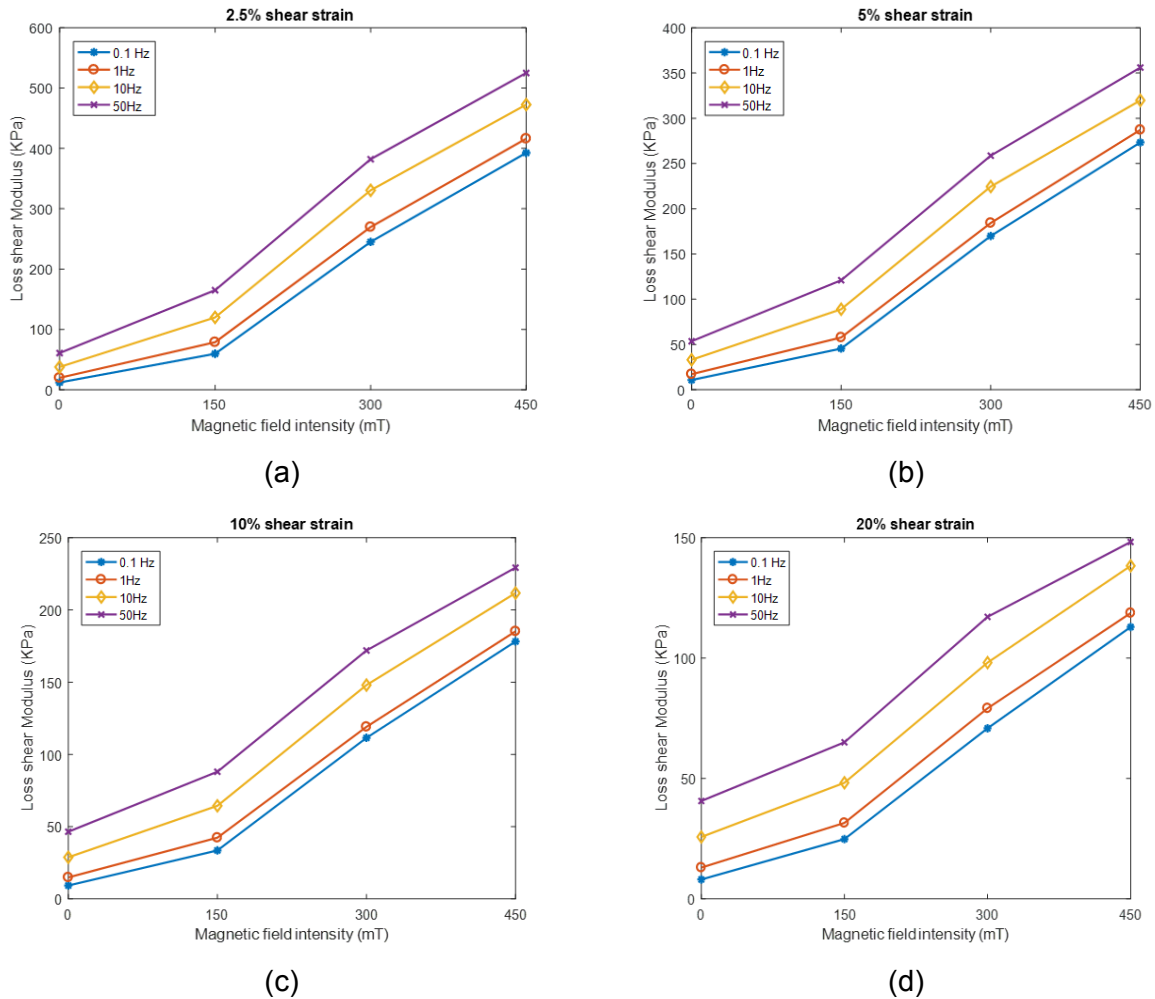


Figure 3.27: Effects of magnetic field intensity on the loss shear modulus of MRE at different excitation frequencies and (a) shear strain amplitude: 2.5%, (b) shear strain amplitude: 5%, (c) shear strain amplitude: 10%, (d) shear strain amplitude: 20%.

3.6 Discussion on factors influencing static and dynamic properties

Due to the viscoelastic nature of MREs, they share similar properties with rubbery type materials. Figure 3.28 shows a typical stress-strain curve of MRE under applied magnetic field obtained from static tests in simple shear mode. The graph is divided into three regions where the strain softening and strain stiffening effects can be observed in transition between region one to region two and region two to region three, respectively. The strain softening effect can be explained by the breakdown of filler aggregates leading to release trapped rubber for allowing more viscous flow, disconnection of dipole-dipole interaction between neighbor particles and filler rubber detachment and reformation that is intensified by increasing the strain amplitude [78].

Additionally, it can be observed from the stress-strain curves of all the fabricated MREs (see Figures 3.14) that the strain softening effect is more pronounced under higher magnetic field intensities. This is mainly due to the fact that increasing the strain will lead to an increase in the distance between the dipoles and at a certain distance, the magnetic network that was structured by the dipoles will break down causing a significant decrease in shear modulus of MRE. On the other hand, the strain stiffening effect is mainly due to the polymeric nature of MREs. The polymeric chains are long enough to form loops causing strain-stiffening, in which the shear modulus of material increases with strain. This effect will help the material to sustain greater orders of stress. The polymeric chain loops do not yield until the chain links break.

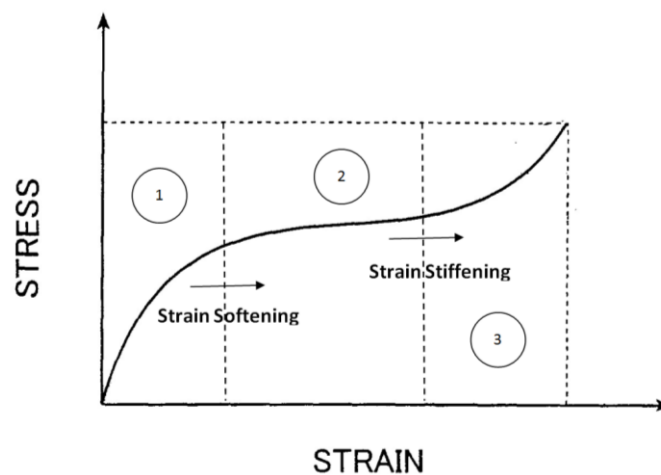


Figure 3.28: A typical stress-strain curve of MRE in simple shear mode under applied magnetic field.

The strain softening and strain stiffening effects can also be seen in the dynamic behavior of MREs. The strain softening effect of rubbers was first studied by Fletcher and Gent [52] and Payne [52] made extensive studies of the effect. The Payne effect also known as Fletcher-Gent effect is a principal feature of stress-strain behavior of rubber, especially rubber compounds containing filler such as carbon black [53]. This phenomena is defined as decrease in the dynamic modulus of rubber by increasing the amplitude of excitation. Due to polymeric nature of MREs, these smart composites also exhibit the Payne effect. Figure 3.29 shows the strain softening effect in a hysteresis loop of MRE type 6 at 20% shear strain. When the amplitude of dynamic excitation is small, only minor reorganization occurs in the network structure formed by the filler particles [18]. By increasing the strain, the particle network structure starts to break which will lead to increase of distance between the dipoles [51]. Therefore, above a critical strain amplitude, the storage modulus of MRE decreases drastically. Sorokin et al. [79] reported that the Payne effect

in the absence of magnetic field begins at 1% and 0.1% amplitude for isotropic and anisotropic MREs, respectively.

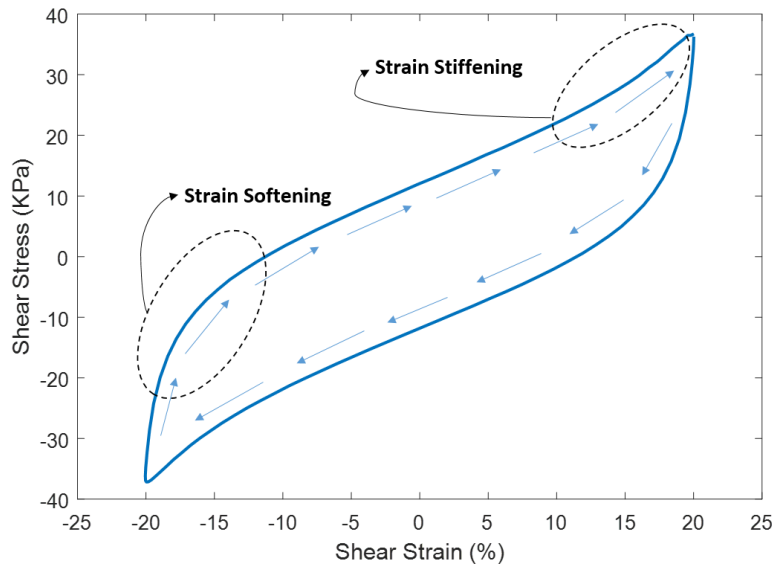


Figure 3.29: Measured stress-strain hysteresis loop of MRE type 6 at 20% shear strain, 0.1 Hz excitation frequency and 300 mT magnetic field intensity.

In this study, the result shows that in the absence of magnetic field, the strain softening effects is minimal while at 10% shear strain the effect is noticeable. However, in the presence of the magnetic field the strain softening behavior is considerable even under small strain amplitudes. In fact, the magnetic filler network is highly active in the presence of the magnetic field which leads to large increase in the dynamic moduli of MRE while it makes the dynamic moduli significantly dependent to strain amplitude [18]. For small deformations, the dipole network is slightly disturbed while large deformations destroys the magnetic particle network resulting in softening of the material [18]. The fact that magnetic field intensifies the Payne effect has been reported in literature as well [80, 81]. On the other hand, strain stiffening effect is noticeable when both the magnetic field intensity and strain amplitude are more than 300 mT and 20%, respectively.

In perfect elastic materials, when the stress is removed the energy within the material is completely recovered while in viscoelastic materials, the viscosity originating from the internal molecular friction slows down the elastic strain response leading to energy loss in the form of heat [18]. In MREs the damping is originated from the viscous flow of the rubber matrix arising from molecular chain motion in the polymer and also interfacial frictional damping at the interface

between the particles and the matrix [82]. Throughout these mechanisms the mechanical energy converts into heat, demonstrating the damping of MREs exhibiting the area inside the hysteresis loop. Therefore, by increasing the amplitude of loading the area enclosed by the hysteresis increases indicating that the amount of energy dissipated per cycle is increased.

The dynamic properties of elastomers is rate dependent and generally, increasing the motion frequency increases the storage and loss moduli of elastomers. MREs also exhibit strain-rate dependent behavior demonstrating strain-rate stiffening effect by increase the excitation frequency. Increasing the strain rate does not provide enough time chain rubber to relax , thus resulting in larger stress orders for a given strain [18]. Consequently, the stiffness of MREs represented by the slope of the major axis of the hysteresis loop and equivalent damping of MRE demonstrated by the area enclosed by the hysteresis are highly frequency dependent. The results of this study also shows that elastic and loss moduli of MREs are increasing by increasing the loading frequency regardless of the applied magnetic field intensity. However, the strain-rate dependency of both stiffness and damping of MRE is greater for higher magnetic field intensities.

3.7 Summary

A double lap shear test set-up is designed to characterize magneto-mechanical properties of different types of fabricated MREs in simple shear mode based on the ISO standard. The test specimens are manufactured using 3D printing technology. Magnetic field is generated using Neodymium permanent magnets and analytical magnetic field analysis is conducted to verify the intensity of the applied magnetic field measured experimentally using Gauss meter. All the 6 types of fabricated MREs are characterized statically under different magnetic field intensities. The effects of the magnetic field on the stress-strain curves and shear modulus of MREs are investigated. It is demonstrated that MRE type 6, by the application of 450 mT magnetic field intensity exhibits a notable relative MR effect of 555% with 181.54 KPa increase in the MRE shear modulus. MRE type 6 which exhibits the highest MRE effect is then chosen for dynamic characterization under the harmonic excitation. Total number of 64 dynamic tests are carried out in a wide range of loading strain amplitudes and frequencies and magnetic field intensities. Effect of loading conditions and the magnetic field intensity on both elastic and loss moduli of MREs are investigated and interpretation of experimental results is performed in details. The strain softening, strain stiffening, strain rate stiffening and magnetic field stiffening are identified as the nonlinear characteristics of the MRE stress-strain hysteresis loops.

Chapter 4: Modeling of Dynamic Properties of MREs

4.1 Introduction

Considerable efforts have been reported for accurate modeling of dynamic behavior of the MREs. Such models are vital for developing control strategies for the adaptive mechanisms based on the MREs. The reported studies have attempted to describe the stress-strain characteristics of the MREs and the hysteresis using two general approaches. These include physics-based models and phenomenological models. The physics-based models, however, involve considerable simplifying assumptions and are generally independent of the strain amplitude and the strain rate [10, 55]. Moreover, for describing properties of different types of MREs, the generalization of physics-based models poses complexities due to widely different physical properties of the MREs [56].

Alternatively, the reported phenomenological models have shown improved ability to predict hysteresis effect in magnetorheological elastomers, and its dependence on loading conditions [3, 34]. The phenomenological hysteresis models can be classified into differential equation-based models and operator-based models. Bouc-Wen model is one of the well-known differential equation-based phenomenological models that has been utilized widely to model hysteretic systems such as smart material actuators [83], MR fluid dampers [84] and MRE-based adaptive devices [2]. The major limitation of the Bouc-Wen model is related to the parameter identification of the differential equation-based model. Furthermore, differential equation-based models are not invertible and thereby, pose complexities for implementation in inverse model-based compensations [56]. On the other hand, operator-based models are considered more suited and relatively simpler for modeling hysteretic systems and design of control algorithms [56, 60, 85]. Prandtl-Ishlinskii operator-based model, in particular, has been considered better suited for controller design due to its analytic invertibility [56, 60]. Although, the operator-based hysteresis models have been widely applied for modeling the nonlinear hysteresis phenomena in smart material actuators [60, 86], their applications to MREs nonlinear hysteresis phenomena have not yet been reported. In this chapter, the classical stop-operator-based Prandtl-Ishlinskii model is formulated to describe the hysteretic stress-strain properties of the MRE, and its validity is demonstrated using the measured data acquired for the fabricated MRE in the simple shear mode. Subsequently, the model is generalized by introducing model parameters dependence on the frequency and magnetic field intensity.

4.2 Classical Prandtl-Ishlinskii model

The Prandtl-Ishlinskii (PI) model either employs summation of either the play or stop operators and a density function to describe the input-output hysteresis relationships of smart materials and actuators. The stop and play operators yield clock-wise and counter clock-wise output-input hysteresis loops, respectively. Considering that the MREs exhibit clock-wise stress-strain hysteresis loops under loading and unloading, the stop operators are used to formulate the PI model. The stop operators and the classical PI model formulations are presented in the following sections.

4.2.1 A Stop hysteresis operator

The stop hysteresis operator, as the fundamental element of the classical Prandtl-Ishlinskii model, has been thoroughly described in [67]. This hysteresis operator is rate-independent, continuous and symmetric. The input-output character of a stop operator, shown in Figure 4.1, is a function of the threshold r , which is a positive constant and directly related to the output-input hysteresis nonlinearity. The stop operator describes the relationship between input v and output $E_r[v](t)$, which was originally proposed to characterize the elastic-plastic behavior in continuum mechanics [70].

Let $C_m[0, T]$ represent the space of piecewise monotone continuous functions, such that the input function v is monotone on the sub-intervals $[t_i, t_{i+1}]$. The output of the stop operator $E_r[v]$ can be analytically described as [67]:

$$\begin{aligned} w(0) &= e_r(v(0)) \\ w(t) &= e_r(v(t) - v(t_i) + w(t_i)); \quad 0 \leq i \leq N - 1 \\ E_r[v](t) &= w(t) \end{aligned} \tag{4.1}$$

Where $t_0 = 0 < t_1 < \dots < t_N = T$ are the intervals within $[0, T]$, and:

$$e_r(r) = \min(r, \max(-r, v)) \tag{4.2}$$

In the above formulation, $w(t)$ is the output of the stop operators. Some of the key properties of the stop operator are briefly summarized below:

- **Lipschitz-continuity:** For a given input $v(t)$ and the threshold $r \geq 0$, the output of the stop operator can be extended to Lipschitz continuous [67]. This property plays an important role for construction of the analytical inverse of the Prandtl-Ishlinskii model required for compensation of hysteresis effects in real time control applications [56].
- **Memory effect:** the stop operator is a hysteresis operator with non-local-memory effect, which implies that the output of the operator depends not only on the current value of the input but also on the previous values of the output [67].

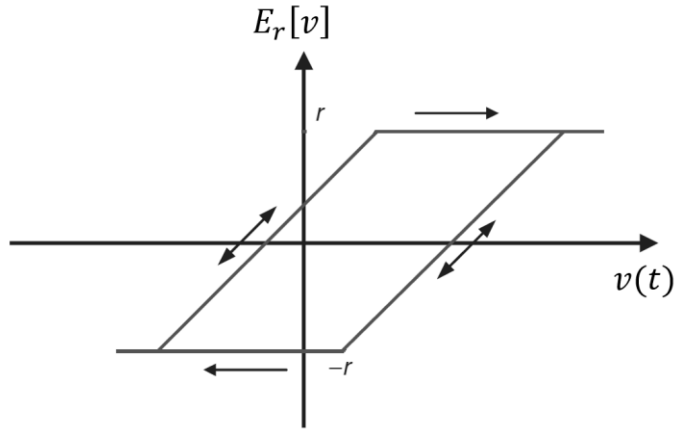


Figure 4.1: The input-output properties of the stop hysteresis operator.

4.2.2 Classical Prandtl-Ishlinskii model

The Prandtl-Ishlinskii hysteresis model is formulated upon integration of a number of weighted stop operators. The relationship between output $\Omega[v](t)$ of the Prandtl-Ishlinskii model and input $v(t)$ can be expressed, as [67]:

$$\Omega[v](t) = \int_0^R p(r)E_r[v](t)dr \quad (4.3)$$

Where $p(r)$ is an integrable density function, satisfying $p(r) > 0$, which provides weighting for the stop operators. In the above model, the integration limit $R = +\infty$. The choice of $+\infty$ as the integration upper limit is only for the sake of convenience, since it is reasonable to assume that the density function p vanishes for large values of r [67]. The density or weighting function is generally identified from the measured output-input properties of the material or the device. Since only a finite number of operators are generally needed to model the output-input hysteresis, the output of the Prandtl-Ishlinskii model can also be expressed by the following summation [56]:

$$\Omega[v](t) = \sum_{j=1}^n p(r_j) E_{r_j}[v](t) \quad (4.4)$$

Where n is the number of stop operators. The key features of the stop operators and the stop operator-based PI model are illustrated using the following simulation example.

Example 4.1: Consider the input of the form $v(t) = 20 \sin(2\pi t)$ and $T = 2$ s. The output-input characteristics of 3 different stop operators are obtained, as shown Figure 4.2 (a). In the simulation example, the threshold values, r_j are considered as:

$$r_j = 3j; \quad (j = 1, 2, \dots, n) \quad (4.5)$$

The output-input characteristics of the PI model integrating only five stop operators are obtained from Eqn. (4.4) using $n = 5$ and the density function of the form:

$$P(r_j) = 2r_j^{-2} \quad (4.6)$$

The results show that output-input relations for each stop operator is in the form of symmetric hysteresis loops, which is attributed to symmetric nature of the stop operator. It is further seen that the width of the hysteresis loop of the stop operator is directly dependent on r . Moreover, the output-input hysteresis curves follow the clockwise direction as observed in the stress-strain hysteresis loops obtained for the MRE samples. Figure 4.2 (b) illustrates the output-input characteristics of the Classical PI model. It is evident that the summation of weighted stop operators yields symmetric output-input hysteresis response. From the results in Figure 4.2, it may be deduced that the stop operator-based classical PI model may be applied for describing symmetric dynamic shear stress-strain characteristics of MREs with strain softening effect (see section 3.5). The classical PI model, however, may lead to small errors under low magnitude and frequency of shear strain as well as low magnetic field intensity, where the nonlinear strain softening effect is negligible and the stress-strain hysteresis loops of the MRE are nearly elliptic.

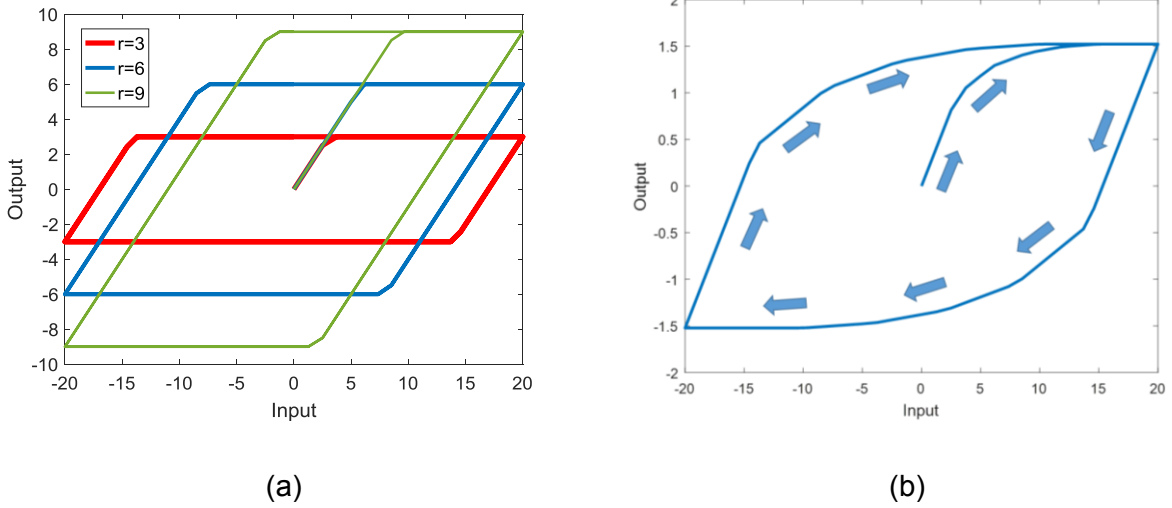


Figure 4.2: Input-output characteristics of: (a) stop hysteresis operators with different threshold values; and (b) the classical Prandtl-Ishlinskii model integrating five stop operators under $v(t) = 20 \sin(2\pi t)$.

4.3 Classical Prandtl-Ishlinskii model for characterizing hysteresis in MREs

Classical Prandtl-Ishlinskii model has been widely used for characterizing symmetric and rate-independent hysteresis properties of the piezo-ceramic and magnetostrictive actuators [56, 87]. In this section, the properties of the classical PI model are explored for describing the hysteresis stress-strain loops of the MREs in simple shear. The measured data, invariably, revealed saturation of the stress under increasing strain, strain rate and magnetic field intensity. It has been suggested that the density function of an exponential form can effectively describe output saturation under increasing input [69]. The density function in the form of a power function is chosen in this study to describe the strain softening effect, such that:

$$p(r_j) = w_1 r_j^{-w_2} \quad (4.7)$$

Where w_1 and w_2 are positive constants. The threshold function is expressed in the exponential form, as:

$$r_j = c_1 e^{-c_2 j} \quad ; \quad j = 1, 2, 3, \dots, n \quad (4.8)$$

Where c_1 and c_2 are positive constants and n is the number stop hysteresis operators to be employed in the model. The proposed density function may also be described as a function of j , such that:

$$p_j = k_1 e^{k_2 j} \quad ; \quad j = 1, 2, 3, \dots, n \quad (4.9)$$

In the above formulations, k_1 and k_2 are positive constants.

4.3.1 Model parameter identification

Owing to the highly nonlinear effects of the strain amplitude, strain rate (frequency) and magnetic field intensity on the shear stress-strain properties of the MREs, the model constants are expected to depend on these factors. The model is initially formulated for the range of strain amplitude considered, for each excitation frequency and field intensity. Subsequently, parameter identification is performed, which resulted in the model parameters as functions of the frequency and the field intensity.

The parameters of the strain amplitude-independent classical Prandtl-Ishlinskii (PI) model Ω were identified through minimization of a sum squared error function J over the range of strain amplitudes for each excitation frequency and magnetic field intensity, expressed as:

$$J(X) = \sum_{q=1}^Q \sum_{m=1}^M W_q (\Omega(v(m, \gamma_q)) - Y(m, \gamma_q))^2 \quad (4.10)$$

Where $\Omega(v(m, \gamma_q))$ is the response of PI model under a given strain amplitude and $Y(m, \gamma_q)$ is the measured shear stress under the same strain amplitude. The index m ($m = 1, 2, \dots, M$) denotes the number of data points considered for each strain amplitude and $Q = 4$ is the number of strain amplitude considered. In the above error function, W_q defines the weighting corresponding to the strain amplitude γ_q . The weighting was defined as the ratio of the peak shear stress at the highest strain amplitude ($\gamma_q = 20\%$) to that under the strain amplitude at γ_q . The minimization problem was solved considering $M = 100$ data points for each strain amplitude for specific frequency and magnetic field intensity. This resulted in a total of 16 sets of model parameters for the range of loading conditions considered, which involved four levels of excitation frequency (0.1, 1, 10 and 50 Hz) and four levels of field intensity (0, 150, 300 and 450 mT). The minimization problem was solved using the nonlinear least squares method in the MATLAB optimization toolbox subject to the following constraints:

$$\{c_1, c_2, k_1, k_2\} > 0.$$

The solutions generally showed very low sensitivity of parameter c_2 on the excitation frequency and the field intensity. An equality constraint ($c_2 = 1.31$) was subsequently introduced on the basis

of the mean value obtained under different excitation conditions. Moreover, the constant c_1 was observed to be nearly insensitive to the magnetic field intensity variations. Equality constraints were defined to ensure variations in c_1 with excitations frequency only.

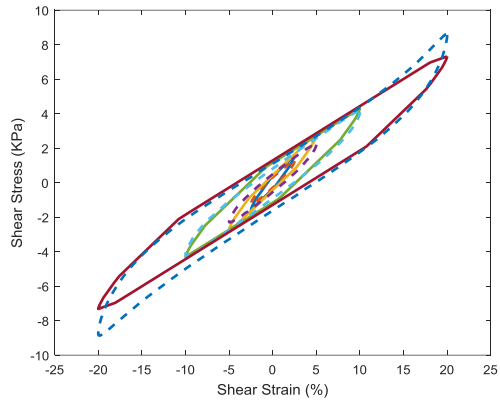
The solution of the minimization problem were subsequently attained for different starting parameter values, which converged to similar solutions. Moreover, the model with ten stop operators could yield reasonably accurate characterization of the MRE stiffness and hysteresis nonlinearities. Table 4.1 summarizes the model parameters identified as functions of the excitation frequency and magnetic field intensity. The result show that the constant c_1 and c_2 and thereby, threshold function r_j is insensitive to the magnetic field. The constants k_1 and k_2 , and ths the density function p_j , however, is strongly dependent on the frequency as well as the magnetic field intensity.

Table 4.1: Variations in parameters of the classical Prandtl-Ishlinskii model with the excitation frequency and magnetic field intensity.

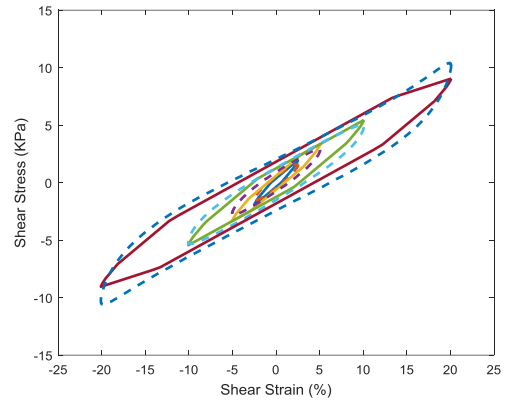
Frequency (Hz)	c_1	c_2	k_1	k_2
Magnetic field intensity = 0 mT				
0.1	13.10	1.31	5.01	0.29
1	12.26	1.31	4.45	0.43
10	11.56	1.31	4.15	0.55
50	10.97	1.31	4.00	0.66
Magnetic field intensity = 150 mT				
0.1	13.10	1.31	5.11	0.50
1	12.26	1.31	4.53	0.59
10	11.56	1.31	4.33	0.69
50	10.97	1.31	4.14	0.78
Magnetic field intensity = 300 mT				
0.1	13.10	1.31	9.55	0.60
1	12.26	1.31	9.29	0.63
10	11.56	1.31	8.46	0.69
50	10.97	1.31	7.50	0.79
Magnetic field intensity = 450 mT				
0.1	13.10	1.31	14.24	0.61
1	12.26	1.31	13.42	0.63
10	11.56	1.31	12.03	0.69
50	10.97	1.31	9.26	0.80

4.4 Model verification

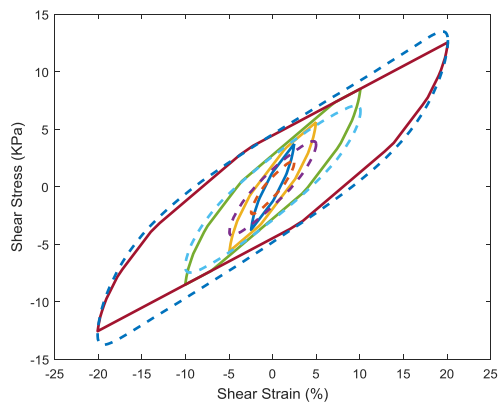
Validity of the stop operator-based Prandtl-Ishlinskii model is investigated by comparing the model responses with the measured data in terms of stress-strain hysteresis loops over the entire range of strain amplitudes, frequencies and magnetic field intensities. Figures 4.3(a) to 4.3(d) compare the stress-strain hysteresis loops obtained from the model and the measured data under 0 mT applied magnetic field intensity and excitation frequencies of 0.1, 1, 10 and 50 Hz, respectively. The comparisons under the application of 0 mT , 150 mT , 300 mT and 450 mT magnetic field intensities are shown in Figures 4.3-6, respectively. The comparisons suggest reasonably good agreements between the model-predicted stress-strain characteristics and the measured data for the loading conditions considered. The comparisons also show notable errors between the model results and the measured data only under 0 mT field intensity. The effectiveness of the model in predicting shear stress-strain characteristics of the MRE is more evident under the application of the magnetic field intensity, as seen in Figures 4.4 to 4.6. It can be seen that the model predict the strain softening effect of the MRE accurately, which has been also reported in studies reporting experimental characterization of MREs [2, 3]. The coefficient of determination (R^2) between the model results and the measured data were generally above 0.98, with the exception of those corresponding to very low strain amplitudes under the application of 0 mT magnetic field intensity.



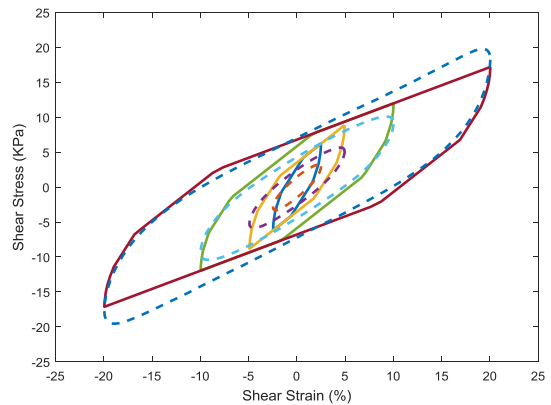
(a)



(b)

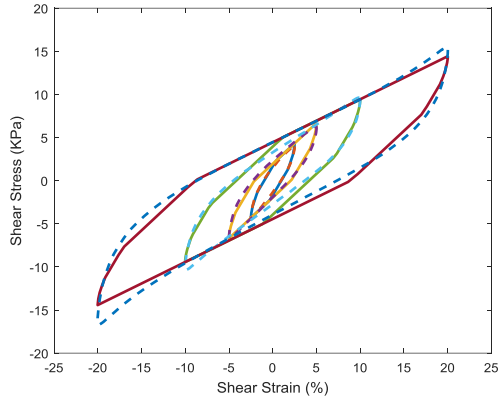


(c)

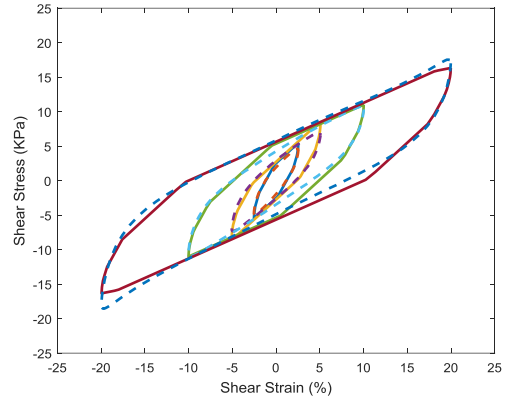


(d)

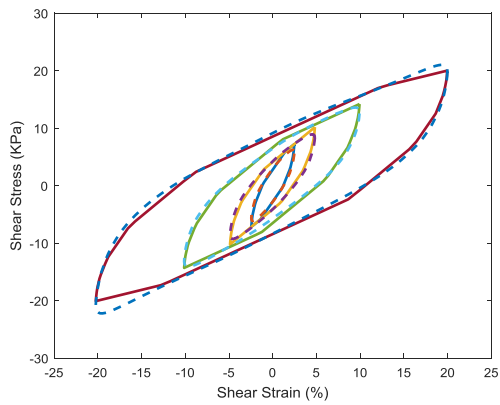
Figure 4.3: Comparisons between of the stress-strain properties obtained from the Classical PI model with the measured data under varying strain amplitudes and $0mT$ magnetic field intensity, and different excitation frequencies (a) 0.1 Hz (b) 1 Hz (c) 10 Hz (d) 50 Hz (- - Measured, - Model).



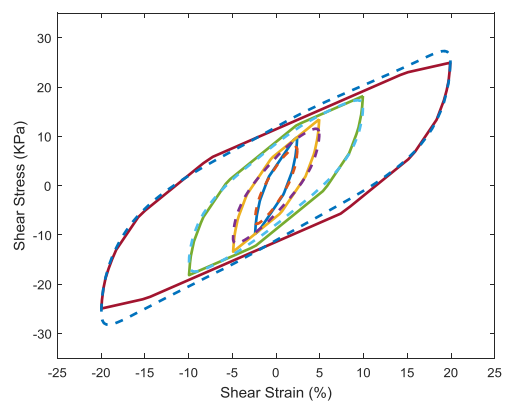
(a)



(b)

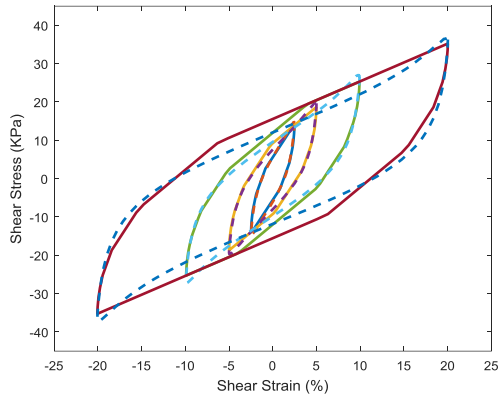


(c)

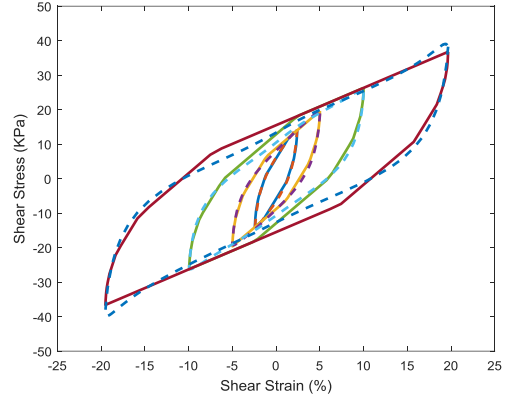


(d)

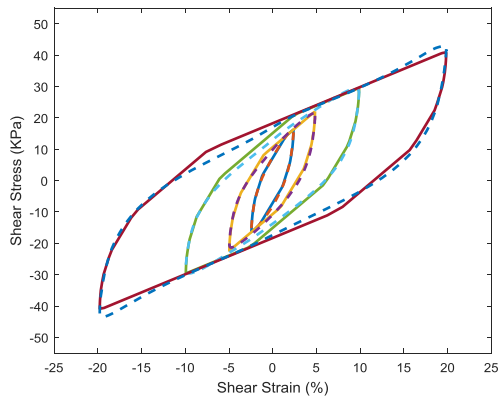
Figure 4.4: Comparison between of the stress-strain properties obtained from the Classical PI model with the measured data under varying strain amplitudes and $150mT$ magnetic field intensity, and different excitation frequencies (a) $0.1 Hz$ (b) $1 Hz$ (c) $10 Hz$ (d) $50 Hz$, (- - Measured, - Model).



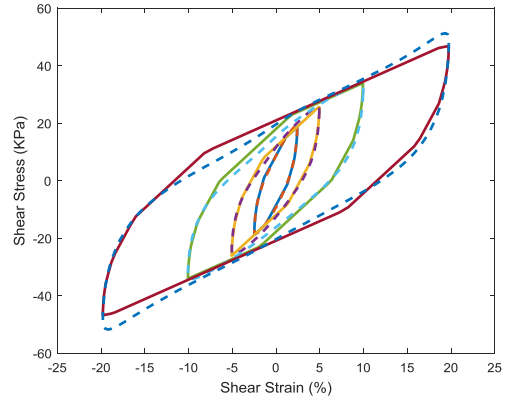
(a)



(b)



(c)



(d)

Figure 4.5: Comparison between of the stress-strain properties obtained from the Classical PI model with the measured data under varying strain amplitudes and $300mT$ magnetic field intensity, and different excitation frequencies (a) $0.1 Hz$ (b) $1 Hz$ (c) $10 Hz$ (d) $50 Hz$, (- - Measured, - Model).

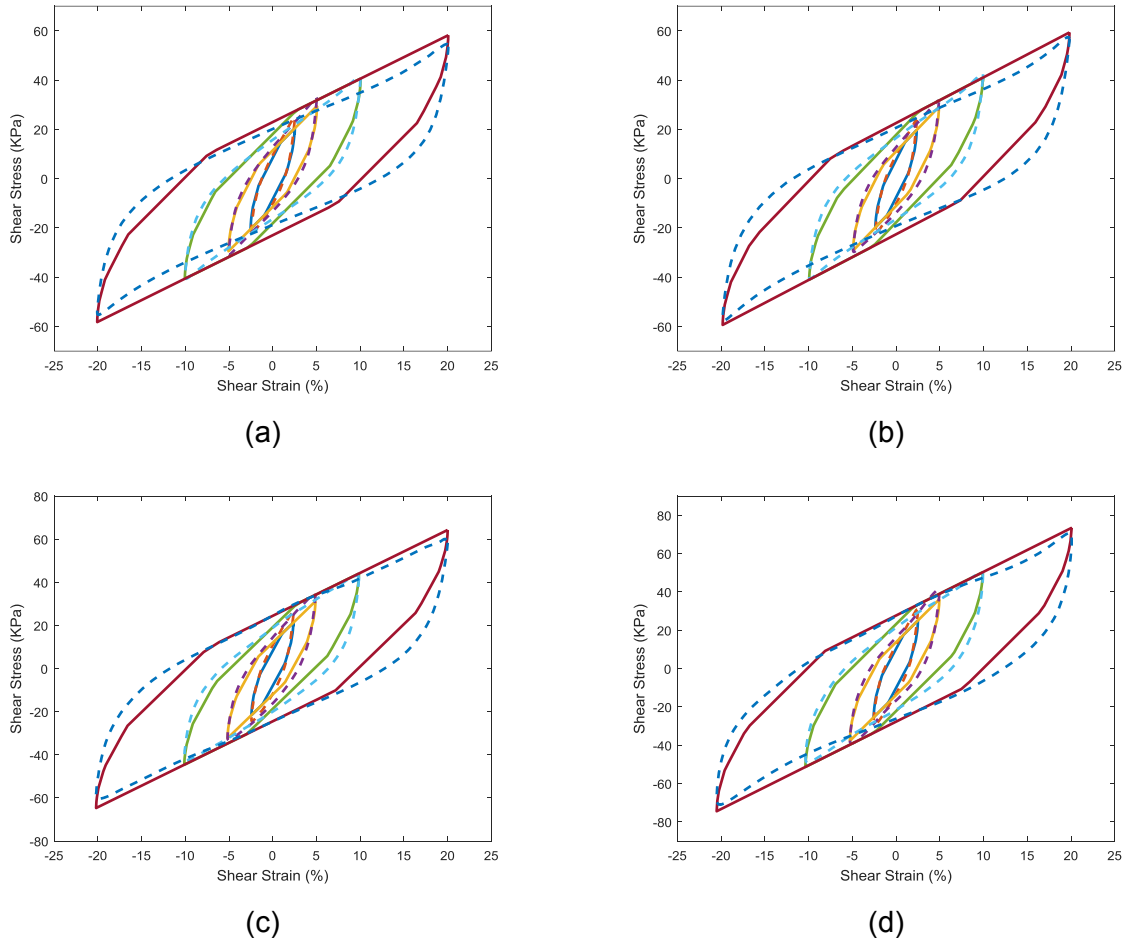


Figure 4.6: Comparison between of the stress-strain properties obtained from the Classical PI model with the measured data under varying strain amplitudes and $450mT$ magnetic field intensity, and different excitation frequencies (a) $0.1 Hz$ (b) $1 Hz$ (c) $10 Hz$ (d) $50 Hz$, (- - Measured, - Model).

The model can predict the stress-strain properties of the MRE under the entire range of the strain amplitudes, while the model parameters show strong dependence on the excitation frequency and the field intensity (table 4.1). The measured stress-strain characteristics presented in section 3.5, invariably revealed decreasing slope of the stress-strain hysteresis loops of the MRE with increasing strain amplitude. This suggest decreasing storage modulus of the MRE with increasing strain amplitude, which has also been reported in [4, 34]. The proposed model, with amplitude independent parameters, can effectively predict this effect in the MRE dynamic behavior. Moreover, fewer number of model parameters are needed to describe the dependence of stress-strain characteristics on the frequency and magnetic field intensity.

4.5 Formulation of a generalized Prandtl-Ishlinskii model

The parameters of the classical Prandtl-Ishlinskii model, presented in section 4.3, show strong dependence on the loading frequency as well as the applied magnetic field intensity. The variations in parameters c_1 , k_1 and k_2 with the loading conditions and magnetic field intensity are further investigated in order to propose a generalized Prandtl-Ishlinskii model for predicting the stress-strain properties of the MRE as functions of the frequency and the magnetic field intensity. Figure 4.7 illustrates variations in constant c_1 with the loading frequency, which suggest that c_1 decreases exponentially with the loading frequency. The dependency of c_1 may thus be described by an exponential or a power function. The second parameter of the threshold function c_2 was observed to be independent of loading frequency and the magnetic field intensity. Moreover, the constant c_1 was also observed to be insensitive to the magnetic field intensity, as seen in table 4.1.

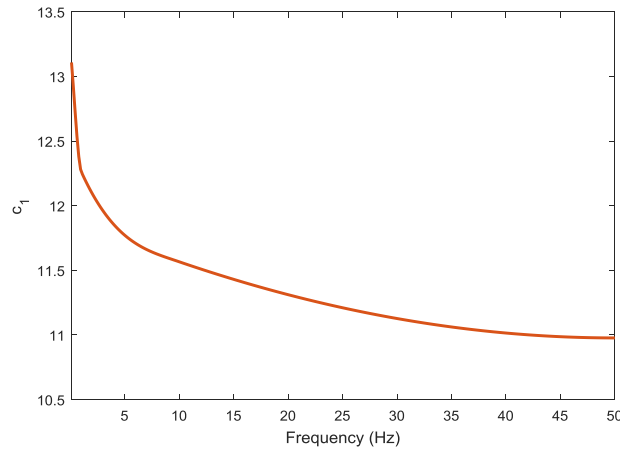


Figure 4.7: Variations in model constant c_1 with the loading frequency.

The parameters of the density function (k_1, k_2) are dependent on both the input frequency as well as the applied magnetic field intensity, as seen Figures 4.8 and 4.9, respectively. The constant k_1 decreases with increasing frequency, while constant k_2 increases with the frequency. The frequency dependence of the constant k_1 , however, is nearly negligible under low magnetic field intensities (0 to 150 mT), while it tends to saturate under higher field intensities, as seen in Figure 4.8(a). The constant k_2 , on the other hand, tends to vary only slightly with the frequency, when the field density is above 150 mT . Although, the peak stress, width of the hysteresis loop and the slope of the stress-strain curve increase with increasing frequency. Irrespective of the

field intensity, constant k_2 tends to saturate and k_1 decreases with increasing frequency. This will lead to decreasing value of the density function p_j with increasing frequency.

Figure 4.8 and 4.9 further show that the constant k_1 and k_2 increase with increasing field density, which will yield increasing value of the density function p_j and thereby the stress output with increasing magnetic field intensity. The exponent k_2 tends to increase substantially with increasing frequency, irrespective of the magnetic field. It tends to approach saturation when field intensity approaches 150 mT . The constant k_1 , on the other hand, varies only slightly up to 150 mT field intensity, but increases rapidly under higher magnitudes of the field intensity. The observation variations in the model constants with excitation frequency and magnetic field intensity suggest that:

The frequency dependence of constant k_1 could be described by either a power or an exponential function in excitation frequency of the form:

$$k_1(f) = a_0 f^{-b_0} \quad (4.11)$$

Where a_0 and b_0 are constants to be identified from the results presented in Figure 4.8 (a). f is the normalized frequency with respect to its maximum value (50 Hz).

The field intensity dependence of constant k_1 , could be adequately described by the following tangent hyperbolic function of the form:

$$k_1(B) = \tanh[a_1 B + a_2] + a_3 \quad (4.12)$$

Where a_1, a_2 and a_3 are constants to be identified from the results presented in Figure 4.8 (b). B is the normalized magnetic field intensity with respect to its maximum value (450 mT).

The frequency and magnetic field dependence of the constant k_2 (Figure 4.9 (a)) could be described by the following exponential function:

$$k_2(f) = \alpha_1(1 - b_2 e^{-b_3 f}) \quad (4.13)$$

$$k_2(B) = \alpha_2(1 - b_4 e^{-b_5 B}) \quad (4.14)$$

Where $\alpha_1, \alpha_2, b_2, b_3, b_4$ and b_5 are model constants to be identified through regression analysis of the data presented in Figure 4.9.

Both the frequency and field intensity dependence of constants k_1 and k_2 can be described by production of the above functions, such that:

$$k_1(f, B) = a_0 f^{-b_0} [\tanh[a_1 B + a_2] + a_3] \quad (4.15)$$

$$k_2(f, B) = b_1(1 - b_2 e^{-b_3 f})(1 - b_4 e^{-b_5 B}) \quad (4.16)$$

The model constant c_1 is also dependent on the excitation frequency, which can be expressed by the following power function:

$$c_1(f) = \beta_1 f^{-\beta_2} \quad (4.17)$$

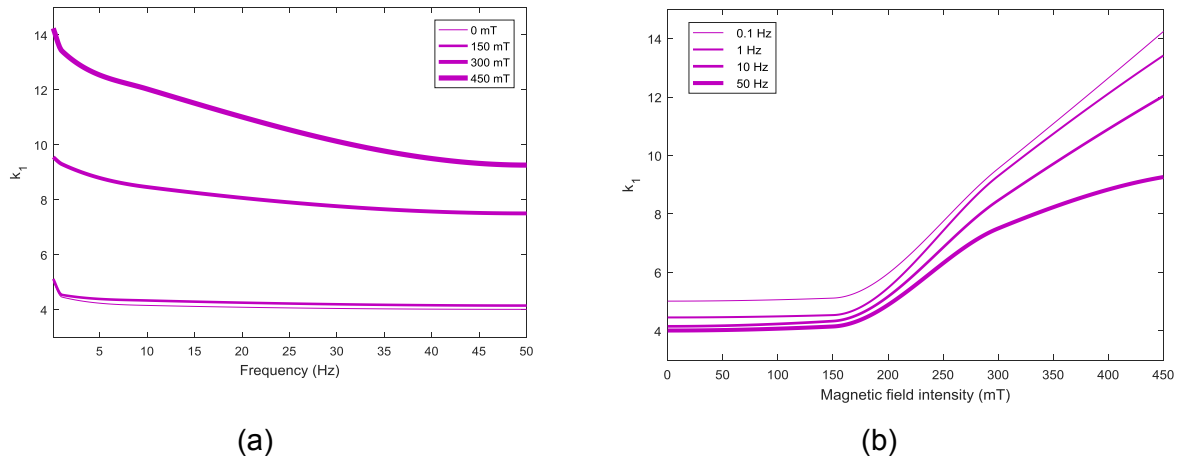


Figure 4.8: Variations in the classical PI model parameter k_1 with: (a) loading frequency; and (b) the magnetic field intensity.

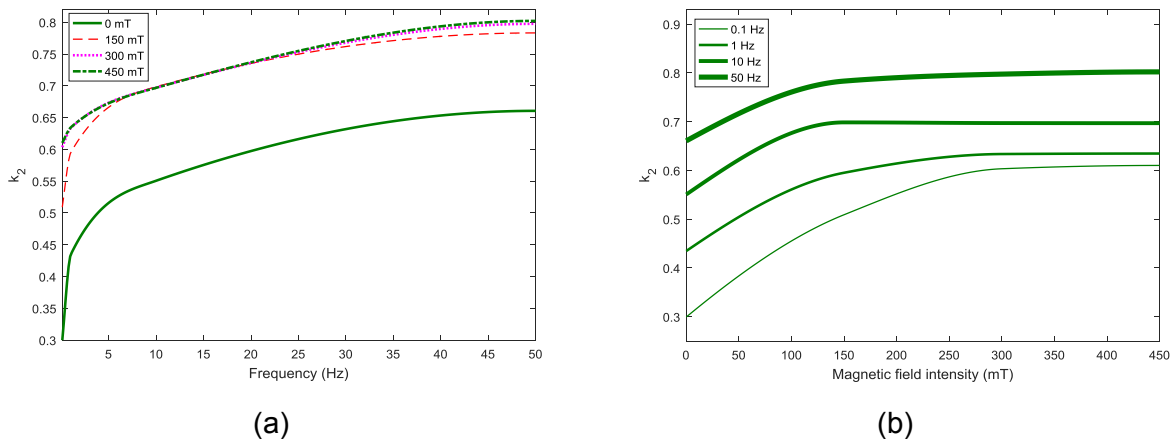


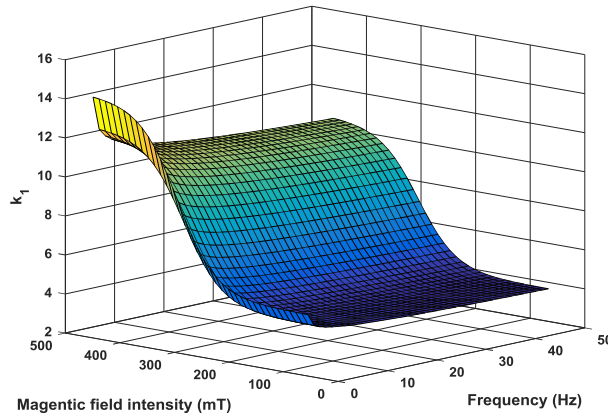
Figure 4.9: Variations in the classical PI model parameter k_2 with: (a) loading frequency; and (b) the magnetic field intensity.

The above regression functions showed excellent correlation with the results presented in Figure 4.7 – 4.9 with correlation coefficient (R^2) in excess of 0.9. Figure 4.10 further illustrates the variation in constants k_1 and k_2 with variations in excitation frequency and the magnetic field intensity. The results show the essential characteristics observed in Figure 4.8 and 4.9.

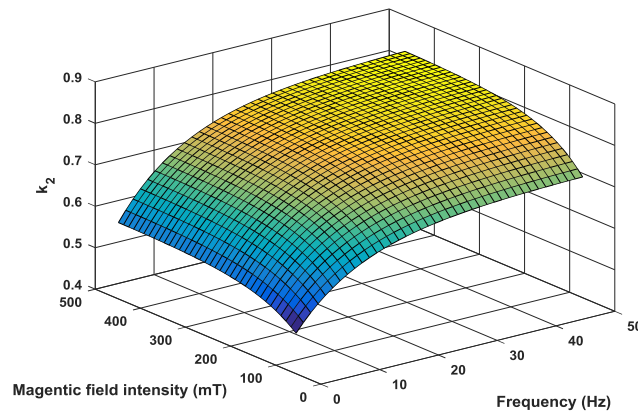
A generalized Prandtl-Ishlinskii model is subsequently designed using the following threshold and density function in both the normalized loading frequency and the normalized field intensity.

$$r_j(f) = c_1(f)e^{-jc_2} \quad ; \quad j = 1,2,3, \dots, n \quad (4.18)$$

$$p_j(f, B) = k_1(f, B)e^{jk_2(f, B)} \quad ; \quad j = 1,2,3, \dots, n \quad (4.19)$$



(a)



(b)

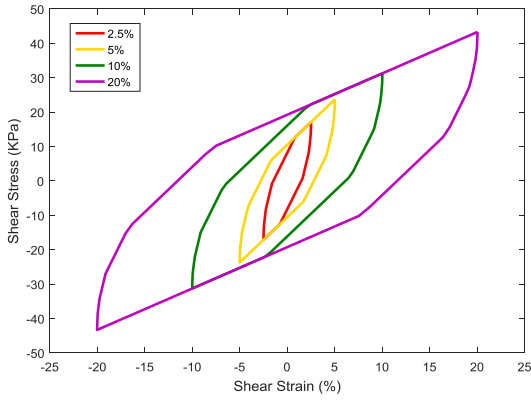
Figure 4.10: The relationships between the model parameters (a) k_1 , (b) k_2 with the loading frequency and the magnetic field intensity.

4.6 Simulation results

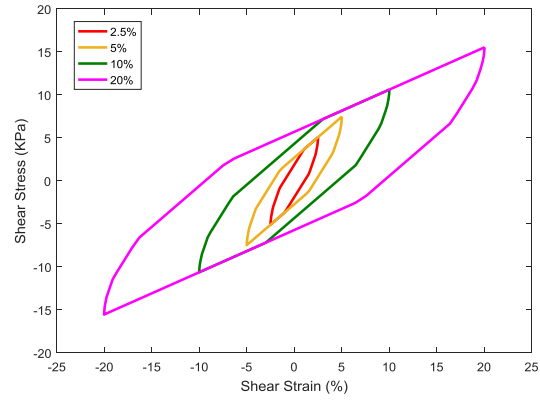
The performance of the proposed generalized Prandtl-Ishlinskii model in predicting the dynamic behavior of the MRE was examined under different loading conditions and magnetic field intensities. The results revealed very good agreements between the peak stress values in the stress-strain hysteresis loops obtained from the generalized PI model and the measured data of the MRE for varying strain amplitudes, frequencies and magnetic field intensities. Figure 4.11(a) illustrates the results obtained from the generalized PI model over the range of strain amplitudes (2.5, 5, 10 and 20%) under 10 Hz excitation frequency and 300 mT applied magnetic field intensity. It was observed that the generalized PI model can effectively predict the decrease in the slope of the stress-strain hysteresis loops with increasing the strain amplitude. Similar results can be observed in Figure 4.11 (b), where the stress-strain hysteresis curves obtained from the generalized PI model are presented over the range of strain amplitudes (2.5-20%) under 1 Hz excitation frequency and 150 mT magnetic field intensity. It was concluded that the proposed generalized model can accurately predict the strain softening effect in the MRE dynamic behavior.

The results of the generalized PI model were also examined over the range of excitation frequencies. Figure 4.12 reveals that both the slope and the area enclosed by the stress-strain hysteresis loops predicted by the generalized PI model increases with increasing the excitation frequency ranging from 0.1 Hz to 50 Hz. Similar trend was observed over all the strain amplitudes as well as the magnetic field intensities, which guaranteed the effectiveness of the proposed generalized PI model in predicting the strain rate stiffening effect in the MRE dynamic behavior.

Finally, the effectiveness of the proposed generalized PI model was investigated over the range of the applied magnetic field intensity. The stress-strain hysteresis curves predicted by the generalized PI model over the range of the magnetic field intensity (0, 150, 300 and 450mT) under 10% shear strain at excitation frequencies 1 Hz and 10 Hz are illustrated in Figure 4.13 (a) and (b), respectively. It was observed that similar to the measured data of the MRE, the slope and the area enclosed by the stress-strain hysteresis drastically increase with intensifying the magnetic field. The Generalized model showed the similar behavior for predicting the effects of the magnetic field intensity on the stress-strain hysteresis loops of the MRE in all the loading conditions considered.

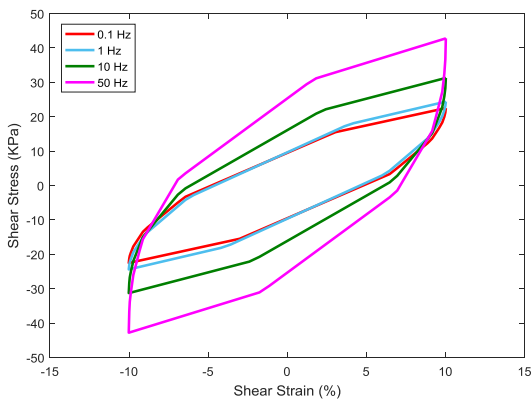


(a)

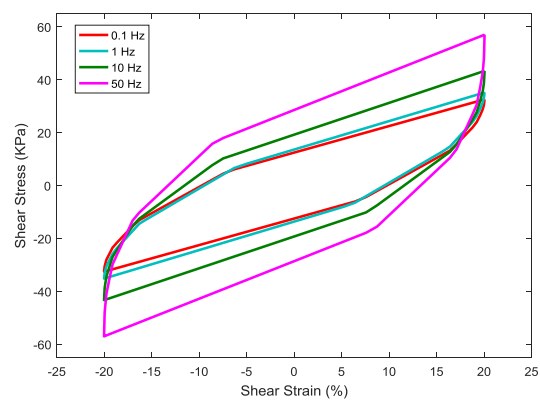


(b)

Figure 4.11: The stress-strain hysteresis loops obtained from the generalized Prandtl-Ishlinskii model over the range of the strain amplitudes (2.5, 5, 10 and 20%) under: (a) 10 Hz excitation frequency and 300 mT magnetic field intensity; and (b) 1 Hz excitation frequency and 150 mT magnetic field intensity.



(a)



(b)

Figure 4.12: The stress-strain hysteresis loops obtained from the generalized Prandtl-Ishlinskii model over the range of the excitation frequencies (0.1, 1, 10 and 50 Hz) under 300 mT magnetic field intensity and the strain amplitude: (a) 10%; and (b) 20%.

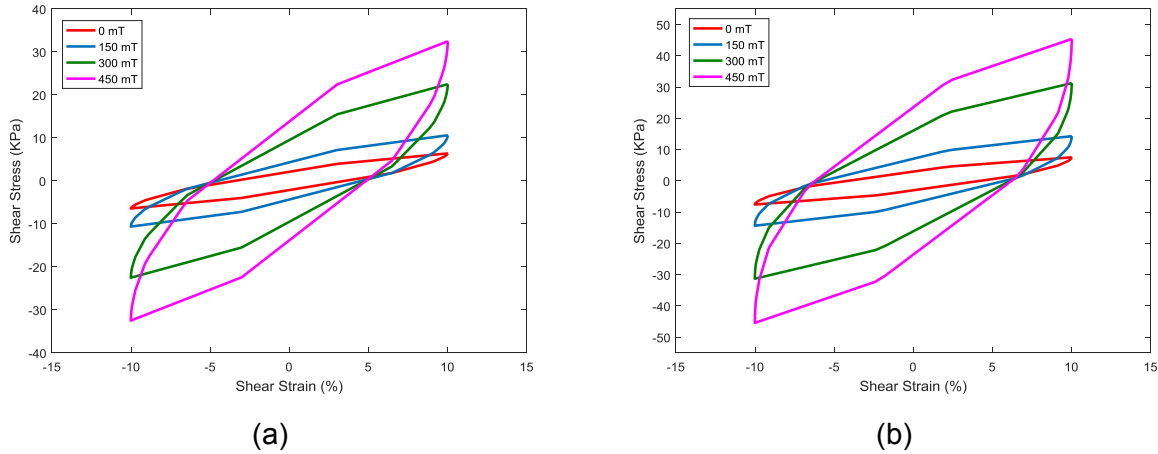


Figure 4.13: The stress-strain hysteresis loops obtained from the generalized Prandtl-Ishlinskii model over the range of the magnetic field intensities (0, 150, 300 and 450 mT) under 10 % strain amplitude and the excitation frequency: (a) 1 Hz; and (b) 10 Hz.

4.7 Summary

The stop operator-based classical Prandtl-Ishlinskii model was formulated for predicting the stress-strain hysteresis nonlinearities of the MREs in wide ranges of input frequency and strain amplitude as well as the applied magnetic field intensity. The measured data was used to identify the parameters of the classical PI model through minimization of the error function between the model and the measured responses over the range of strain amplitudes. Validity of the proposed model was examined by comparing the model responses with the measured data in terms of stress-strain hysteresis loops over the entire range of strain amplitudes, frequencies and magnetic field intensities. The coefficient of determination (R^2) between the model results and the measured data were generally observed to be above 0.98, with the exception of those corresponding to the very low strain amplitudes under the application of 0 mT magnetic field intensity. The identified parameters of the classical Prandtl-Ishlinskii model showed strong dependence on the loading frequency as well as the applied magnetic field intensity. This dependency was further investigated in order to propose a generalized Prandtl-Ishlinskii model for predicting the stress-strain characteristics of the MRE as functions of the frequency and the magnetic field intensity. Finally, the performance of the generalized model was examined, which revealed the effectiveness of the generalized PI model in designing the stress-strain hysteresis loops of MRE as well as predicting the strain softening, strain rate stiffening and magnetic field stiffening effects in the MRE dynamic behavior.

Chapter 5: Conclusions and Recommendation for Future Studies

5.1 Major contributions

The main focus of this dissertation was to provide an in-depth investigation on the magneto-mechanical characteristics of a new class of active materials, namely magnetorheological elastomers (MREs). These composites are composed of an elastomeric matrix impregnated by micron-sized ferromagnetic particles. Due to their alterable mechanical properties by the application of an external magnetic field, MREs are promising materials with a broad range of possible engineering applications. The key contributions of this thesis include experimental characterization and a phenomenological model for describing the static and dynamic responses of MREs. The contributions of this dissertation research are summarized below:

- (i) Development of a simple MRE fabrication methodology;
- (ii) Design and manufacturing six types of MREs containing variable contents of rubber matrix and ferromagnetic particles;
- (iii) Design of an experimental set-up for static and dynamic characterization of MRE in the simple shear mode under varying magnetic field intensity;
- (iv) Static and dynamic characterization of magneto-mechanical properties of six different MRE samples under wide ranges of loading conditions and applied magnetic field intensities;
- (v) Formulation of a stop-operator based classical Prandtl-Ishlinskii model for modeling the hysteresis nonlinearities of MREs;
- (vi) Formulation of a generalized Prandtl-Ishlinskii model to predict the dynamic behavior of the MRE over wide ranges of loading frequencies and amplitudes as well as magnetic field intensities.

5.2 Major conclusions

This dissertation research presents nonlinear stress-strain characteristics of magnetorheological elastomers as well as modeling of hysteresis properties of the smart composite using stop operator-based Prandtl-Ishlinskii model. Major conclusions drawn from the dissertation research are summarized below:

- (i) Content of ferromagnetic particles has a significant influence on the magneto-mechanical properties of the MRE. Increasing the iron particles volume percentage in the elastomeric matrix magnifies notably the MR effect defined as the degree of change in the modulus of MRE in presence of the magnetic field. Additionally, higher relative MR effect could be achieved by softening the matrix material either by adding a diluting agent like silicone oil or by selecting a softer matrix material.
- (ii) Owing to their viscoelastic nature, the MREs exhibit significant hysteresis in the input strain and the output stress, which is symmetric about the output in simple shear mode. The enclosed area and the slope of the major axis of MRE hysteresis loops are highly dependent on the loading frequency, strain amplitude as well as the applied magnetic field intensity. The strain softening, strain stiffening, strain rate stiffening and the magnetic field stiffening phenomena are identified as the nonlinear hysteresis properties of the MREs.
- (iii) Up to 2500% increase in the elastic shear modulus of the MRE was observed in the storage modulus under 2.5% strain amplitude at a frequency of 50 Hz and 450 mT magnetic field intensity compared to that achieved under 20% strain amplitude at 0.1 Hz input frequency in the absence of the magnetic field. Such a substantial MR effect of the MRE offers considerable potential for its applications in controllable vibration isolators.
- (iv) The stop-operator based classical Prandtl-Ishlinskii model can accurately predict the nonlinear hysteresis properties of the MREs. The coefficient of determination between the measured and model responses was found to be in the order of 98%, suggesting effectiveness of the classical PI model in capturing the stress-strain hysteresis loops of the MREs. The parameters of the classical PI model revealed strong dependence on the loading frequency as well as the magnetic field intensity.
- (v) The generalized Prandtl-Ishlinskii hysteresis model, proposed in this study, could accurately predict the stress-strain characteristics of the MRE over wide ranges of applied shear strain, strain rate and magnetic field intensity.

5.3 Recommendations for future work

This dissertation research presents the methodologies for fabrication and experimental characterization of MREs in addition to the phenomenological modeling. A repeatable and effective process for isotropic MRE fabrication is successfully developed and experimental characterization is performed under different loading conditions. Additionally, the hypothesis that the complementary properties of the stop operator-based Prandtl-Ishlinskii model could be employed to predict the hysteresis nonlinearities of MREs is explored. Comparisons between the simulation and experimental results supports the limitless potential of the Prandtl-Ishlinskii model. The experimental data suggests highly complex effects of many design and loading factors such as volume fractions of ferromagnetic particles, matrix compound properties, strain amplitude, strain rate and magnetic field intensity. Furthermore, the proposed model involves identification of large number of parameters for describing the rate and field dependence of the MR effect and magneto-mechanical properties. Some of the recommended areas to be further investigated either experimentally or theoretically are listed below:


- (i) Fabricate anisotropic magnetorheological elastomers containing different contents of ferromagnetic particles to compare the magneto-mechanical properties with the corresponding isotropic MRE. The anisotropic MREs may exhibit greater MR effect but may impose additional complexities during fabrication.
- (ii) Perform experimental characterization of MREs in the tension/compression modes to acquire in-depth understanding of MRE behavior in the other operation modes.
- (iii) Investigate the effects of size of the ferromagnetic particles that may influence the MR effect substantially.
- (iv) Explore the rate-dependent density function as well as rate-dependent threshold function in an attempt to develop a more efficient rate dependent Prandtl-Ishlinskii model with fewer parameters.
- (v) Formulate threshold and density functions in strain amplitudes and strain rate in order to enhance the effectiveness of a generalized Prandtl-Ishlinskii model.
- (vi) Explore modeling the hysteresis nonlinearities of MREs using the differential equation-based phenomenological models such as the Bouc-Wen model for predicting the nonlinear properties of MREs under wide ranges of loading conditions and magnetic field intensities.

Appendix


A Material properties

Ecoflex® Series

Super-Soft, Addition Cure Silicone Rubbers



Certified
ISO 10993-10
SKIN SAFE



SMOOTH-ON
SINCE 1988

Cured Material
Certified Skin Safe!

www.smooth-on.com

PRODUCT OVERVIEW

Ecoflex® rubbers are platinum-catalyzed silicones that are versatile and easy to use. Ecoflex® rubbers are mixed 1A:1B by weight or volume and cured at room temperature with negligible shrinkage. Low viscosity ensures easy mixing and de-airing, or you can choose to mix and dispense using our convenient dispensing cartridges. Cured material is skin safe and certified by an independent laboratory to ISO 10993-10, Biological evaluation of medical devices, Part 10: Tests for irritation and skin sensitization.

Cured rubber is very soft, very strong and very “stretchy”, stretching many times its original size without tearing and will rebound to its original form without distortion. Ecoflex® rubbers are water white translucent and can be color pigmented with Silc Pig® pigments for creating a variety of color effects. You can also add Smooth-On’s Silicone Thinner® to further lower the viscosity. THI-VEX® silicone thickener can be added by weight to Ecoflex® silicones for brushable applications.

Soft, Softer, Softest . . . Ecoflex® rubbers are based on Smooth-On’s Dragon Skin® technology and are currently available in four different hardness: Shore A-5, Shore 00-10, 00-20, 00-30 and 00-50. They are suitable for a variety of applications including making prosthetic appliances, cushioning for orthotics and special effects applications (especially in animatronics where repetitive motion is required). Ecoflex® 5 has a pot life of 1 minute and a demold time of 5 minutes – Available only in dispensing cartridges.

Note: Ecoflex® 00-10 cures with a “tacky” surface.

TECHNICAL OVERVIEW

	Mixed Viscosity (ASTM D-2393)	Specific Gravity (g/cc) (ASTM D-1475)	Specific Volume (cu. in./lb.) (ASTM D-1475)	Pot Life (ASTM D-2471)	Cure Time	Shore Hardness (ASTM D-2240)	Tensile Strength (ASTM D-412)	100% Modulus (ASTM D-412)	Elongation at Break % (ASTM D-412)	Die B Tear Strength (ASTM D-624)	Shrinkage (in./in.) (ASTM D-2566)
Ecoflex® 5	13,000 cps	1.07	25.8	1 min.	5 min.	5A	350 psi	15 psi	1000%	75 pli	< .001 in./in.
Ecoflex® 00-50	8,000 cps	1.07	25.9	18 min.	3 hours	00-50	315 psi	12 psi	980%	50 pli	< .001 in./in.
Ecoflex® 00-30	3,000 cps	1.07	26.0	45 min.	4 hours	00-30	200 psi	10 psi	900%	38 pli	< .001 in./in.
Ecoflex® 00-20	3,000 cps	1.07	26.0	30 min.	4 hours	00-20	160 psi	8 psi	845%	30 pli	< .001 in./in.
Ecoflex® 00-10	14,000 cps	1.04	26.6	30 min.	4 hours	00-10	120 psi	8 psi	800%	22 pli	< .001 in./in.

*All values measured after 7 days at 73°F/23°C

Mix Ratio: 1A:1B by volume or weight **Useful Temperature Range:** -65°F to 450°F (-53°C to 232°C)
Color: Translucent **Dielectric Strength** (ASTM D-147-97a): >350 volts/mil

PROCESSING RECOMMENDATIONS

PREPARATION... Safety – Use in a properly ventilated area (“room size” ventilation). Wear safety glasses, long sleeves and rubber gloves to minimize contamination risk. Wear vinyl gloves only. Latex gloves will inhibit the cure of the rubber.

Store and use material at room temperature (73°F/23°C). Warmer temperatures will drastically reduce working time and cure time. Storing material at warmer temperatures will also reduce the usable shelf life of unused material. These products have a limited shelf life and should be used as soon as possible.

Cure Inhibition – Addition-cure silicone rubber may be inhibited by certain contaminants in or on the pattern to be molded resulting in tackiness at the pattern interface or a total lack of cure throughout the mold. Latex, tin-cure silicone, sulfur clays, certain wood surfaces, newly cast polyester, epoxy, tin cure silicone rubber or urethane rubber may cause inhibition. If compatibility between the rubber and the surface is a concern, a small-scale test is recommended. Apply a small amount of rubber onto a non-critical area of the pattern. Inhibition has occurred if the rubber is gummy or uncured after the recommended cure time has passed.

Because no two applications are quite the same, a small test application to determine suitability for your project is recommended if performance of this material is in question.

To prevent inhibition, one or more coatings of a clear acrylic lacquer applied to the model surface is usually effective. Allow any sealer to thoroughly dry before applying rubber. Note: Even with a sealer, platinum silicones will not work with modeling clays containing heavy amounts of sulfur. Do a small scale test for compatibility before using on your project.

Figure A.1: Technical bulletin of Ecoflex series silicone rubber (Page 1)

Safety First!

The Material Safety Data Sheet (MSDS) for this or any Smooth-On product should be read prior to use and is available upon request from Smooth-On. All Smooth-On products are safe to use if directions are read and followed carefully.

Keep Out of Reach of Children

Be careful. Use only with adequate ventilation. Contact with skin and eyes may cause irritation. Flush eyes with water for 15 minutes and seek immediate medical attention. Remove from skin with waterless hand cleaner followed by soap and water.

Important: The information contained in this bulletin is considered accurate. However, no warranty is expressed or implied regarding the accuracy of the data, the results to be obtained from the use thereof, or that any such use will not infringe upon a patent. User shall determine the suitability of the product for the intended application and assume all risk and liability whatsoever in connection therewith.

Applying A Release Agent - Although not usually necessary, a release agent will make demolding easier when pouring into or over most surfaces. Ease Release® 200 is a proven release agent for use with silicone rubber. Mann Ease Release® products are available from Smooth-On or your Smooth-On distributor.

IMPORTANT: To ensure thorough coverage, lightly brush the release agent with a soft brush over all surfaces of the model. Follow with a light mist coating and let the release agent dry for 30 minutes.

If there is any question about the effectiveness of a sealer/release agent combination, a small-scale test should be made on an identical surface for trial.

MEASURING & MIXING...

Before you begin, pre-mix Part B thoroughly. After dispensing required amounts of Parts A and B into mixing container (1A:1B by volume or weight), **mix thoroughly for 3 minutes making sure that you scrape the sides and bottom of the mixing container several times.** After mixing parts A and B, vacuum degassing is recommended to eliminate any entrapped air. Vacuum material for 2-3 minutes (29 inches of mercury), making sure that you leave enough room in container for product volume expansion.

POURING, CURING & MOLD PERFORMANCE...

For best results, pour your mixture in a single spot at the lowest point of the containment field. Let the rubber seek its level up and over the model. **A uniform flow will help minimize entrapped air.** The liquid rubber should level off at least 1/2" (1.3 cm) over the highest point of the model surface.

Curing / Post Curing - Allow rubber to cure as prescribed at room temperature (73°F/23°C) before demolding. Do not cure rubber where temperature is less than 65°F/18°C. **Optional:** Post curing the mold will aid in quickly attaining maximum physical and performance properties. After curing at room temperature, expose the rubber to 176°F/80°C for 2 hours and 212°F/100°C for one hour. Allow mold to cool to room temperature before using.

If Using As A Mold - When first cast, silicone rubber molds exhibit natural release characteristics. Depending on what is being cast into the mold, mold lubricity may be depleted over time and parts will begin to stick. No release agent is necessary when casting wax or gypsum. Applying a release agent such as Ease Release® 200 (available from Smooth-On) prior to casting polyurethane, polyester and epoxy resins is recommended to prevent mold degradation.

Thickening Ecoflex® Silicones - THI-VEX® is made especially for thickening Smooth-On's silicones for vertical surface application (making brush-on molds). Different viscosities can be attained by varying the amount of THI-VEX®. See the THI-VEX® **technical bulletin** (available from Smooth-On or your Smooth-On distributor) for full details.

Thinning Ecoflex® Silicones - Smooth-On's Silicone Thinner® will lower the viscosity of Ecoflex® silicones for easier pouring and vacuum degassing. A **disadvantage** is that ultimate tear and tensile are reduced in proportion to the amount of Silicone Thinner® added. **It is not recommended to exceed 10% by weight of total system (A+B).** See the Silicone Thinner® technical bulletin (available from Smooth-On or your Smooth-On distributor) for full details.

Mold Performance & Storage - The physical life of the mold depends on how you use it (materials cast, frequency, etc.). Casting abrasive materials such as concrete can quickly erode mold detail, while casting non-abrasive materials (wax) will not affect mold detail. Before storing, the mold should be cleaned with a soap solution and wiped fully dry. Two part (or more) molds should be assembled. Molds should be stored on a level surface in a cool, dry environment.



Call Us Anytime With Questions About Your Application.

Toll-free: (800) 381-1733 Fax: (610) 252-6200

The new www.smooth-on.com is loaded with information about mold making, casting and more.

071316-JR

Figure A.1: Technical bulletin of Ecoflex series silicone rubber (Page 2)

PRODUCT OVERVIEW

Slacker® is one component translucent clear fluid that is added to our translucent **platinum-cure silicones** such as Dragon Skin® and Ecoflex® products. **Slacker®** will change the “feel” of the silicone rubber to a softer and more “flesh-like” material. It also alters the rebound properties of the silicone, making it feel more like human tissue.

Slacker® allows the user to vary the degree of tackiness to the cured silicone, allowing for the creation of self-sticking silicone appliances. The amount of tackiness is in direct proportion to the amount of **Slacker®** added. Pieces created with **Slacker® will not exude silicone oil**, eliminating a common problem with other softening methods.

Slacker® can be added in larger proportions to Smooth-On’s super soft and stretchy platinum silicones (for example, Dragon Skin® FX-Pro®) to make silicone gel that can be used to create gel-filled silicone prosthetic appliances. Gel-filled appliances will flex, bend, and even wrinkle like human flesh. Silicone gels created with **Slacker®** can also be used to create **cushioning materials** for medical applications (anaplastology). **Use Skin Tite® adhesive to temporarily, but securely, adhere silicone appliances to the skin.**

PROCESSING RECOMMENDATIONS

PREPARATION...

Temperature - Store and use all products at room temperature (73°F / 23°C). This product has a limited shelf life and should be used as soon as possible. Wear safety glasses, long sleeves and vinyl gloves to minimize contamination risk.

MEASURING & MIXING...

Measuring Is Done By Volume Or Weight – Whether using an Ecoflex® product or a Dragon Skin® product, the proper mix ratio is 100 Parts A + 100 Part B + X Parts Slacker®. Everyone’s application and desired level of stickiness or “tack” will vary. The following chart should be used as a reference for you to achieve your own desired effect.

1 Part A + 1 Part B + 1 Part Slacker® Result - “Tacky”	1 Part A + 1 Part B + 2 Parts Slacker® Result - “Very Tacky”
1 Part A + 1 Part B + 3 Parts Slacker® Result - “Extremely Tacky / Gel-like”	1 Part A + 1 Part B + 4 Parts Slacker® Result - “Super Soft Tacky Silicone Gel”

Example - 50 grams Dragon Skin® FX-Pro® part A + 50 grams Dragon Skin® FX-Pro® part B + 150 grams Slacker® (3 parts) will give you an “Extremely Tacky / Gel-like” result.

USING SLACKER® WITH DRAGON SKIN® OR ECOFLEX® PRODUCTS...

Adding Color - Silc Pig® silicone pigments can be added and mixed thoroughly into the silicone rubber prior to adding Slacker® for matching a specific skin tone, etc.

Mixing – Ecoflex® or Dragon Skin® silicones with Slacker® added can be hand mixed. Aggressively hand mix for 3 minutes, making sure that you scrape the sides and bottom of your mixing container several times.

Release Agent - When using a platinum silicone mold, Ease Release® 200 should be used. **If there is any question** about the effectiveness of a release agent combination, a small scale test should be made on an identical surface for trial.

Pouring - For best results, pour your mixture in a single spot at the lowest point of the mold. Let the rubber seek its level in the mold. **A uniform flow will help minimize entrapped air.**

CREATING SILICONE GEL FILLED MAKEUP APPLIANCES...

Using An Encapsulator – When creating a gel-filled appliance, use a platinum silicone as your membrane for best results. Dragon Skin® FX-Pro® works very well as a membrane for gel filled appliances.

Applying A Mold Release – Appliances appliances made with Slacker® can be cast into platinum silicone molds, urethane resin molds (Shell Shock®) or rigid gypsum molds. Ease Release® 200 can be used as a mold release. Another release option is to apply a soap solution (1 part unscented dish soap to 2 parts 99% isopropyl alcohol works well) with a clean brush over all mold surfaces. Allow release to dry for at least 30 minutes.

Figure A.2: Technical bulletin of slacker (Page 1)

Safety First!

The Material Safety Data Sheet (MSDS) for this or any Smooth-On product should be read prior to use and is available upon request from Smooth-On. All Smooth-On products are safe to use if directions are read and followed carefully.

Keep Out of Reach of Children

BE CAREFUL - Avoid contact with eyes. Silicone polymers are generally non-irritating to the eyes however a slight transient irritation is possible. Flush eyes with water for 15 minutes and seek medical attention. Remove from skin with waterless hand cleaner followed by soap and water. Children should not use this product without adult supervision.

IMPORTANT - The information contained in this bulletin is considered accurate. However, no warranty is expressed or implied regarding the accuracy of the data, the results to be obtained from the use thereof, or that any such use will not infringe upon a patent. User shall determine the suitability of the product for the intended application and assume all risk and liability whatsoever in connection therewith.

ADHERING APPLIANCE TO THE SKIN...

After the casting is fully cured, the mold release should be removed. Soap based release can be removed using warm water, Ease Release® 200 can be removed using isopropyl alcohol. Smooth-On's Skin Tite® adhesive can be used to temporarily adhere the piece to the skin. Theatrical makeup can be used to further blend and color the piece. If using Skin Tite® as an adhesive, remove the piece slowly after use. You can use baby oil or makeup remover to assist in removal.

We recommend that you do a small scale test on the back of your hand to ensure that you have no allergic reaction to silicone. If you notice any type of skin reaction, do not use product.

CURING & PERFORMANCE...

Curing - The cure time of the silicone will be lengthened when Slacker® is added. As platinum-cure silicones are heat sensitive, curing can be accelerated by applying heat. Do not cure rubber where temperature is less than 65°F /18°C.

Cure Inhibition - Platinum-cure silicone rubber may be inhibited by certain contaminants in or on the pattern to be molded (such as sulfur based clays, polyesters, certain wood surfaces, epoxies, urethane rubber and tin-cured silicone rubber) resulting in tackiness at the mold interface or a total lack of cure throughout the piece.

If compatibility between the rubber and the mold is a concern, a small-scale test is recommended. Apply a small amount of rubber onto a non-critical area of the mold. Inhibition has occurred if the rubber is uncured after the recommended cure time has passed.

Because no two applications are quite the same, a small test application to determine suitability for your project is recommended if performance of this material is in question



Call Us Anytime With Questions About Your Application.

Toll-free: (800) 762-0744

Fax: (610) 252-6200

The new www.smooth-on.com is loaded with information about moldmaking, casting and more.

080310-JR

Figure A.2: Technical bulletin of slacker (Page 2)

Silicone Thinner®

Silicone Rubber Thinning Fluid



www.smooth-on.com

Silicone Thinner® is a non-reactive silicone fluid that will lower the mixed viscosity of tin cure (condensation) or platinum cure (addition) silicone rubber products.

Silicone Thinner® offers the following advantages:

- A lower mixed viscosity (A+B) means that the rubber will de-air faster when vacuuming.
- Mixed rubber (A+B) will flow better over intricate model detail.
- Silicone Thinner® will lower the ultimate shore hardness (durometer) of cured silicone rubber.
- Pot life (working time) is increased in proportion to the amount of Silicone Thinner® used.

Disadvantage: Ultimate tear and tensile strength are reduced in proportion to the amount of Silicone Thinner® added, however knotty tear properties of the Mold Max® series rubbers are unaffected. The following test data is offered as an example of the effects of Silicone Thinner® on Mold Max® 30 silicone rubber (your results may vary):

Value	Mold Max® 30 0% Silicone Thinner*	Mold Max® 30 5% Silicone Thinner*	Mold Max® 30 10% Silicone Thinner*
Mixed Viscosity (A+B)	25,000 cps	19,000 cps	13,800 cps
Shore Hardness (after 7 days)	30 A	26 A	23 A
Tensile Strength (after 7 days)	400 psi	350 psi	330 psi
Tear Strength (Die B) (after 7 days)	130 pli	115 pli	110 pli

Directions: Materials should be stored and used in a warm environment (73° F / 23° C). This material has a limited shelf life and should be used as soon as possible. Wear safety glasses, long sleeves and rubber gloves to minimize contamination risk.

***Silicone Thinner® is added as a percentage of the total Part A+Part B rubber system. An accurate gram scale must be used. Weigh out and pre-mix required amount of Silicone Thinner® with Part A of silicone rubber before adding Part B.** Mix all components thoroughly and vacuum as directed on mold rubber technical bulletin. **It is not recommended to exceed 10% by weight of total system (A+B).**

Because no two applications are quite the same, a small test application to determine suitability for your project is recommended if performance of this material is in question.

Safety First!

The material safety data sheet (MSDS) for this or any Smooth-On product should be read before using and is available on request or on our website at www.smooth-on.com. All Smooth-On products are safe to use if directions are read and followed carefully. **Keep Out of Reach Of Children.** **IMPORTANT** - The information contained in this bulletin is considered accurate. However, no warranty is expressed or implied regarding the accuracy of the data, the results to be obtained from the use thereof, or that any such use will not infringe a copyright or patent. User shall determine suitability of the product for the intended application and assume all associated risks and liability.



Call Us Anytime With Questions About Your Application.

Toll-free: (800) 762-0744

Fax: (610) 252-6200

The new www.smooth-on.com is loaded with information about mold making, casting and more.

22510 - JR

Figure A.3: Technical bulletin of silicone thinner (Page 2)

Technical data sheet

Product name: Bio-Flex® V 135001 (trial grade)
Date of issue: 28 July 2014 Version: 4.0

Designation of product, preparation and manufacturer

Trade name: Bio-Flex® V 135001 (trial grade)
Use of product: Polymer blend based on poly lactid acid, suitable for the production of 3D printing filaments.
Manufacturer: FKUR Kunststoff GmbH
 Siemensring 79
 D - 47 877 Willich
 Phone: + 49 (0) 2154 / 92 51-0
 Fax: + 49 (0) 2154 / 92 51-51
 Mail: info@fkur.com
 Web: www.fkur.com

Mechanical properties

Modulus of elasticity	2,960	[MPa]	ISO 527
Tensile strength	61.5	[MPa]	ISO 527
Tensile strain at tensile strength	5.3	[%]	ISO 527
Tensile stress at break	38	[MPa]	ISO 527
Tensile strain at break	10.5	[%]	ISO 527
Flexural modulus	3,295	[MPa]	ISO 178
Flexural strain at break	no break	[%]	ISO 178
Flexural stress at 3.5 % strain	88.8	[MPa]	ISO 178
Notched impact strength (Charpy), RT	2.8	[kJ/m ²]	ISO 179-1/1 eA
Impact Strength (Charpy), RT	30.8	[kJ/m ²]	ISO 179-1/1 eU
Shore D hardness	n/a	[-]	DIN 53505
Density	1.24	[g/cm ³]	ISO 1183
Bulk density	n/a	[kg/m ³]	ISO 60

The values listed have been established on standardized test specimens (DIN EN ISO 3167, type A) at standard temperature and humidity conditions.

Thermal properties

Melting temperature	> 155	[°C]	ISO 3146-C
Vicat A softening temperature	n/a	[°C]	ISO 306
Heat distortion temperature HDT B	n/a	[°C]	ISO 75
Melt volume rate (190 °C/2.16 kg)	n/a	[cm ³ /10 min]	ISO 1133
Melt flow rate (190 °C/2.16 kg)	3.0 - 5.0	[g/10 min]	ISO 1133

Legal notice

The figures should be regarded as guide values only. Under certain conditions the properties can be influenced to a significant extent by the processing conditions.

Neither FKUR Kunststoff GmbH nor its marketing affiliates shall be responsible for the use of this information or of any product, method or equipment mentioned. Customers must undertake their own determination of this product's suitability and completeness for their own use, for the protection of the environment, for the health and safety of their employees and purchasers of their products. No warranty is made of the merchantability or fitness of any product, and nothing herein waives any of the seller's conditions of sale. The current version of General Conditions of Sale of FKUR Kunststoff GmbH is valid.

The brands „FKuR – Plastics made by nature“ and „BIO-FLEX“ are registered trademarks of FKUR Kunststoff GmbH, according to the international `Nice-Classifications' (NCL9), no. 01, 02 and 17.

Figure A.4: Material Properties of specimens manufactured by 3D print technology

References

- [1] M. Kallio, *The elastic and damping properties of magnetorheological elastomers*: VTT Technical Research Centre of Finland, 2005.
- [2] M. Behrooz, X. Wang, and F. Gordaninejad, "Modeling of a new semi-active/passive magnetorheological elastomer isolator," *Smart Materials and Structures*, vol. 23, no. 4, pp. 045013, 2014.
- [3] J. Yang, H. Du, W. Li, Y. Li, J. Li, S. Sun, and H. Deng, "Experimental study and modeling of a novel magnetorheological elastomer isolator," *Smart Materials and Structures*, vol. 22, no. 11, pp. 117001, 2013.
- [4] M. Norouzi, S. M. S. Alehashem, H. Vatandoost, Y. Q. Ni, and M. M. Shahmardan, "A new approach for modeling of magnetorheological elastomers," *Journal of Intelligent Material Systems and Structures*, 2015.
- [5] M. Behrooz, X. Wang, and F. Gordaninejad, "Performance of a new magnetorheological elastomer isolation system," *Smart Materials and Structures*, vol. 23, no. 4, pp. 045014, 2014.
- [6] Z. Yang, C. Qin, Z. Rao, N. Ta, and X. Gong, "Design and analyses of axial semi-active dynamic vibration absorbers based on magnetorheological elastomers," *Journal of Intelligent Material Systems and Structures*, 2014.
- [7] W. Li, K. Kostidis, X. Zhang, and Y. Zhou, "Development of a force sensor working with MR elastomers.", *Advanced Intelligent Mechatronics*, pp. 233-238, 2009.
- [8] H. Böse, R. Rabindranath, and J. Ehrlich, "Soft magnetorheological elastomers as new actuators for valves," *Journal of Intelligent Material Systems and Structures*, 2012.
- [9] G. Hu, M. Guo, W. Li, H. Du, and G. Alici, "Experimental investigation of the vibration characteristics of a magnetorheological elastomer sandwich beam under non-homogeneous small magnetic fields," *Smart materials and structures*, vol. 20, no. 12, pp. 127001, 2011.
- [10] L. Davis, "Model of magnetorheological elastomers," *Journal of Applied Physics*, vol. 85, no. 6, pp. 3348-3351, 1999.
- [11] H. Böse, and R. Röder, "Magnetorheological elastomers with high variability of their mechanical properties.", *Journal of Physics*, vol 149, no. 1, p. 012090, 2009.
- [12] F. Gordaninejad, X. Wang, and P. Mysore, "Behavior of thick magnetorheological elastomers," *Journal of Intelligent Material Systems and Structures*, vol. 23, no. 9, pp. 1033-1039, 2012.
- [13] Vincent J, Staten, "Magnetic fluid clutch and brake," U.S. Patent 2,573,065, 1951.
- [14] Z. Rigbi, and L. Jilkén, "The response of an elastomer filled with soft ferrite to mechanical and magnetic influences," *Journal of Magnetism and Magnetic Materials*, vol. 37, no. 3, pp. 267-276, 1983.

- [15] M. R. Jolly, J. D. Carlson, B. C. Muñoz, and T. A. Bullions, "The Magnetoviscoelastic Response of Elastomer Composites Consisting of Ferrous Particles Embedded in a Polymer Matrix," *Journal of Intelligent Material Systems and Structures*, vol. 7, no. 6, pp. 613-622, 1996.
- [16] R. J. Mark, J. D. Carlson, and C. M. Beth, "A model of the behaviour of magnetorheological materials," *Smart Materials and Structures*, vol. 5, no. 5, pp. 607, 1996.
- [17] L. Yancheng, L. Jianchun, L. Weihua, and D. Haiping, "A state-of-the-art review on magnetorheological elastomer devices," *Smart Materials and Structures*, vol. 23, no. 12, pp. 123001, 2014.
- [18] V. Hossein, N. Mahmood, A. Seyed Masoud Sajjadi, and K. S. Stoyan, "A novel phenomenological model for dynamic behavior of magnetorheological elastomers in tension-compression mode," *Smart Materials and Structures*, vol. 26, no. 6, pp. 065011, 2017.
- [19] J. D. Carlson, and M. R. Jolly, "MR fluid, foam and elastomer devices," *Mechatronics*, vol. 10, no. 4-5, pp. 555-569, 2000.
- [20] W. Li, X. Zhang, and H. Du, "Magnetorheological elastomers and their applications," *Advances in Elastomers I*, pp. 357-374: Springer, 2013.
- [21] J. M. Ginder, M. E. Nichols, L. D. Elie, and S. M. Clark, "Controllable-stiffness components based on magnetorheological elastomers.", *Proceedings-SPIE The international Society For Optical Engineering*, pp. 418-425, 2000.
- [22] A. A. Lerner, and K. A. Cunefare, "Performance of MRE-based vibration absorbers," *Journal of Intelligent Material Systems and Structures*, 2007.
- [23] N. Hoang, N. Zhang, W. Li, and H. Du, "Development of a torsional dynamic absorber using a magnetorheological elastomer for vibration reduction of a powertrain test rig," *Journal of Intelligent Material Systems and Structures*, vol. 24, no. 16, pp. 2036-2044, 2013.
- [24] S. Sun, Y. Chen, J. Yang, T. Tian, H. Deng, W. Li, H. Du, and G. Alici, "The development of an adaptive tuned magnetorheological elastomer absorber working in squeeze mode," *Smart Materials and Structures*, vol. 23, no. 7, pp. 075009, 2014.
- [25] S. Sun, H. Deng, J. Yang, W. Li, H. Du, and G. Alici, "Performance evaluation and comparison of magnetorheological elastomer absorbers working in shear and squeeze modes," *Journal of Intelligent Material Systems and Structures*, 2015.
- [26] H.-x. Deng, and X.-l. Gong, "Application of magnetorheological elastomer to vibration absorber," *Communications in Nonlinear Science and Numerical Simulation*, vol. 13, no. 9, pp. 1938-1947, 2008.
- [27] H.-x. Deng, X.-l. Gong, and L.-h. Wang, "Development of an adaptive tuned vibration absorber with magnetorheological elastomer," *Smart materials and structures*, vol. 15, no. 5, pp. N111, 2006.
- [28] X.-M. Dong, Y. Miao, C.-R. Liao, and W.-M. Chen, "A new variable stiffness absorber based on magneto-rheological elastomer," *Transactions of Nonferrous Metals Society of China*, vol. 19, pp. s611-s615, 2009.

- [29] J. M. Ginder, W. F. Schlotter, and M. E. Nichols, "Magnetorheological elastomers in tunable vibration absorbers.", *Proc. SPIE*. vol. 4331, no. 1, pp. 103-110, 2001.
- [30] S. Sun, H. Deng, J. Yang, W. Li, H. Du, G. Alici, and M. Nakano, "An adaptive tuned vibration absorber based on multilayered MR elastomers," *Smart Materials and Structures*, vol. 24, no. 4, pp. 045045, 2015.
- [31] B. Kavlicoglu, B. Wallis, H. Sahin, and Y. Liu, "Magnetorheological elastomer mount for shock and vibration isolation.", *Active and Passive Smart Structures and Integrated Systems*, pp. 79770Y, 2011.
- [32] Y. Li, J. Li, W. Li, and B. Samali, "Development and characterization of a magnetorheological elastomer based adaptive seismic isolator," *Smart Materials and Structures*, vol. 22, no. 3, pp. 035005, 2013.
- [33] Y. Li, J. Li, T. Tian, and W. Li, "A highly adjustable magnetorheological elastomer base isolator for applications of real-time adaptive control," *Smart Materials and Structures*, vol. 22, no. 9, pp. 095020, 2013.
- [34] Y. Yu, Y. Li, J. Li, and X. Gu, "A hysteresis model for dynamic behaviour of magnetorheological elastomer base isolator," *Smart Materials and Structures*, vol. 25, no. 5, pp. 055029, 2016.
- [35] T. Shiga, A. Okada, and T. Kurauchi, "Magnetorheological behavior of composite gels," *Journal of Applied Polymer Science*, vol. 58, no. 4, pp. 787-792, 1995.
- [36] J. M. Ginder, M. E. Nichols, L. D. Elie, and J. L. Tardiff, "Magnetorheological elastomers: properties and applications.", *Proc. SPIE*. vol.3675, pp. 131-138, 1999.
- [37] M. Lokander, and B. Stenberg, "Performance of isotropic magnetorheological rubber materials," *Polymer Testing*, vol. 22, no. 3, pp. 245-251, 2003.
- [38] X. Gong, X. Zhang, and P. Zhang, "Fabrication and characterization of isotropic magnetorheological elastomers," *Polymer testing*, vol. 24, no. 5, pp. 669-676, 2005.
- [39] C. Bellan, and G. Bossis, "Field dependence of viscoelastic properties of MR elastomers," *International Journal of Modern Physics B*, vol. 16, no. 17n18, pp. 2447-2453, 2002.
- [40] M. Farshad, and A. Benine, "Magnetoactive elastomer composites," *Polymer testing*, vol. 23, no. 3, pp. 347-353, 2004.
- [41] P. R. von Lockette, J. Kadlowec, and J.-H. Koo, "Particle mixtures in magnetorheological elastomers (MREs).", *Proc. SPIE*. vol.6170, 2006.
- [42] I. Agirre-Olabide, J. Berasategui, M. J. Elejabarrieta, and M. M. Bou-Ali, "Characterization of the linear viscoelastic region of magnetorheological elastomers," *Journal of Intelligent Material Systems and Structures*, pp. 1045389X13517310, 2014.
- [43] J. M. GINDER, S. M. CLARK, W. F. SCHLOTTER, and M. E. NICHOLS, "MAGNETOSTRICTIVE PHENOMENA IN MAGNETORHEOLOGICAL ELASTOMERS," *International Journal of Modern Physics B*, vol. 16, no. 17n18, pp. 2412-2418, 2002.

- [44] M. Lokander, and B. Stenberg, "Improving the magnetorheological effect in isotropic magnetorheological rubber materials," *Polymer Testing*, vol. 22, no. 6, pp. 677-680, 2003.
- [45] A. B. a. S. Awietjan, "Microstructure and Properties of Magnetorheological Elastomers," *Advanced Elastomers - Technology, Properties and Applications*: InTech, 2012.
- [46] K. Danas, S. Kankanala, and N. Triantafyllidis, "Experiments and modeling of iron-particle-filled magnetorheological elastomers," *Journal of the Mechanics and Physics of Solids*, vol. 60, no. 1, pp. 120-138, 2012.
- [47] S.-H. Eem, H.-J. Jung, and J.-H. Koo, "Modeling of magneto-rheological elastomers for harmonic shear deformation," *IEEE Transactions on Magnetics*, vol. 48, no. 11, pp. 3080-3083, 2012.
- [48] M. Lokander, "Performance of magnetorheological rubber materials", *Diss. Fiber-och polymerteknologi*, 2004.
- [49] G. Stepanov, S. Abramchuk, D. Grishin, L. Nikitin, E. Y. Kramarenko, and A. Khokhlov, "Effect of a homogeneous magnetic field on the viscoelastic behavior of magnetic elastomers," *Polymer*, vol. 48, no. 2, pp. 488-495, 2007.
- [50] A.-M. Albanese, and K. A. Cunefare, "Properties of a magnetorheological semi-active vibration absorber.", *Proc. SPIE*, vol. 5052, pp. 36-43, 2003.
- [51] M. Kallio, T. Lindroos, S. Aalto, E. Järvinen, T. Kärnä, and T. Meinander, "Dynamic compression testing of a tunable spring element consisting of a magnetorheological elastomer," *Smart Materials and Structures*, vol. 16, no. 2, pp. 506, 2007.
- [52] W. Fletcher, and A. Gent, "Nonlinearity in the dynamic properties of vulcanized rubber compounds," *Rubber Chemistry and Technology*, vol. 27, no. 1, pp. 209-222, 1954.
- [53] A. Payne, and R. Whittaker, "Low strain dynamic properties of filled rubbers," *Rubber chemistry and technology*, vol. 44, no. 2, pp. 440-478, 1971.
- [54] E. Galipeau, and P. P. Castañeda, "A finite-strain constitutive model for magnetorheological elastomers: magnetic torques and fiber rotations," *Journal of the Mechanics and Physics of Solids*, vol. 61, no. 4, pp. 1065-1090, 2013.
- [55] Y. Shen, M. F. Golnaraghi, and G. Heppler, "Experimental research and modeling of magnetorheological elastomers," *Journal of Intelligent Material Systems and Structures*, vol. 15, no. 1, pp. 27-35, 2004.
- [56] M. Al Janaideh, "Generalized Prandtl-Ishlinskii hysteresis model and its analytical inverse for compensation of hysteresis in smart actuators," PhD Thesis, Concordia University, Montreal, Quebec, Canada, 2009.
- [57] W. Li, Y. Zhou, and T. Tian, "Viscoelastic properties of MR elastomers under harmonic loading," *Rheologica acta*, vol. 49, no. 7, pp. 733-740, 2010.
- [58] W. J. Choi, "Dynamic analysis of magnetorheological elastomer configured sandwich structures," Doctoral Thesis, School of Engineering Sciences, University of Southampton, 2009.

- [59] J.-T. Zhu, Z.-D. Xu, and Y.-Q. Guo, "Magnetoviscoelasticity parametric model of an MR elastomer vibration mitigation device," *Smart Materials and Structures*, vol. 21, no. 7, pp. 075034, 2012.
- [60] M. Al Janaideh, S. Rakheja, and C.-Y. Su, "An analytical generalized Prandtl–Ishlinskii model inversion for hysteresis compensation in micropositioning control," *IEEE/ASME Transactions on mechatronics*, vol. 16, no. 4, pp. 734-744, 2011.
- [61] P. Ge, and M. Jouaneh, "Tracking control of a piezoceramic actuator," *IEEE Transactions on control systems technology*, vol. 4, no. 3, pp. 209-216, 1996.
- [62] Y.-K. Wen, "Method for random vibration of hysteretic systems," *Journal of the engineering mechanics division*, vol. 102, no. 2, pp. 249-263, 1976.
- [63] D. Hughes, and J. T. Wen, "Preisach modeling of piezoceramic and shape memory alloy hysteresis," *Smart materials and structures*, vol. 6, no. 3, pp. 287, 1997.
- [64] K. Kuhnen, "Modeling, identification and compensation of complex hysteretic nonlinearities: A modified Prandtl-Ishlinskii approach," *European journal of control*, vol. 9, no. 4, pp. 407-418, 2003.
- [65] X. Tan, and H. K. Khalil, "Control of unknown dynamic hysteretic systems using slow adaptation: Preliminary results.", *American Control Conference, ACC'07*. IEEE, pp. 3294-3299, 2007.
- [66] F. Preisach, "Über die magnetische Nachwirkung," *Zeitschrift für Physik A Hadrons and Nuclei*, vol. 94, no. 5, pp. 277-302, 1935.
- [67] M. Brokate, and J. Sprekels, *Hysteresis and phase transitions*: Springer Science & Business Media, 2012.
- [68] M. A. Krasnosel'skii, and A. V. Pokrovskii, *Systems with hysteresis*: Springer Science & Business Media, 2012.
- [69] M. Al Janaideh, C.-Y. Su, and S. Rakheja, "Development of the rate-dependent Prandtl–Ishlinskii model for smart actuators," *Smart Materials and Structures*, vol. 17, no. 3, pp. 035026, 2008.
- [70] R. V. Iyer, and X. Tan, "Control of hysteretic systems through inverse compensation," *IEEE Control Systems*, vol. 29, no. 1, pp. 83-99, 2009.
- [71] S. K. De, and J. R. White, *Rubber Technologist's Handbook*: Rapra Technology Limited, 2001.
- [72] P. Zając, J. Kaleta, D. Lewandowski, and A. Gasperowicz, "Isotropic magnetorheological elastomers with thermoplastic matrices: structure, damping properties and testing," *Smart Materials and Structures*, vol. 19, no. 4, pp. 045014, 2010.
- [73] International Standards, "ISO 1827: Rubber, vulcanized or thermoplastic - Determination of shear modulus and adhesion to rigid plates - Quadruple-shear methods," 2011.
- [74] International Standards, "ISO 4664-1: Rubber, vulcanized or thermoplastic - Determination of dynamic properties . Part 1: General guidance," 2011.
- [75] "ASTM D5992-96(2011), Standard Guide for Dynamic Testing of Vulcanized Rubber and Rubber-Like Materials Using Vibratory Methods," 2006.

- [76] Z. Yang, T. Johansen, H. Bratsberg, G. Helgesen, and A. Skjeltop, "Potential and force between a magnet and a bulk $Y1Ba2Cu3O7-\delta$ superconductor studied by a mechanical pendulum," *Superconductor Science and Technology*, vol. 3, no. 12, pp. 591, 1990.
- [77] J. Camacho, and V. Sosa, "Alternative method to calculate the magnetic field of permanent magnets with azimuthal symmetry," *Revista mexicana de física E*, vol. 59, no. 1, pp. 8-17, 2013.
- [78] M. Rendek, and A. Lion, "Amplitude dependence of filler-reinforced rubber: Experiments, constitutive modelling and FEM – Implementation," *International Journal of Solids and Structures*, vol. 47, no. 21, pp. 2918-2936, 2010/10/15/, 2010.
- [79] V. V. Sorokin, E. Ecker, G. V. Stepanov, M. Shamonin, G. J. Monkman, E. Y. Kramarenko, and A. R. Khokhlov, "Experimental study of the magnetic field enhanced Payne effect in magnetorheological elastomers," *Soft Materials*, vol. 10, no. 43, pp. 8765-8776, 2014.
- [80] V. S. Molchanov, G. V. Stepanov, V. G. Vasiliev, E. Y. Kramarenko, A. R. Khokhlov, Z. D. Xu, and Y. Q. Guo, "Viscoelastic properties of magnetorheological elastomers for damping applications," *Macromolecular Materials and Engineering*, vol. 299, no. 9, pp. 1116-1125, 2014.
- [81] H. An, S. J. Picken, and E. Mendes, "Nonlinear rheological study of magneto responsive soft gels," *Polymer*, vol. 53, no. 19, pp. 4164-4170, 2012.
- [82] A. Fuchs, Q. Zhang, J. Elkins, F. Gordaninejad, and C. Evrensel, "Development and characterization of magnetorheological elastomers," *Journal of Applied Polymer Science*, vol. 105, no. 5, pp. 2497-2508, 2007.
- [83] M. Rakotondrabe, "Bouc–Wen modeling and inverse multiplicative structure to compensate hysteresis nonlinearity in piezoelectric actuators," *IEEE Transactions on Automation Science and Engineering*, vol. 8, no. 2, pp. 428-431, 2011.
- [84] X. Q. Ma, S. Rakheja, and C.-Y. Su, "Development and Relative Assessments of Models for Characterizing the Current Dependent Hysteresis Properties of Magnetorheological Fluid Dampers," *Journal of Intelligent Material Systems and Structures*, vol. 18, no. 5, pp. 487-502, 2007.
- [85] C.-Y. Su, Q. Wang, X. Chen, and S. Rakheja, "Adaptive variable structure control of a class of nonlinear systems with unknown Prandtl-Ishlinskii hysteresis," *IEEE Transactions on automatic control*, vol. 50, no. 12, pp. 2069-2074, 2005.
- [86] O. Aljanaideh, M. Al Janaideh, S. Rakheja, and C.-Y. Su, "Compensation of rate-dependent hysteresis nonlinearities in a magnetostrictive actuator using an inverse Prandtl–Ishlinskii model," *Smart Materials and Structures*, vol. 22, no. 2, pp. 025027, 2013.
- [87] C. Visone, "Hysteresis modelling and compensation for smart sensors and actuators.", *Journal of Physics*, vol. 138. no.1, p. 012028, 2008.